A polarisation study of spiral galaxies

Ward-Thompson, Derek

A Polarisation Study of Spiral Galaxies

Derek Ward-Thompson M A (Oxon) M Sc (Dunelm)

September 1987

Thesis presented for the degree of Ph.D

University of Durham

To My Parents

Preface

The work carried out in this thesis is a report of three years of research carried out by the author, while he was a member of the Durham University Polarimetry Group, within the Department of Physics, under the supervision of Dr.S.M.Scarrott. Much guidance from Dr.Scarrott is gratefully acknowledged, but the result is chiefly the author's own original work, with the following exception: The work presented in Chapter 3 is the joint work of the author along with Drs. Scarrott and Warren-Smith, and has already been published (Scarrott et al. 1987a).

During the three years the author attended several meetings of the Royal Astronomical Society, the Anglo Australian Telescope Symposium held at St. Andrews' University in September 1984, and the conference on Cosmical Gas Dynamics held at Manchester University in April 1985. The author addressed the Royal Astronomical Society in April 1986, at the annual out-of-town meeting held at Leeds University.

The author also visited the Wise Observatory of Tel-Aviv University, Israel, to use the $1-m$ telescope, and the La Palma Observatory, to use the $1-m$ Jacobus Kapteyn Telescope and the $2.4-m$ Isaac Newton Telescope. Much of the data contained in this thesis was taken at these times, but the remainder was taken by members of the Polarimetry Group, and the author acknowledges Drs. Scarrott and Warren-Smith, and Messrs. Draper and Gledhill.

Contents

List of figures

List of Tables

Abstract

Optical polarimetry results are presented for four spiral galaxies: NGC 5194 (M51), NGC 1068, NGC 4565 and NGC 4594 (M104). M51 and NGC 1068 show spiral polarisation patterns which are interpreted as indicating a spiral magnetic field in each case. NGC 4565 and M104 show polarisations in their dust lanes which are parallel to their galactic planes, and which are interpreted in terms of a magnetic field in the plane of each.

It is hypothesised that the observed magnetic fields may be linked to galactic shocks. A discussion of the origin of galactic magnetic fields concludes that there is no evidence which necessitates a primordial magnetic field.

Chapter 1

Morphology of Galaxies

1.1 Introduction

This thesis is divided into three parts. The first two chapters deal with previous research which has been carried out in the field of formation of spiral galaxies, and magnetic fields in spiral galaxies. In the next three chapters data are presented and interpreted of optical polarimetry of four spiral galaxies. The last chapter contains a discussion of the results, and their implications for existing theories.

It is the aim of this chapter to review current theories of why spiral galaxies exhibit the shapes which are observed and what formed those shapes. To do this, it is first necessary to describe briefly the different types of galaxies which are observed, and to show where spiral galaxies fit into the overall picture.

1.2 Observed galaxy types

Each galaxy can be classified into one of four main categories according to its appearance. The classification which will be outlined here follows that in the Hubble Atlas of Galaxies (Sandage 1961). The categories are ellipticals, lenticulars, spirals, and irregulars (see Fig 1.1). Each of these categories is then sub-divided as follows:

Elliptical galaxies are designated E0-E7, where the number describes the degree of ellipticity. That is: E0 is spherical through increasing ellipticity to E7, which is lenticular. Spiral galaxies are categorised in two types - normal spirals (S), and barred spirals (SB). These are then split into sub-groups a, b and c to denote early, intermediate and late-type spirals. There are also types S0 and SB0 which are seen as links between ellipticals and spirals, and are disk galaxies with no discernible spiral arms.

The three subdivisions denote the degree of spirality. Sa and SBa show very tightly wrapped spiral structure, Sb and SBb have slightly more open spirals, while Sc and SBc have very clear open spiral structure.

There are also irregular galaxies (Irr), which show no spiral structure at all and are divided into two groups - Type I and Type II. Irr I galaxies are differentiated because they can be resolved into groups of highly luminous O and B stars and HII regions. Irr II galaxies cannot be resolved in this manner, and many have irregular dark lanes. Finally there are ring galaxies and peculiar galaxies which are seen as side branches of the main categories.

To say that Fig 1.1 represents an evolutionary chart of a

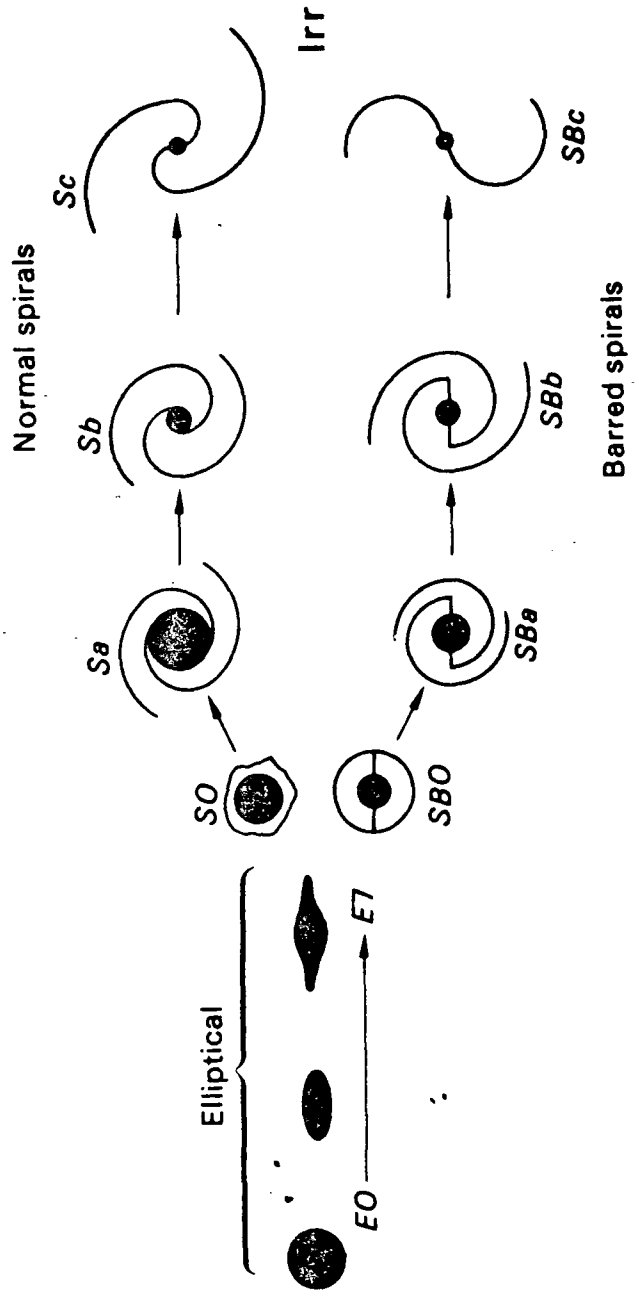

Figure 1.1: The Hubble classification of galaxies.

galaxy, in the same way that the Hertzsprung - Russell diagram is for stars, would be incorrect. There is a large, fundamental difference between ellipticals and spirals. This concerns the amount of dust which they contain. Elliptical galaxies generally contain little or no dust, while spirals contain large quantities of dust, often forming extensive dust lanes. The amount of dust in a galaxy directly affects the star formation rate within that galaxy. Elliptical galaxies show only limited or no star formation while spiral galaxies contain many young stars and star-forming regions.

Elliptical galaxies cannot evolve into spiral galaxies, therefore there must be some initial conditions during the formation of a galaxy which determine the ultimate morphological type. In this chapter the effects of gravitational and mechanical forces will be considered. The dynamics of large structures of disk-like matter will be discussed in terms of spiral density waves and shocks. In the next chapter the further effects of magnetic fields will be included.

1.3 Galaxy formation

Consider a volume of the Universe at some time after the Hot Big Bang. This volume contains a certain amount of matter with mass M, which begins to collapse under self-gravitation. Exactly what first triggers this collapse within an expanding universe is still an issue for speculation. Whether it be superstrings, or perturbations in the quantum fields which existed in the very early Universe, or whichever particular theory one adheres to, (see, for example: Gott,1977; Jones & Gonzalez,1984; Shanks,1985) is beyond the bounds of this thesis.

Regardless of the trigger mechanism, the mass collapses to create a protogalaxy. There are several initial parameters of such a protogalaxy which affect the nature of this collapse. These include the initial mass, volume, angular momentum, magnetic field and the degree of uniformity of density of the protogalaxy. The following discussion in this chapter and the next explores what effect the variation of each of these parameters has on the properties of the galaxy which is formed.

1.4 Elliptical galaxies

The first initial parameter to look at is the angular momentum vector ω. If a protogalaxy is considered which has low angular momentum, the matter coalesces to form stars, whilst continuing the collapse. This goes on until an equilibrium state is reached, when the majority of the mass of the newly-formed galaxy is in the form of stars.

The stars are all in orbit about the common centre of mass of the galaxy, and the galaxy formed is elliptical in shape. That is to say that its three semi-major axes are in general of different lengths. The exact shape of the galaxy is determined by the modulus and direction of ω. The axis which is closest to being parallel to ω is the shortest, and the axis nearest to perpendicular to ω is the longest. The smaller the initial value of ω the more nearly spherical the galaxy. It must be remembered that our view of a galaxy is in one direction only, and so methods such as luminosity profiles must be used to determine its true shape in three dimensions.

1.5 Spiral galaxies

A collapsing protogalaxy with a large angular momentum collapses much more readily along the axis of rotation than in any other direction. So the protogalaxy collapses to a large, flattened rotating disk and star formation occurs. Featureless disk galaxies are seen (S0 and SB0), likewise, irregular and ring galaxies are seen which could be disk galaxies which have broken up due to tidal forces caused by neighbouring galaxies. However, to create and maintain the patterns which are observed in spiral galaxies it is necessary to consider in more detail the dynamics of a disk of stars, gas and dust.

A typical rotation period of a galaxy is around 10^8 years and the age of galaxies is typically 10^{10} years. Hence an average galaxy could be expected to have completed approximately 100 revolutions by the present day. So there is a problem as to why the spiral patterns have not become so tightly wound up that they are no longer visible. Early work concentrated on this problem.

Observations of the spatial distribution of the stars in a spiral galaxy show that, whereas the luminosity exhibits a spiral structure, the stars are in fact more uniformly distributed. This is because the majority of stars in a galaxy are older than 10^8 years and their velocity dispersion increases with stellar age (Wielen 1974). Typically, stars of 10^7 years old have a dispersion of $7km/s$. That for stars aged $10^8 - 10^9$ years is $10 - 20km/s$, and for the oldest stars (10^{10} years) the velocity dispersion can be up to $50km/s$. However the more massive, short-lived stars (of order 10^6 years) are also the most luminous, and it is these highly luminous stars which trace out the

spiral pattern of a galaxy most clearly.

Significant steps toward the solution of the problem of creating and maintaining spiral structure have been made within the last 20 years. One theory is that the spiral pattern is created by a spiral density wave in the gas and dust of the interstellar medium.

The spiral dark lanes correspond to compression regions in the density of the interstellar gas and dust. When this gas and dust passes through a compression region, a burst of star formation is triggered. So, immediately after the compression, there appears a region of very bright, young, highly luminous stars. Thus is created the pattern of alternate bright and dark spirals.

B.Lindblad (1964), discussed a circulation theory, which stated that there is a spiral structure of density waves (in spiral galaxies) which rotates in effect as if it were a solid body, whilst the matter of the galaxy orbits in a Keplerian fashion with an angular velocity which is dependent upon the radius of the orbit from the galactic centre. Thus, in general, the stars, gas and dust in a spiral galaxy orbit at a different angular velocity from the spiral pattern.

The radius of corotation is defined as the radius at which the matter is orbiting at the same angular velocity as the spiral pattern. This radius separates the two regimes in a spiral galaxy. Within the corotation radius matter rotates faster than the pattern. Outside of the corotation radius the matter appears to orbit in a retrograde fashion relative to the pattern. Lindblad hypothesised that in this latter region the matter flows outwards along a spiral arm, before leaving the trailing edge and falling back to the next arm. This is the essence of

the circulation theory.

The radius of corotation of a typical galaxy is large, and encloses the majority of the visible disk of the galaxy. Hence the matter rotates in the same direction as, and overtakes the spiral pattern throughout the major part of a galaxy, so the circulation theory does not explain spiral structure in galaxies.

Kalnajs (1973) considered a ring of test particles rotating about a galactic centre in an elliptical orbit. This ellipse was then precessed, and a superposition of several such ellipses, with decreasing major axes, gives the impression of a spiral pattern (see Fig 1.2).

Lynden-Bell (1974) also discussed how spiral patterns might be set up in the interstellar medium without spirality in the stellar distribution. He stated that a star in a typical orbit around a galaxy describes an open orbit. However, relative to a rotating frame of reference the orbit can appear closed (see Fig 1.3).

Some specific orbits, in the frame of reference rotating with the spiral structure, can appear elliptical. These are known as resonant orbits because stars in such orbits can transfer angular momentum radially outwards and set up distortions in the gravitational field of the galaxy which could form shock waves in the interstellar medium (shocks are discussed in Section 1.7).

P.O.Lindblad (1974) pointed out that there are two important parameters to consider: The angular frequency of the matter, ω, and the frequency of radial oscillations, or epicyclic frequency, κ. Matter in a typical open orbit can be deemed to be orbiting in a precessing ellipse and the angular frequency of

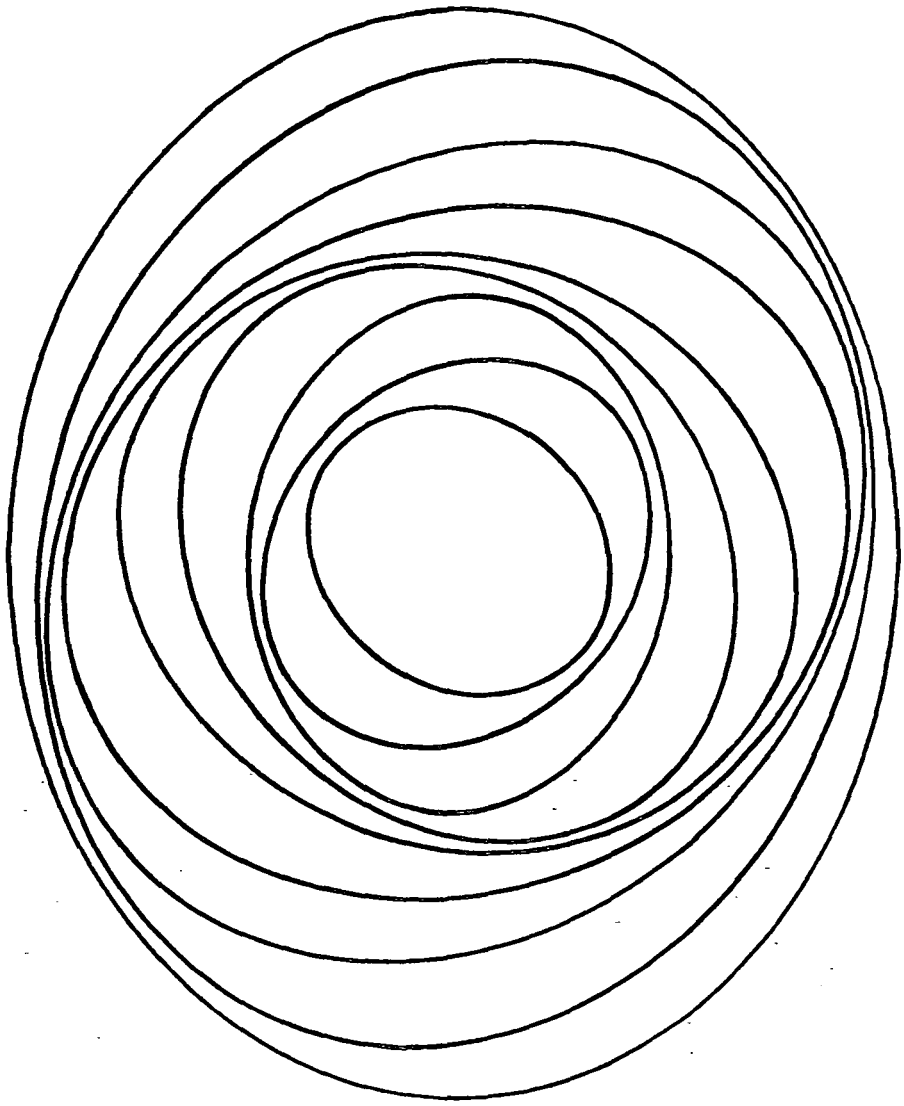

Figure 1.2: A set of precessing ellipses gives the impression of a spiral pattern (Kalnajs 1973).

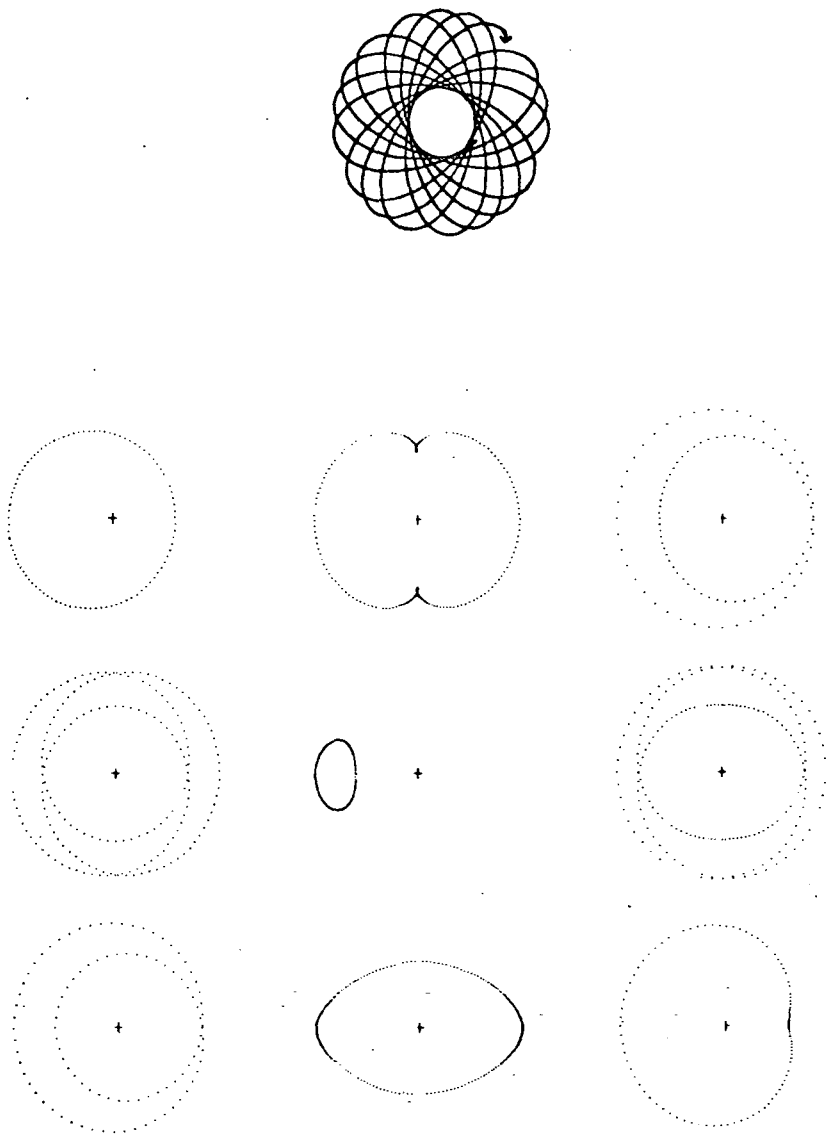

Figure 1.3: An open orbit (top) and its appearance in different rotating frames of reference (Lynden-Bell 1974).

this ellipse is given by:

$$\Omega_e = \omega - \frac{\kappa}{2} \tag{1.1}$$

Observations of our Galaxy and several others have shown that the quantity $\omega - (\kappa/2)$ is very nearly constant over the main part of each galaxy studied. This constancy means that if a set of orbits, such as is illustrated in Fig 1.2, should occur, then the pattern persists for some time, and spiral density waves are set up, which move with pattern angular frequency Ω_p. If $\Omega_p > \omega - (\kappa/2)$, there are three interesting resonant radii: Corotation ($\Omega_p = \omega$) was mentioned earlier. The other two cases are:

$$\Omega_p = \omega - \frac{\kappa}{2} \tag{1.2}$$

$$\Omega_p = \omega + \frac{\kappa}{2} \tag{1.3}$$

These radii are called the inner Lindblad resonance (ILR), and the outer Lindblad resonance (OLR) respectively. At ILR the precessing ellipse rotates at the same rate as the pattern. At OLR a closed elliptical orbit precesses with the pattern velocity, but the matter orbits in a retrograde fashion relative to the direction of precession. Thus the density wave pattern does not extend within ILR nor beyond OLR.

This work has given some insight as to how spiral patterns could be maintained once they are set up, but does not explain why they are set up in the first place. As mentioned earlier Lynden-Bell suggested that stars in resonant orbits can transport angular momentum outwards, and hence lower the rotational energy of the system. Other workers have tried to explain this further by starting at different places and attacking the problem in other ways.

Among the best efforts at deriving spiral patterns mathematically from wave dispersion relations are those of Lin and Shu (1964). They assumed that a galaxy is an infinitesimally thin disk with an appropriate surface density, ρ. They ignored the velocity dispersion of the stars and started with an initial distribution function in the disk, ρ_0, for ρ with relevant boundary conditions at $r = 0$ and $r \rightarrow \infty$. They then wrote down the equations of this function and introduced a small perturbation, but note that the initial cause of the perturbation was still unknown. The solution of this for the surface density ρ in cylindrical polar coordinates (r, θ, z) is:

$$\rho' = Re(\rho_1(r)e^{i(\omega t - n\theta)}) \quad * \tag{1.4}$$

where n is an integer subsequently found to be equal to the number of arms in the spiral, and ω is a variable depending solely on r. This is a density wave equation which is spiral in nature. The form of the spiral satisfies the following equation:

$$\theta = \frac{1}{n} \times (F(r) + const) \tag{1.5}$$

where F(r) is a function which varies rapidly with r. If $F(r) < 0$ the arms are trailing, and if $F(r) > 0$ the arms are leading.

In a typical galaxy F(r) should change by 4π over a typical galactic radius. More recent work by Shu et al. (1985) on the density waves in Saturn's rings led them to believe that Fourier analysis of non-linear density waves could eventually fully account for spiral patterns in galaxies.

Another theory is that spiral structure is seen most clearly in galaxies which have a massive companion, and it is probably the presence of the gravitational influence of the companion

* where: $\rho = \rho_0(r) + \rho'$

$\rho_1(r) = e^{iF(r)}$

$\omega = \omega_r + i\omega_i$

which sets up the spiral pattern. Toomre (1981) deduced that a form of positive feedback occurs in which clear open spiral structure is set up rapidly after an encounter with a neighbouring galaxy.

This structure survives for several rotations after closest approach. But this still does not account for spiral structure in galaxies which have no near neighbours any more, as the pattern is not long-lived. Nonetheless it is worth noting that some of the most obvious open spiral patterns occur in galaxies with near neighbours (eg:M51 and M81). So it is highly likely that the proximity of another galaxy can at the very least amplify an already existing spiral pattern, but some initial pattern is still required.

Spiral density wave hypotheses have even been used to explain inter-arm spurs within a two-armed spiral structure. Byrd (1983) performed calculations on an inter-arm spur in M31. He showed that the angle of the spur is such as to be caused by a massive object orbiting in the galactic disk. The mass of such an object was calculated to be $5 - 9 \times 10^7$ solar masses.

1.6 Stability against bar formation

Numerous N-body simulations have been carried out in recent years in an effort to create the spiral density variations discussed above. Among the most successful of these was a study performed by Hohl (1971), who started with a rotating self - gravitating disk of stars, with an initial velocity dispersion and modeled the variation of the surface density distribution with time. He found that after two rotations a bar-shaped structure formed in the central portion of the disk (see Fig 1.4). Note

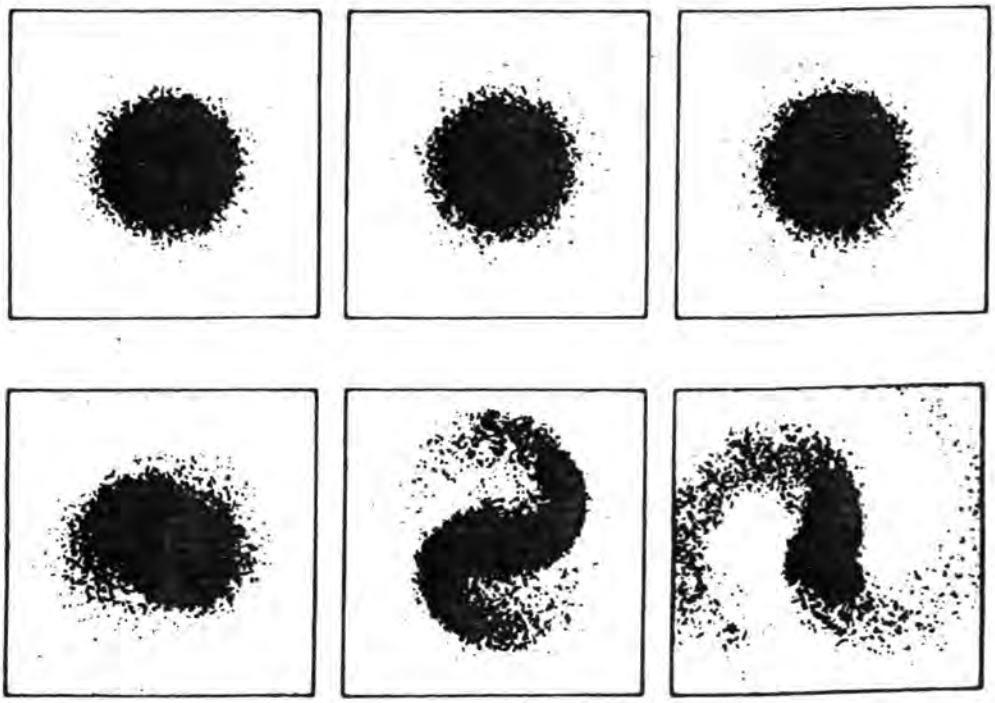

Figure 1.4: N-body simulation showing the formation of a bar (Hohl 1971).

that this model differed from that of Lin and Shu, where zero velocity dispersion of the stars was assumed. This formation of a bar does not, however, appear to be a major set-back, as among the 1000 brightest spiral galaxies, roughly 2/3 contain bar-like features.

A more disturbing set-back of this model is that it did not succeed in creating truly long-lived spiral patterns existing for 100 or more revolutions. After about 3 rotations of the barred spiral the structure degenerated to a more oval shape which had a roughly exponential z variation. Other authors have come to similar conclusions (eg: Kalnajs 1976 a & b), creating spiral patterns which are not long-lived.

An important discovery was made by two workers in the field and is known as the Ostriker-Peebles criterion (Ostriker & Peebles 1973). These authors considered an N-body simulation of a disk of stars which have both ordered kinetic energy of rotation about the galactic centre and also random kinetic energy of irregular motion. The criterion which they found states that, in a galaxy composed of a disk of stars: The ratio of the kinetic energy of rotation of the stars about the galactic centre to the total gravitational potential energy of the galaxy must be less than, or equal to, 0.14. If this criterion is not fulfilled then a bar-like instability is created in the centre of that galaxy.

They further noted that there are many galaxies in which the random stellar motions are small compared to the systematic circular motion. This lead them to the conclusion that such a galaxy must contain a massive halo, such that the ratio of halo-to-disk mass is of the order of 1 to 2.5.

Kalnajs and Athanassoula-Georgala (1974) said that an al-

ternative solution to satisfy the Ostriker-Peebles criterion would be a galaxy with an active nucleus. It is now believed that active galactic nuclei are a more common phenomenon than was previously thought to be the case. It is therefore possible that enough energy may arise from this source to avoid the above-mentioned instability to bar formation.

However, if the nucleus of a galaxy undergoes a violent explosion the effects can be seen on the ISM. Sanders and Bania (1976) carried out hydrodynamical calculations on the effects of galactic explosions in spiral galaxies, and found that the spiral gas distribution is somewhat distorted. A ring is formed which disappears after 10^8 years, then the spiral structure returns. Further discussion of active galactic nuclei is presented in Chapter 4 - a study of the Seyfert galaxy NGC 1068.

One way in which a spiral pattern may be set up is that there is a large halo of dark matter surrounding each galaxy, which is massive but non-luminous (Hohl 1974). The gravitational attraction of such a massive halo sets up standing waves in the interstellar medium, rather in the manner of shepherding satellites creating the gaps in Saturn's rings. However in Hohl's models the major stumbling block is the ratio of disk mass to halo mass. He also found that if the halo mass was less than that of the disk, then a bar was formed, which subsequently left an oval distribution of stars. Furthermore the only spiral patterns which lasted more than a couple of revolutions were from those models in which the mass of the disk component represented only $10 - 20\%$ of the total mass of the galaxy.

The feasibility of a massive halo (5-10 times as masive as the disk) may, at first sight, be questioned. However evidence exists which suggests that this may, in fact, be the case (see

Illingworth 1981 for a review). Extensive sets of HI rotation curve data now exist for many galaxies. The majority of these curves are very flat at large radii. This implies that M/L increases strongly with radius, hence that a large part of the galaxy's mass may exist in a dark halo. Further work on this could prove if this is true for all galaxies. Toomre (1982) performed further calculations on stellar orbits in composite disk-plus-halo systems and confirmed that such systems are stable.

Other experimental evidence includes the detection of an optical halo around the Sb galaxy NGC 4565 (Hegyi and Gerber 1977). This halo has a brightness of 0.1% sky brightness at a radius of 34kpc, comparable to the radius of the visible disk. They also state that the colour data suggest the halo to be composed of stars of spectral type $K7$ or redder. Hence the halo has a large mass to luminosity ratio, as required by the theory above.

Van Albada and Roberts (1981) studied the gas component of galaxies with a barred spiral gravitational field variation. Their gas dynamical calculations were performed at a higher resolution than previous attempts, and they found that a shock forms along the leading edge of the bar, which gradually moves back across the bar with time. They associated shocks with the dark lanes seen in barred spiral galaxies. However they state that further work is necessary in order to completely remove the spurious effects of the resolution of the numerical analysis.

Ambastha and Varma (1983) performed similar calculations upon disk systems of gas and stars which had varying sizes of halo. They succeeded in creating many different spiral patterns, some of them barred, but still none of them long-lived.

1.7 Spiral shocks

One of the main advantages of the spiral density wave pattern hypothesis is that it accounts for the triggering of star-formation in narrow spiral arm regions. This is the galactic washboard model (Roberts 1974). This model predicts the following: There is a gravitational field within the plane of a galaxy which contains regular fluctuations in the form of a spiral pattern. However the intensity of these fluctuations is relatively small.

Gas orbiting in a galaxy experiences this periodic variation in gravitational potential energy. This then creates a large variation in the density of the gas. The reason for this is that the density response of a component of the galaxy to a potential variation is roughly proportional to the inverse square of the characteristic speed of that component (Shu 1973). The sound velocity in the inter-stellar gas is typically much less than the random velocity of the stars, hence the density response of the gas is very much greater. Fig 1.5 shows the response of the gas density to a varying gravitational potential around an orbit, and what form at the potential minima of the gravitational field are shock fronts in the inter-stellar medium.

The strength of these shocks depends upon the amplitude of the driving potential variation. However it is also dependent on the ratio of the total velocity component of the gas normal to a spiral arm, to the sound velocity in the inter-stellar gas. Two different cases occur—one in which the gas velocity exceeds the sound velocity and one in which the reverse is true. In the first case a fractional change in gravitational field of only 5% produces a strong, narrow shock. This leads to a galaxy with

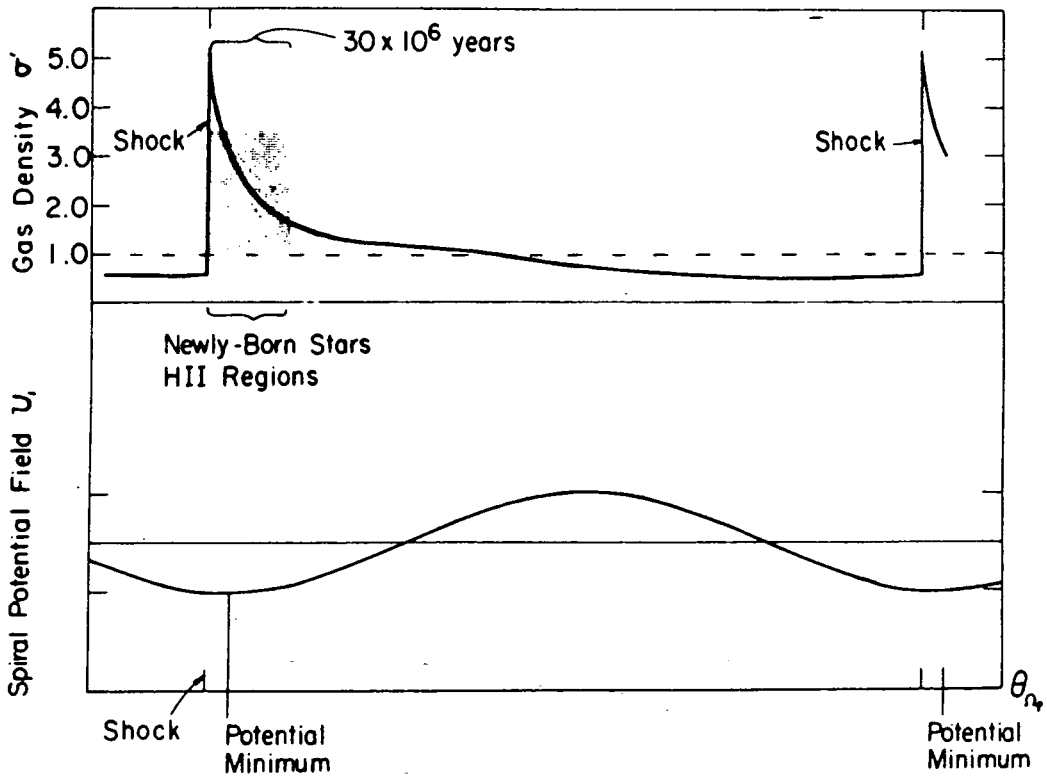

Figure 1.5: Gas density response to varying gravitational potential (Roberts 1974).

narrow, clearly delineated spiral arms. In the second instance only broad, weak shocks are produced, leading to broad, diffuse spiral arms.

Roberts et al. (1974) confirmed this experimentally for a sample of 25 galaxies. They found a good correlation between the shock strength and the luminosity and clarity of the spiral arm structure in their sample. The strength, as already mentioned, scales with the square of the rotation velocity of the interstellar medium perpendicular to the arm v_p. Hence their galaxies had detailed rotation curve data already available, and had all been classified by van den Bergh (1960). They found that galaxies containing bright, well-developed spiral arms have strong shocks: $v_p = 15 - 25 km/s$. Galaxies with patchy, less clearly defined arms have intermediate strength shocks: $v_p = 10 - 15 km/s$. Those with only a trace of spiral structure have only very weak shocks: $v_p < 10 km/s$.

Shu (1974) did some calculations on star formation within shock front models and specifically on the relative distribution of HI and HII in a galactic disk. The mass of HI (MI) in an annulus of width r at radius R is:

$$MI = 2\pi RDr \tag{1.6}$$

where D is the surface density of HI at galactic radius R. Whereas, assuming that HII formation only occurs at the triggering points of galactic shock waves, then the mass of HII within the same annulus is:

$$MII = smLft \tag{1.7}$$

where s is the flux of HI across the shock front:

$$s = DR(\omega - \Omega_p)sini \tag{1.8}$$

ω is the angular velocity of the matter at radius R, Ω_p is the angular velocity of the shock pattern, i is the opening angle of the spiral, m is the number of shock fronts around the annulus, which is equal to two for a bisymmetric spiral. L is the length of the shock front within the annulus: $L = r/(sini)$, f is the fraction of the mass of HI induced to form HII by the passage of the shock, an efficiency factor, and t is the average life-time of an HII region.

So, dividing the mass of HII by the mass of HI in the annulus gives:

$$\frac{MII}{MI} = (\omega - \Omega_p)\frac{ftm}{2\pi} \tag{1.9}$$

Assuming t is independent of radius: $m(\omega - \Omega_p)$ is a monotonically decreasing function from $R = 0$ up to the radius of corotation. $f \rightarrow 0$ within the inner Lindblad resonance, because the spiral shocks do not extend within that radius.

Hence the abundance ratio of $[HII]/[HI]$ increases with increasing radius to a point just beyond the ILR and then decreases once more. Quantitative examination of the last equation can produce a curve which closely fits the observed abundances in galaxies, and, for instance, explains the 5kpc ring in our own Galaxy.

Problems still remain with sustaining shocks (Toomre 1977), associated with damping and dissipation of energy. However Sanders & Huntley (1976) succeeded in creating spiral shocks in the gas density distribution from oval distributions in gravitational potential variations. These shocks were not long-lived, however they do serve to illustrate that spiral shocks can occur without spiral density waves.

1.8 Spiral patterns without spiral shocks

More recent work on star formation in spiral galaxies was carried out by Roberts and Hausman (1984). They treated the ISM as an N-body system of particles representing the molecular gas clouds present in all galaxies. They modelled a system of inelastic collisions between clouds in which star formation occurred, and also collisions with supernova remnants (SNRs) formed from young stars after an appropriate delay time.

They assumed an initial velocity dispersion based upon observation, and then subjected all to a spiral variation of the galactic gravitational field of the kind outlined in Section 1.5. Their model assumed a steady state solution for the energy of the system. In other words: Energy which was taken from the system by cloud-cloud collisions was replaced by cloud-SNR collisions, in which the cloud was accelerated by the shock from the SNR.

They discovered that after just over 10^8 years an equilibrium situation was reached in which the molecular clouds vaguely traced out the spiral variations of the gravitational field. However, far more striking was the fact that the young stellar associations exactly traced out the spiral pattern of the field after only 10^8 years. This pattern remained visible until at least 10^9 years. Although the number of parameters which had to take assumed values was large, still this theory looks like a viable alternative to spiral shock wave theories.

In the subsequent paper (Hausman and Roberts 1984) they discovered that if the stellar associations had a lifetime of more than 2×10^9 years they no longer traced out such clear spiral features. This is exactly what was mentioned earlier as the

observed distribution of stars in galaxies. Finally, these authors claimed that by varying the parameters over physically reasonable limits they could reproduce a wide variety of the observed morphologies of spiral galaxies.

An alternative approach was produced by Sellwood and Carlberg (1984), who claimed that spiral features in galaxies are purely transitory, but that they are recurrent.

They considered a typical galaxy as composed of gas and stars, and global spiral instabilities of the kind discussed by proponents of spiral density waves. However they made no attempt to make the spiral instabilities in the gaseous or stellar response long-lived. They also started with a large initial halo mass which gradually decreased over the age of a galaxy.

They found that if a galaxy reaches a state where it no longer contains any gas, then the disk stabilises and no further spiral features are observed. However any star formation or collisions between molecular clouds destabilises the disk. A spiral instability lasts typically for a few revolutions before it decays and another instability occurs. In order to produce a steady state situation with a balance between heating (increasing the random velocities of the stars) and cooling (star formation and cloud-cloud collisions) they found a necessary star formation rate of a few solar masses per year, over the whole of a galactic disk.

1.9 Summary

A review has been presented of recent attempts to explain the regular spiral patterns observed in many galaxies. The present situation is the following: Spiral density wave models have

been made which can artificially produce normal spiral patterns, as well as barred spirals. Furthermore, such density wave variations can create spiral patterns through collisions between molecular clouds. Exactly what starts the initial perturbations from which the spiral density variations grow, is still unclear.

However it has been shown that small density variations can create large-scale shocks in the interstellar medium which could be sufficient to trigger star formation. It is also possible that spiral shocks can arise in other ways. The major remaining problem is how to maintain the spiral structure throughout the greater part of a galaxy's lifetime. Clearly there are other effects which must be taken into consideration. The most important component of a galaxy which has been neglected so far is the magnetic field. The role which this may play is discussed in the next chapter.

Chapter 2

Review of Magnetic Fields in Galaxies

2.1 Introduction

In this chapter a review is presented of previous studies of large-scale magnetic fields in galaxies. Firstly the different observational techniques which could be used to detect magnetic fields in other galaxies are outlined, and their chief results are listed. Then theories concerning the origin of galactic magnetic fields are discussed.

Finally the predictions of the various theories are compared with the existing observational evidence. In the next three chapters the results of a survey carried out in the Durham University Polarimetry Group are presented, and in the last chapter the effect of the new data on an understanding of the theories is outlined.

2.2 Previous observations

Observations which can be made of magnetic fields in galaxies include: Studies of cosmic rays, although these tell us primarily about the field in our own Galaxy, and examination of the linear polarisation states of electromagnetic radiation emanating from other galaxies. Other observations which could be made include looking at the Zeeman splitting of the HI line in a magnetic field, and circular polarisation effects. Neither of these latter have been carried out due to the experimental difficulties involved and the strength of the fields required to produce measurable effects. This section will concentrate on linear polarisation studies which have been undertaken in the past in two regions of the electromagnetic spectrum - optical and radio.

2.2.1 Optical linear polarisation measurements

Optical linear polarisation arises from a variety of mechanisms. The most important of these in the study of galaxies are: Scattering of starlight by interstellar dust grains, and preferential extinction by magnetically aligned non-spherical dust grains.

Scattering creates a polarisation state in which the **E**-vector of the scattered light is perpendicular to the scattering plane. Hence nebulosity which is illuminated by a point source (eg: a single star) displays a centro-symmetric pattern which is centred upon the illuminating source. Typical levels of polarisation created by scattering in an optically thin reflection nebula (ie: where single scattering dominates) are around $10-20\%$— eg: NGC 6729, illuminated by RCrA (Ward-Thompson et al.

1985). However, levels of polarisation up to 70% can be created by scattering, depending on the scattering geometry.

The process by which polarisation is caused by magnetically aligned dust grains is known as the Davis-Greenstein mechanism (Davis and Greenstein 1951). These authors assumed that interstellar dust grains are composed mainly of hydrogen compounds, with about 12% by mass of iron in compounds, although most researchers now claim that silicate compounds predominate. The means of orientation outlined by Davis and Greenstein was later revised by Jones and Spitzer (1967), and it is these latter authors who are now generally believed to be correct, but note that the alignment produced by the revision is in the same direction as that discovered by Davis and Greenstein.

The exact method of alignment, however, still remains a matter of debate. More recent theories have included the pinwheel theory (Purcell 1973), otherwise known as suprathermal alignment. This was shown to be merely a more general case of the Davis-Greenstein mechanism (Cugnon 1985). Note that all researchers agree over the direction of the alignment. The method of alignment most widely accepted is known as paramagnetic relaxation (not ferromagnetic, as was thought by Davis and Greenstein), and can be achieved in fields of only a few microgauss. This works as follows:

Consider a region of interstellar space containing gas and dust, and permeated by a magnetic field **B**. The dust grains within this region are spinning rapidly ($10^6 rad/sec$), such that their angular momentum vector ω is oriented randomly. Thus, in general **B** and ω are not parallel. Hence the grain experiences a sinusoidally varying magnetic field, which induces an

internal magnetisation of all paramagnetic grains within the region. Because of paramagnetic relaxation, the induced magnetisation lags behind the external field by some phase angle. Furthermore the magnetic torque experienced by the dust grain is perpendicular to **B**.

This torque is dissipative, tending to increase the internal energy of the grain. However a dust grain radiates efficiently, so that the increase in internal energy does not significantly increase the grain's internal temperature. Jones and Spitzer considered the gas kinetic temperature T_g and the grain internal temperature T_i, where, in general:

$$T_i < T_g \tag{2.1}$$

The impulsive torques caused by grain-atom collisions are random, and so cancel, hence the total net value of this torque tends to zero. This leaves the paramagnetic torque due to the field, which tends to cause the grain to spin such that its angular momentum vector ω is parallel to the magnetic field vector **B**. Furthermore, if such a grain is non-spherical, it will rotate about its shorter axis.

Hence dust grains in a region containing a magnetic field show a tendency to spin with their longer axis **perpendicular** to the field. Grains of dust in the interstellar medium scatter visible light, and they scatter more of the component of light which is vibrating parallel to their longer axis.

The light which then passes through a region of such aligned grains becomes polarised in a direction which is **perpendicular** to the long axis of the grains. Hence light which has passed through a region of magnetically aligned grains is polarised **parallel** to the field in that region.

So the polarisation of light from a distant object can trace the transverse component (projected onto the plane of the sky) of the magnetic field foreground to that object. Typical levels of polarisation created in this way are around 2−5%, depending on the extinction within the region of aligned dust grains.

Early attempts to map magnetic fields in galaxies proved most successful within our own Galaxy. The now classic measurements of interstellar polarisation (Hall 1949, Hiltner 1949) were attributed to a large scale magnetic field within our Galaxy. This field appeared to be confined to the plane of the Galaxy and to run parallel to that plane. Clearly this method can tell the direction of a field, though not its sense. This was confirmed by Mathewson and Ford (1970). Axon and Ellis (1976) catalogued the polarisation results of other authors for over 5000 stars, and found also that the percentage polarisation increases with increasing distance. This is as expected if the magnetic field uniformly permeates the major part of the Galaxy, and is ordered on a large scale.

Serkowski et al. (1975) studied the wavelength (λ) dependence of polarisation (P) caused by preferential extinction due to aligned grains in the interstellar medium. They deduced a relation of the following form:

$$\frac{P_\lambda}{P_{max}} = e^{-1.15ln^2(\lambda_{max}/\lambda)} \tag{2.2}$$

where maximum polarisation P_{max} occurs at wavelength λ_{max}. They went on to infer that the ratio of total to selective interstellar extinction:

$$R = \frac{A_V}{E_{B-V}} \tag{2.3}$$

is given by:

$$R = 5.5\lambda_{max} \tag{2.4}$$

The relation between polarisation and extinction at different wavelengths is explored in Chapter 5, where a multicolour polarimetric survey of M104 is detailed.

Endeavours to measure polarisation in other galaxies proved difficult. However Elvius managed to measure polarisations of a few percent in several galaxies: eg: M63 (Elvius 1951), NGC 7331 (Elvius 1956) and M31 (Elvius and Hall 1964). Problems arise over sky polarisation which swamps the polarisation in the object, also over the extreme faintness of the objects under observation.

Measurements were made of the peculiar galaxy NGC 5128 (Elvius and Hall 1964) which were interpreted in terms of a magnetic field parallel to the plane of that galaxy. A far more complete survey was carried out by Berry (1985), who concluded that the polarisation in NGC 5128 is in fact caused by extinction by nonspherical dust grains aligned by a toroidal magnetic field in the plane of the galaxy. He further concluded that the strength of this field is of roughly the same strength as the field in our own Galaxy - of the order of a few microgauss. Elvius (1973) performed a few measurements on NGC 4565 and again found polarisation parallel to the dust lane.

Bingham et al. (1976) mapped the optical polarisation in M82, and this work was further detailed by Pallister (1976). These authors found moderately high levels of polarisation (of the order of 10%) caused by scattering from dust grains. They also found that departures from the expected centrosymmetry in the brightest regions indicated an extended illuminating source. Perkins (1978) modelled the polarisation as scatter-

ing, on the assumption that M82 had drifted into a giant dust cloud. Chesterman and Pallister (1980) further discussed the polarisation of M82 in terms of scattering, and invoked a tilted disk model.

Scarrott et al. (1977) performed a series of measurements on M104, in which they observed polarisations of the order of $2 - 4\%$ running parallel to the dust lane of the galaxy. They attributed this to a large scale magnetic field within the plane of M104 causing alignment of nonspherical grains.

Elvius (1978 a & b)) described observed polarisation in the Seyfert galaxy NGC 1068 as possibly due to scattering. Angel et al. (1976) also performed optical polarimetry on NGC 1068, and concluded that polarisation was caused by dust scattering, although this will be discussed further in Chapter 4. Elvius (1978c) found polarisation running along the spiral arms of NGC 4216 and NGC 3623.

It can be seen that, despite experimental difficulties, a growing volume of evidence has been amassed which points to the fact that magnetic fields in galaxies are strongest in the planes of galaxies. However the exact geometry of such fields, whether it be circular, spiral, or otherwise, has yet to be determined.

2.2.2 Radio linear polarisation measurements

Radio polarisation arises chiefly from synchrotron radiation. Electrons spiralling in a magnetic field emit linearly polarised radiation at short radio wavelengths. The plane of polarisation observed is **perpendicular** to that component of the magnetic field transverse to the line of sight. Levels of polarisation created in this way can be as high as 50%.

However, if the linearly polarised radiation passes through a magnetic field with a component parallel to the direction of propagation, then the Faraday effect causes the plane of polarisation to rotate. The equation governing Faraday rotation (Burn 1966) is:

$$\theta_{obs} = \theta_{int} + (RM) \times \lambda^2 \qquad (2.5)$$

where θ_{obs} is the observed polarisation angle (in radians) of the radiation of wavelength λ, θ_{int} is the intrinsic polarisation angle before the radiation has passed through the magnetic field, and the constant (RM) is called the rotation measure.

It is necessary to measure the polarisation at several wavelengths in order to calculate the RM. Alternatively it is possible to measure the polarisation at such a high frequency that the Faraday rotation is negligible. This is why Faraday rotation can be ignored in optical polarisation measurements.

Observations of this kind have been carried out (Segalowitz 1976, Segalowitz et al. 1976) on M51 and M81. In both of these the authors found tangential magnetic fields. They could not interpret the exact field morphology in the case of M81 because of slight uncertainty over the Faraday rotation. However for M51, data were obtained at two different wavelengths and it was found that the field was spiral in nature. Limitations still remain over the resolution of radio measurements, so for instance the field could not be mapped right into the centre of M51.

However, Faraday rotation can be useful in that it enables the field parallel to the line of sight to be calculated. Caution must be exercised as the rotation is caused by all of the fields in the line between source and observer. The magnetic

field within our own Galaxy can be taken as constant across the small angular size of the object under study. Similarly the intergalactic field, which is considerably smaller anyway, can be assumed constant. Thus the variation in RM across a galaxy can be attributed to the environs of that galaxy. The expression for calculating the RM (Sofue et al. 1986) is:

$$RM = 0.81 \int nBdl \tag{2.6}$$

where n is the number of electrons per cubic centimetre in the observed galaxy, B is the component of the magnetic field parallel to the line of sight in microgauss and l is the path length within the field in parsecs. This method of calculating the variation of RM across a galaxy can be used to decide between the various field geometries.

Consider a galaxy inclined at some angle to the line of sight. Fig 2.1 illustrates the dependence of the variation of RM across the face of a galaxy with magnetic field geometry. In the case of a circular field the variation of RM along the major axis is such as to be positive on one side of the galactic nucleus (field directed towards observer) and negative on the other side (field away from observer). In the case of a bisymmetric spiral (BSS) field the RM is symmetrical about the galactic nucleus along the major axis. This is a very powerful observational technique, despite difficulties with obtaining the necessary resolution. The field strengths in all of the galaxies studied in this way are of the order of $3 - 15 microgauss$.

Tosa and Fujimoto (1978) observed M51 and found it to have a BSS structure (see Chapter 3). Sofue et al. (1980) did the same for M81 and M33 and found both to have BSS fields. Sofue and Fujimoto (1983) tried to determine the field con-

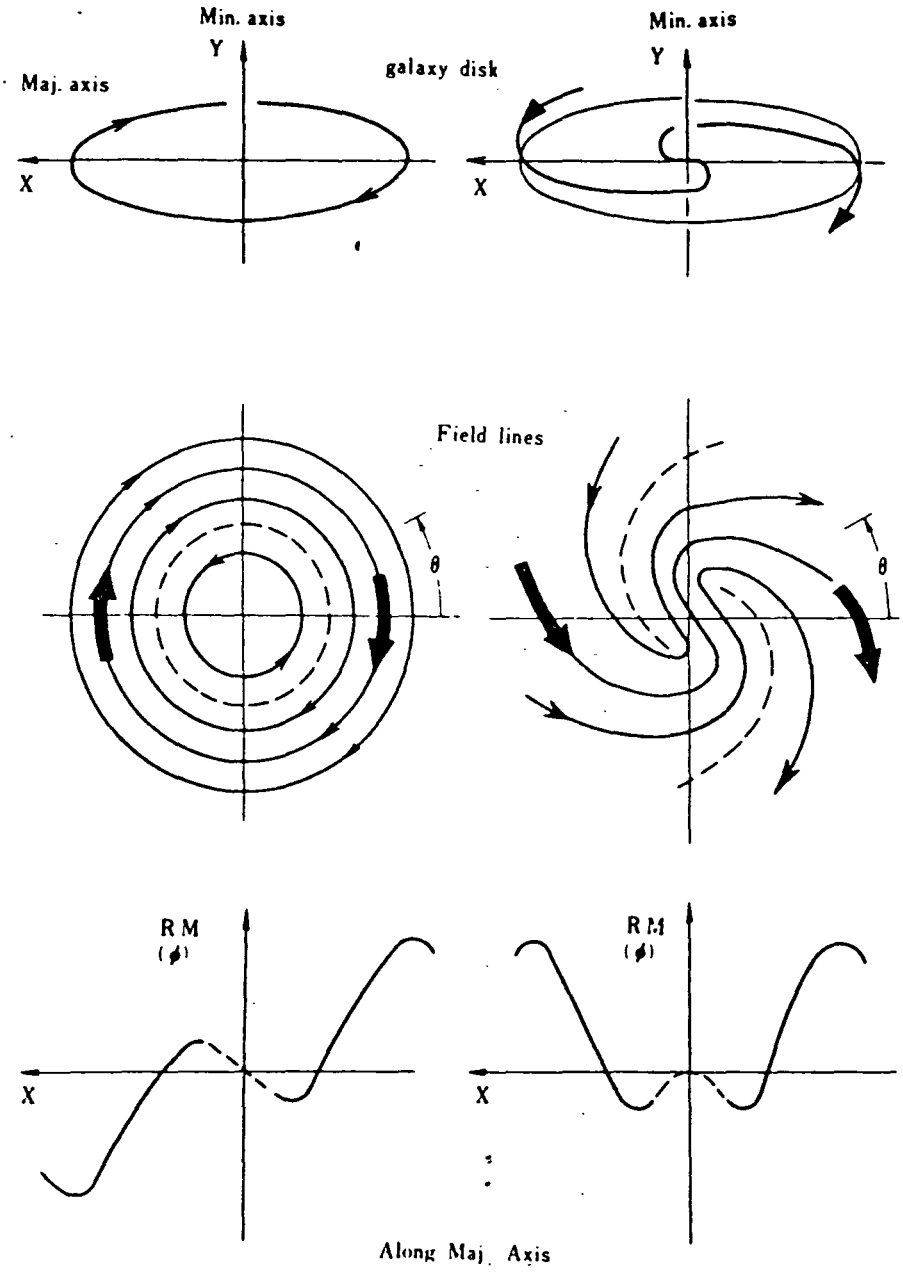

Figure 2.1: Rotation measures for a circular field and a BSS field configuration (Sofue et al. 1986)

figuration of our Galaxy. They performed a series of rotation measurements on a large number of extra-galactic objects. In a way this was the opposite method to that just outlined. It has been mentioned that the RM depends not only on the field in the distant galaxy but also on the field in our own Galaxy. If each measurement is made to cover the whole of an external galaxy then each galaxy will give a single value of RM.

Then if sufficient numbers of RM determinations are made across the whole of the sky, a picture will be built up of the variation of RM with galactic latitude and longitude. This picture will contain a random element (the individual RM of each galaxy) superposed upon that caused by the Faraday effect in the Galaxy. These authors managed to separate the two by smoothing their data, and discovered that the field configuration in the Galaxy is a bisymmetric spiral. Thus the field reverses its direction from one spiral arm to the next.

However Vallee (1984) cast serious doubts on the findings of Sofue and Fujimoto. He claimed that the region of our Galaxy which contains the solar system also contains four interstellar magnetic bubbles (IMBs) which these authors did not take into account. An IMB can be created by a young stellar association, where each star has a very large stellar wind. The combined effects of these stellar winds is to create a cavity in the interstellar medium and in the magnetic field - this is called an IMB. Alternatively a supernova by exploding can also create a cavity in the interstellar medium and the magnetic field.

Vallee claimed that Sofue and Fujimoto ignored these four IMBs and the effects they have on RM observations. Instead they ascribed the effects of the local IMBs to distant galaxies, and thus smoothed them out. If they had taken them into

consideration they would have found the magnetic field of our Galaxy to be circular and not spiral, according to Vallee.

Krause et al. (1987a) studied the radio linear polarisation of M81 and deduced a BSS field configuration following the spiral arms. This was further confirmed by their RM observations. Buczilowski (1987) did the same for M33 and concluded that it too has a BSS field. He tried the same for NGC 6946 but was unable to arrive at a firm conclusion due to its proximity on the sky to the Galactic Plane, and hence contamination by foreground Faraday rotation. Previous to this Klein et al. (1982) measured the polarisation of NGC 6946 at 2.8cm and found traces of a BSS pattern at typical levels of around 10%. From the fact that this pattern was not so pronounced as that found by Segalowitz et al. (1976) in M51, and from the fact that there was an absence of compression regions in the non-thermal emission from NGC 6946, they deduced that density waves are less important in the latter than in M51.

Ondrechen (1985) performed a series of radio polarisation measurements on M83, a barred spiral galaxy. He found linear polarisation in the spiral arms, which runs perpendicular to the arms. This can be explained by synchrotron emission in a magnetic field which runs parallel to the arms. He went on to postulate that spiral shocks cause the observed spiral dust lanes in M83, and that the spiral shocks also enhance the magnetic field along the arms. This is discussed in the next section.

One exception to this trend of BSS fields in spiral galaxies appears to be M31, which according to Beck (1982) has a circular magnetic field. He stated that this field reaches a maximum of about $5 microgauss$ in a ring of radius $10 kpc$ from the

galactic nucleus. He interpreted his results in terms of a primordial field which has been wound up by differential rotation to create a circular field.

However Sofue (1987) found that if an exactly circular component of the field is subtracted, then a BSS field remains. Hence he suggested that M31 has a BSS field superposed on a circular field. Also Loiseau et al. (1987) and Berkhuijsen et al. (1987), using radio polarisation measurements, found a combination of BSS and circular fields in M31. Such a field is known as an axisymmetric spiral (ASS) field. A similar configuration has been observed in IC 342 (Krause et al. 1987b, Grave and Beck 1987).

Vallee (1984) reviewed the evidence of spiral and circular fields in spiral galaxies, and arrived at the conclusion that all could be explained by the tidal effects of massive companion galaxies (cf: Toomre 1981). That is to say that spiral galaxies which have a massive neighbour have spiral magnetic fields, whilst galaxies with no near neighbour, or only a relatively small neighbour, have circular fields. For example our Galaxy has a circular field (according to Vallee) because its neighbour (Large Magellanic Cloud) is only 1/15 the mass of the Galaxy. Whereas M51 has a spiral field because its neighbour (NGC 5195) is 1/3 of the mass of M51 itself.

This theory also predicts a tidal radius for each galaxy. That is to say a radius within which the spiral tidal effects should not penetrate. In the case of M51 this radius is $10kpc$. Hence in this theory the spiral field of M51 should not extend far inside a $10kpc$ radius of the galactic centre. This point is taken up in Chapter 3.

Magnetic fields outside of galactic planes have also been

studied. Allen et al. (1978) used arguments of equipartition of cosmic ray and magnetic field energy densities in a study of NGC 891 to deduce a magnetic field of a few microgauss extending about $5kpc$ from the galactic plane. Sofue (1987) used earlier measurements of RMs in pulsars (Sofue et al. 1979) to deduce a halo field in our Galaxy of a few microgauss. This is similar to the magnitude of the disk field.

Seiradakis et al. (1985) discovered strong radio polarisation in the general direction of the Galactic Centre, but at high Galactic latitude. They deduced that this was a tracer of the field outside the Galactic Plane, running perpendicular to the Plane. Uchida et al. (1985) interpreted this as a poloidal magnetic field component of the Galaxy. The significance of these discoveries is discussed in Section 2.3.1.

2.3 Theories of the origin of magnetic fields

Despite the fact that Welter et al. (1984) described attempts at modelling galactic magnetic fields as heroic, various theories have arisen to account for magnetic fields in galaxies. Basically they split into two kinds: Theories invoking a primordial field (field which existed before the galaxies were formed), and dynamo theories (field which was created at the same time as, or later than, the galaxies). Each of these theories will be outlined and their predictions listed.

2.3.1 Primordial magnetic field

Very little is known about the epoch when magnetic fields originated. There are various options which have been suggested.

The first possibility is a truly primordial origin—a magnetic field was created in the Big Bang, along with the matter. Such a field, if it existed, would have had to have been very small for it not to have affected the very early universe to an extent which would be noticeable today. For instance a field of greater than $10^{-9} gauss$ would alter nucleo-synthesis arguments, but even a field strength of $10^{-20} gauss$ might suffice to provide a seed for the fields observed today (Rees 1986).

The next possibility to be considered is the creation of a magnetic field via symmetry breaking associated with phase transitions in the very early universe. Contemporary Grand Unifying Theories suggest the formation of magnetic monopoles when symmetry breaking occurs. Parker (1979) puts a limit on the number of monopoles formed, because too high a density would destroy existing fields. Inflationary models of the Big Bang require only a low density of monopoles, but more work is required on this theory to ascertain its viability.

Another way in which a field could be set up in the very early universe would be by means of rotational perturbations in the universal medium before recombination (Harrison 1970). In the radiation dominated era of the Universe, small turbulent rotations were set up in localised regions—with the net angular momentum of the Universe remaining unchanged. Ions and electrons in a rotating region thereby set up a magnetic field.

One problem remaining with these theories is that such a field should decay in timescales short compared to the age of the universe. Furthermore, even a field which survived until the formation of the galaxies would decay in only about 2% of a galaxy's life-time: Parker (1975) illustrated that a field permeating a galaxy would undergo turbulent dissipation, and

hence would escape from the surface of a galaxy in less than 10^9 years.

So there must be some regenerating mechanism to continue the survival of the magnetic field for us to observe such a field today. This will be discussed in the next subsection, but first the consequences of a primordial field are outlined, and a summary of how such a field might affect galaxy formation is presented.

Nucleo-synthesis calculations of what matter is formed in a Hot Big Bang show that the only elements present in any quantity are ionised Hydrogen and Helium. Elementary particles are also created, some of which carry charge.

The charges and the magnetic field are effectively locked together, and it is most convenient to think of the whole as a magnetic fluid. The matter moves most freely along the lines of the magnetic field, in other directions it experiences a magnetic resistance and tries to drag the field lines along with it. However it has already been seen that matter collapses along the axis of rotation of a protogalaxy. So if a protogalaxy has a significant angular momentum ω and also a significant initial magnetic field $\mathbf{B}$ then clearly the important consideration is the angle between the initial field and the axis of rotation. The following scenario was first outlined by Piddington (1964).

Consider first the case of a protogalaxy whose initial magnetic field $\mathbf{B}$ is parallel to its initial axis of rotation ω: The collapse occurs most strenuously along this axis, where there is least resistance from magnetic braking and least resistance from rotation. Collapse continues until the disk galaxy situation is reached. Then the rotation of the matter around the major axis drags the field around into a helical shape. Such a

field, seen face-on, would appear to have a spiral configuration.

The next case for consideration is that where the magnetic field is perpendicular to the axis of rotation. Here the two effects of rotation and magnetic resistance are most in competition. The matter collapses in some complex fashion, twisting the field lines of the magnetic fluid. Rotational potential energy is converted to magnetic potential energy as the lines of magnetic flux feel a mutual repulsion as they are twisted together. It is possible that this energy could be released in the form of a directed outflow of matter in the two opposite directions of the rotation axis.

Such outflows have been observed in the radio region: A central source galaxy is seen between two lobes of high energy radio emission, one of which may be blue-shifted while the other is red-shifted. These lobes are believed to be regions of high energy plasma, of order $100kpc$ in diameter, which have been ejected from the central galaxy, and are known as plasmons.

The emission per unit volume of a radio galaxy is about 10^4 times the emission of a normal galaxy. Likewise, the magnetic field strength in a radio galaxy is about 20 times that in a normal galaxy, giving a magnetic flux of 2×10^{42} gauss * square centimetre in a radio galaxy. It can be shown (Piddington 1964) that this value of flux can be obtained in about 8 revolutions of the protogalaxy in the case where the original **B** and ω are perpendicular, and the value of the original **B**-field is of the order of a few microgauss. The helical field formed constrains the outflow to the axis of rotation, and creates the observed phenomena.

Recently Turner (1986) cast doubt on the likelihood of this

scenario in cases where galactic jets are observed. He took NGC 6251 as an example and noted that the jets emit synchrotron radiation. According to Turner's calculations, once the magnetic energy has been converted to gravitational and kinetic energy in the outflows, there is insufficient magnetic potential energy left to fuel the jet synchrotron radiation. However this is merely one case, and he does admit that the calculations may be model dependent.

The intermediate case of a protogalaxy where the rotation axis and the field are at some angle between 0 and 90 degrees is still more complex, and the field may end up in some spiral configuration. Furthermore, some slightly less energetic outflows could occur. Other effects which could arise in this case include galaxies with warped disks, and other asymmetries.

Comparing the expectations of a primordial field theory with the observations listed in the previous section, a high degree of agreement is apparent. The majority of galactic fields mapped by radio astronomers exhibit BSS structure, and this is exactly what is set up by a primordial field. However, one remaining problem associated with this theory is to maintain the spiral configuration of the field over a galactic life span and avoid it from becoming so tightly wrapped that it becomes a circular field.

It could be that the field decouples from the matter and becomes locked to the galactic spiral density waves or spiral shock waves. Exactly how this mechanism might work in practice is difficult to see. One suggestion (Fujimoto 1987) is that turbulent diffusion of the magnetic field serves to decouple the field from the matter. Alternatively Sofue (1987) claims that the halo field of a galaxy (see Section 2.2.2) can act as a reservoir

for the disk field, thus perpetuating the latter.

Sofue (1987) pointed out that one prediction of a primordial field which can be tested is the setting up of a poloidal component of a galactic magnetic field: If a galactic field is observed which has a component perpendicular to the plane of the galaxy, and which is open to intergalactic space, that would be strong evidence in favour of a primordial magnetic field. He claimed that a field of this nature of around $10 nanogauss$ would be created and maintained in the central few hundred parsecs of a galaxy if the strength of the primordial field was of the order of one or two nanogauss. This was exactly what was reported by Seiradakis et al. (1985). Sofue (1987) also claimed that a primordial magnetic field origin can explain all of the available observational evidence.

2.3.2 Dynamo theories

The other side of the argument to the theories just presented is to explain galactic magnetic fields in terms of the dynamo action of the ISM. Several authors have propounded versions of this theory (eg: Parker 1979, Ruzmaikin 1987). The basic theory starts with the assumption of a very weak seed field set up either by the first stars to form, or by circling motions of charges in a collapsing protogalaxy. Another site for the possible creation of a seed field is in active galactic nuclei. Ruzmaikin (1987) claimed that the size of such a seed field need only be of the order of $1 nanogauss$. Note that such a field could equally be primordial in origin, and any problems mentioned earlier of maintaining a field to the present day can be solved by the following arguments.

This weak seed field is amplified by the hydro-dynamical motions of ionised gas in the ISM. The emf required to set up the field is $10^{10}V$, and can be generated by the random motions in only 5×10^8 years provided the process is at least 10% efficient (Ruzmaikin 1987). Thereafter the back reaction of the motions caused by the field stabilises the field.

Parker (1979) derived the equations of a galactic dynamo, the chief results of which are now discussed. Gas in the ISM is subject to the downward (towards the plane of the disk) force of gravity as well as the upward forces of gas pressure, magnetic field pressure and CR pressure. Gas clouds have typical velocities of around $10km/s$ and hence rise and fall distances of the order of $200pc$, the scale height of the disk. Differential rotation gives rise to shearing, which causes the clouds to rotate.

Consider a point in the plane of a galaxy and define it to be the origin of a coordinate system (x, y, z) such that x is in the radial direction, y is tangential and z is perpendicular to the galactic plane (see Fig 2.2). The azimuthal velocity of a gas cloud v_y decreases with increasing x, so (dv_y/dx) is negative, and this is known as the shear factor G. Thus a cloud rising above the plane $(+z)$ rotates anti-clockwise when viewed from large positive z. This sets up a loop in the magnetic field, and an equivalent cloud leaving the plane in the opposite direction $(-z)$ sets up a loop there (the closed lines in Fig 2.2).

The total of many such loops sets up a circulation of the magnetic field in the $x - z$ plane (dotted lines), which has the effect of directing the field towards the galactic centre in the galactic plane, hence B_x is negative. At $z = \pm h$ the field is lost to the intergalactic medium. Parker (1979) derived an equation

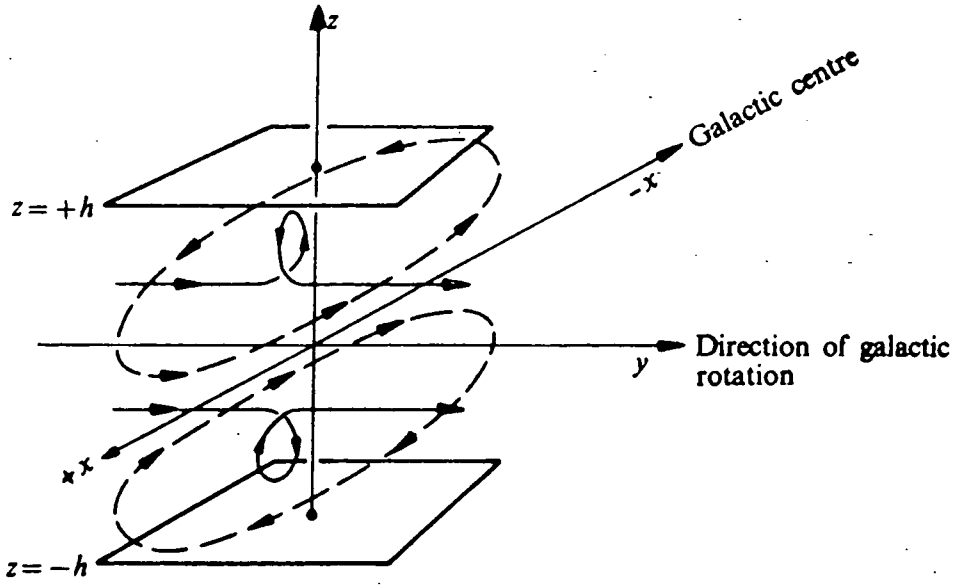

Figure 2.2: The galactic dynamo (Parker 1979)

governing these variables, ignoring resistive dissipation:

$$\frac{\partial B_y}{\partial t} = GB_x \tag{2.7}$$

It has just been shown that both G and B_x are negative, so $(\partial B_y/\partial t)$ is positive. Thus the azimuthal field increases with time, and this is how the galactic dynamo works. Including resistive dissipation reduces the dynamo efficiency to the point where an equilibrium state is reached between flux generation and flux leakage. Parker (1971) performed some rough calculations and concluded that the differential rotational energy of the Galaxy is sufficient to maintain the generation of the Galactic field for more than 10^{10} years.

The easiest field configuration to produce in this case is a circular field. This field is buoyed up by cosmic rays in the ISM. This gives a pressure scale height of around $200pc$ (half height half maximum density) for a typical galactic field. However about every $1kpc$ around a circular line of flux an instability occurs (Parker 1979). This Parker instability is a potential minimum in the magnetic field. The effect of this is that HII and other ionised gases flow along the magnetic field lines and are most dense in the potential minimum. Hence star formation occurs most vigorously there.

Another consequence of the cosmic ray (CR) pressure in a galactic magnetic field is that it enables an estimate to be made of the strength of the field. It is assumed that the sources of cosmic rays (eg: supernovae) produce CRs until an equilibrium situation is reached. The same number are being created as are escaping through the magnetic field. Hence the CR pressure P is equal to the magnetic field pressure $(B^2/8\pi)$. P is also equal to $(U/3)$, where U is the CR energy density. Hence direct

observations of the local CR energy density yield an estimate of the local Galactic field strength of $3-5 microgauss$ (Parker 1979). This is in good agreement with estimates from other methods mentioned earlier.

Other field configurations can also be produced in this model: Fujimoto (1987) started with the kinematic dynamo equations and found BSS solutions. He put typical values into these equations and showed that the field is in a steady or growing state for the region of the galaxy in the solar neighbourhood, forming a spiral pattern. Furthermore, a pattern angular velocity of $15-20 kms^{-1}kpc^{-1}$ can be maintained over a wide range of radius. Hence a BSS pattern of magnetic field can rotate rigidly in space. Further discussion of this matter is pursued in Chapter 6.

2.4 Summary

A review has been presented of current knowledge of galactic magnetic fields and the observational evidence available to date has been outlined. A variety of conflicting theories as to the origin and maintenance of fields have been discussed, but clearly further observations are necessary before significant theoretical progress can be made. In the next three chapters data are presented of an optical polarimetric study of four spiral galaxies, then in Chapter 6 the effects of the new observations on the theories are discussed.

Chapter 3

NGC5194 (M51) and NGC5195

3.1 Introduction

Results are presented in the next three chapters of an optical polarimetric survey of four spiral galaxies carried out by the Durham University Polarimetry Group between June 1984 and December 1986. The extent of this data is summarised in Table 3.1.

The first column of the table lists the NGC catalogue number of the galaxy, as well as its Messier number, where applicable. The second column gives the inclination to the line of sight. This is the angle between the line of sight and the perpendicular to the plane of a galaxy. Hence a face-on galaxy has an inclination of 0 degrees and an edge-on galaxy has an inclination of 90 degrees. The horizontal lines denote the chapter divisions.

Object	Incl (deg)	Type	Dates Observed	Tele-scope	Filt	Expo-sures	
NGC5194 (M51)	35	Sc	85-Feb:12-18	Wise	NF	64	80
NGC5195	-	Irr	85-Feb:12-18	"	NF	64	80
NGC1068	32	Sb	84-Aug:23rd	"	NF	20	76
(M77)	"	"	86-Aug:6th	"	NF	12	4
"	"	"	86-Aug:7th	"	V	8	13
"	"	"	86-Aug:11-12	"	R	12	6
"	"	"	86-Dec:31st	INT	R	12	4
NGC4594	84	Sab	84-Jun:1st	Wise	NF	16	24
(M104)	"	"	86-Mar:14th	"	NF	16	24
"	"	"	86-Jul:8th	"	V	8	40
"	"	"	86-Jul:6th	"	R	8	24
"	"	"	86-Jul:7th	"	I	8	32
NGC4565	86	Sb	84-Jun:3rd	"	NF	24	96
"	"	"	86-Mar:12th	"	NF	32	122

Table 3.1: The Data (see text)

The third column lists galaxy type, as taken from the Hubble Atlas (Sandage 1961), and the fourth column gives the date upon which each set of data was taken. The fifth column lists the telescope upon which the data were recorded: Wise stands for the $1-m$ telescope of the Wise Observatory of the University of Tel-Aviv, Israel, where the $f/13.5$ focus was used, and INT stands for the $2.4m$ Isaac Newton Telescope of the La Palma Observatory, where the $f/15$ focus was used.

Column six lists the colours available in the observations of

each galaxy, where V,R and I denote broad band optical filters covering the wavebands $480 - 660nm$, $560 - 890nm$ and $680 - 1000nm$ respectively, with peak response at $550nm$, $650nm$ and $745nm$ respectively, and NF means that the CCD was used without a filter (see below). The last columns give the number of exposures and the total exposure time (in min) respectively, in each data set.

3.2 Observation and reduction notes

All data were observed through the Durham Imaging Polarimeter, described by Scarrott et al. (1983). The detector used was a CCD system using a GEC P8600 chip, as outlined by Wright and MacKay (1981). The typical CCD readout noise is 8 electrons per pixel. The image scale of the Wise telescope is $1.2arcsec$ per pixel and of the INT is $0.43arcsec$ per pixel. The unfiltered band pass of the CCD is $450 - 1000nm$, with peak response at $750nm$. The operating system of the CCD was written by P.W.Draper—see Draper (1987). For a discussion of the polarisation of light and its measurement see Ward-Thompson (1984).

The reduction procedure is described by Warren-Smith (1979) and Scarrott et al. (1983) with modifications by Draper and Warren-Smith (see Draper 1987). The procedure runs on the Durham node of STARLINK. The errors inherent in the Durham Polarimetry System are discussed briefly by Scarrott et al. (1983), and in more detail by Warren-Smith (1979). All of the errors quoted for data in this thesis are given to one standard deviation.

3.3 NGC5194 (M51)

The data presented in this chapter have already been published by Scarrott et al. (1987a), and briefly summarised in Scarrott et al. (1987b). The data comprise a total of 16 overlapping fields in the region of NGC5194/5, with four exposures in each. Each exposure simultaneously recorded both object and surrounding sky in two orthogonal polarisation states. Common field stars were used to align the images. The resolution of the final data set was $3.5 arcsec$, being a combination of mean seeing throughout the period of the observations and the effects of aligning many images.

Fig 3.1 illustrates a grey-scale intensity image of NGC 5194 and NGC 5195. North is at the top, east is at the left. The east-west diameter of the visible part of the disk of M51 is $5 arcmin$. The spiral arms of M51 can be clearly seen, as can the dust lanes on the inner edges of the spiral arms.

Fig 3.2 displays the entire polarisation data set at a bin size of $18 arcsec$ square, with the bin spacing being $12 arcsec$ square, north is at the top, east at the left. The polarisation map is superposed on an isophotal contour map of the region. The contours are spaced logarithmically at intervals of $1.1 magnitudes$. The polarisation of the nucleus of M51 was not detected, thus it can be concluded that there is no foreground interstellar polarisation to M51. Hence all of the polarisation observed is associated with the object itself.

A description of the polarisation map follows: The central region of the galaxy displays a spiral pattern of vectors, which lie parallel to the spiral arms. This can be seen in this map to extend to a radius of about $1 arcmin$. Typical levels of

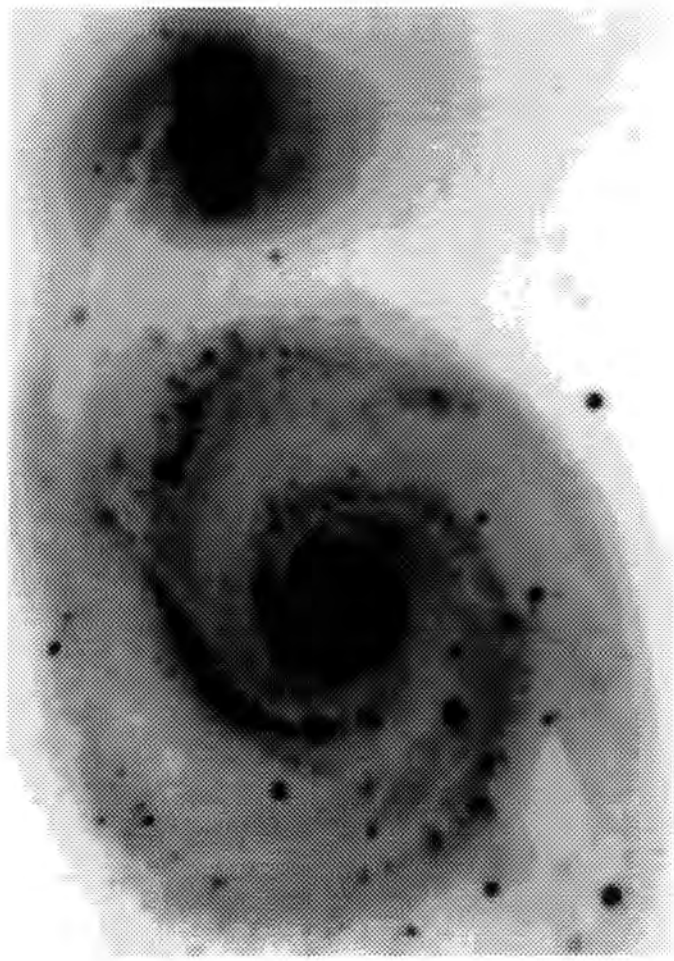

Figure 3.1: Intensity image of NGC 5194/5 (see text)

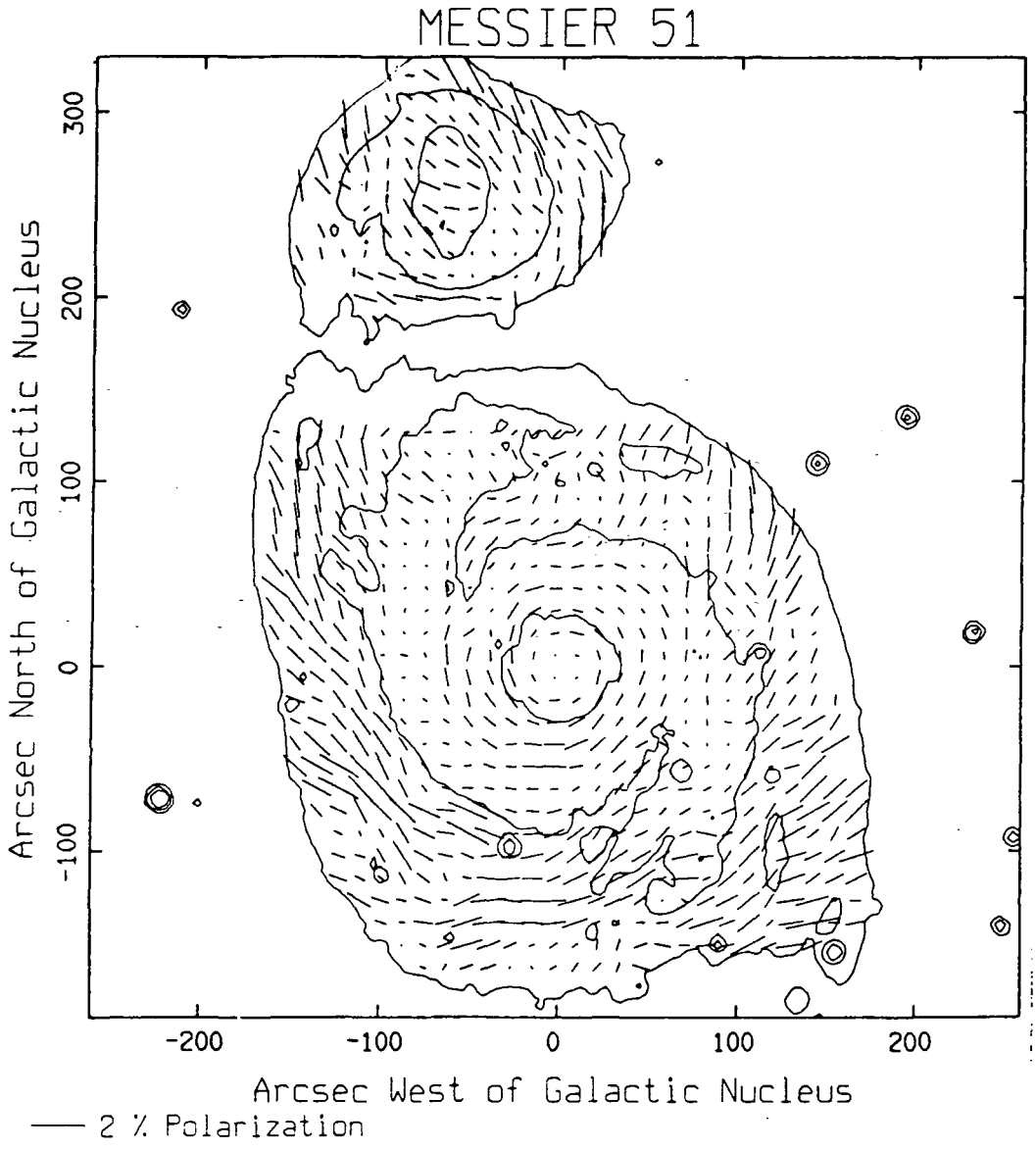

Figure 3.2: Polarisation map of NGC5194/5 (see text)

polarisation in this region are $1 \pm 0.5\%$. The angle error on a measurement here is typically $\pm 15 degrees$. Beyond this radius due east and due west of the nucleus the two spiral arms of M51 extend to the north and south respectively. The polarisation in these areas is so small as to be unmeasurable.

In the areas centred on $100 arcsec$ due northeast and southwest of the nucleus it can be seen that the polarisation lies perpendicular to the spiral arm at a level of $0.7 \pm 0.3\%$, with angle error $\pm 12 degrees$. Both of these areas lie within a spiral arm. The polarisation of the two interarm regions centred on $120 arcsec$ due east and due southwest of the nucleus is around 1.5% and lies parallel to the spiral arms. Note also that the polarisation of the two interarm regions at galactic radius $1 arcmin$ due northeast and southwest is also parallel to the spiral arms.

This pattern of polarisations—parallel to the spiral arms in the interarm regions, and perpendicular to the spiral arms within the arms themselves— was observed by Kunkel (1977), who performed a limited polarisation study of M51, and merely measured the polarisation in apertures centred on first the spiral arms, then the dark interarm lanes. He saw the pattern just described. He accounted for the observed polarisation in terms of simple scattering considerations:

He hypothesised that all of the polarisation which he saw was due to single scattering of nearly unpolarised starlight by interstellar dust grains. As was stated in the previous chapter, the direction of polarisation created in this way is perpendicular to the plane of incidence of the scattered photon. Thus any anisotropy in the illumination of a region of dust can be seen in the polarisation.

A region of dust within a spiral arm is chiefly illuminated from ahead and behind on the arm itself. This produces a polarisation which is perpendicular to the spiral arms. A region between two spiral arms is illuminated by the arms to either side, and hence has a polarisation parallel to the spiral arms.

However Kunkel's hypothesis breaks down in the central region of M51. Fig 3.3 shows a polarisation map of this region, with integration bins $8.4 arcsec$ square, spaced at $6 arcsec$ intervals. The polarisation map is superposed on an isophotal contour map of the region, again with logarithmically spaced contours, this time at intervals of $0.75 magnitudes$. Here it can be seen that in the central region, from a radius of less than $10 arcsec$ to $70 arcsec$, there is a spiral polarisation pattern at $0.7 \pm 0.4\%$ with angle error $\pm 15 degrees$, but it was not possible to measure the polarisation of the nucleus.

It was mentioned in the previous chapter that Segalowitz et al. (1976) published a $6cm$ radio polarisation map of M51—this was also published in Segalowitz (1976). In an endeavour to understand the results of the current survey the data were binned to circular integration bins of roughly $50 arcsec$ diameter, coincident with the $6cm$ measurements of Segalowitz et al.

This is illustrated in Fig 3.4, which is superposed on the same contour map as Fig 3.2. The light lines are the optical polarisation vectors, and the dark lines are the radio measurements. The scale in the diagram is for the optical vectors. The same length of vector corresponds to 20% radio polarisation. This indicates that the optical polarisation levels are around $0.6 \pm 0.3\%$ with angle error $\pm 15 degrees$, while the radio polarisation levels are between 15 and 20%. Furthermore in 29 of the 38 apertures the two sets of vectors are perpendicular to

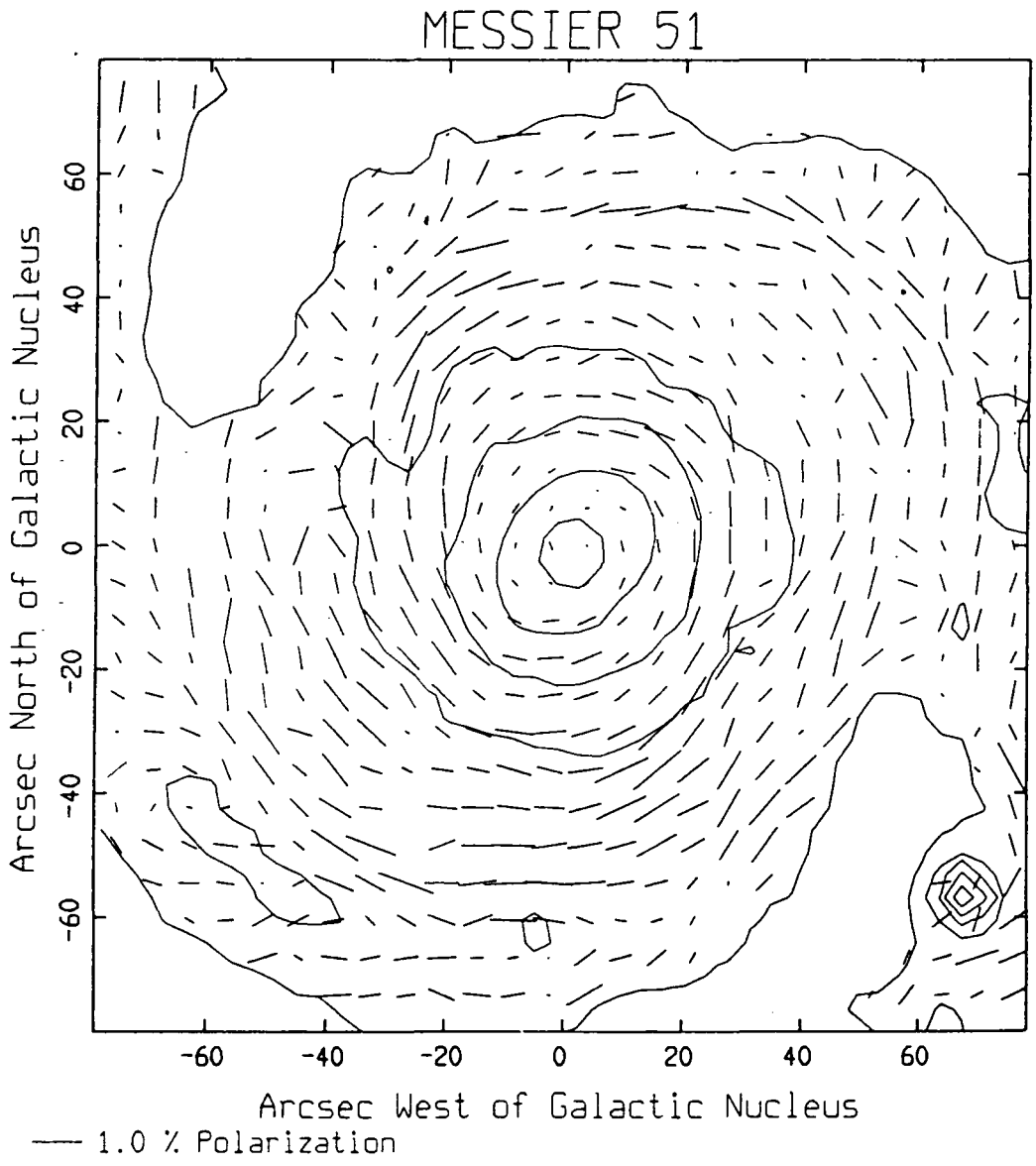

Figure 3.3: Polarisation map of the central region of M51 (see text)

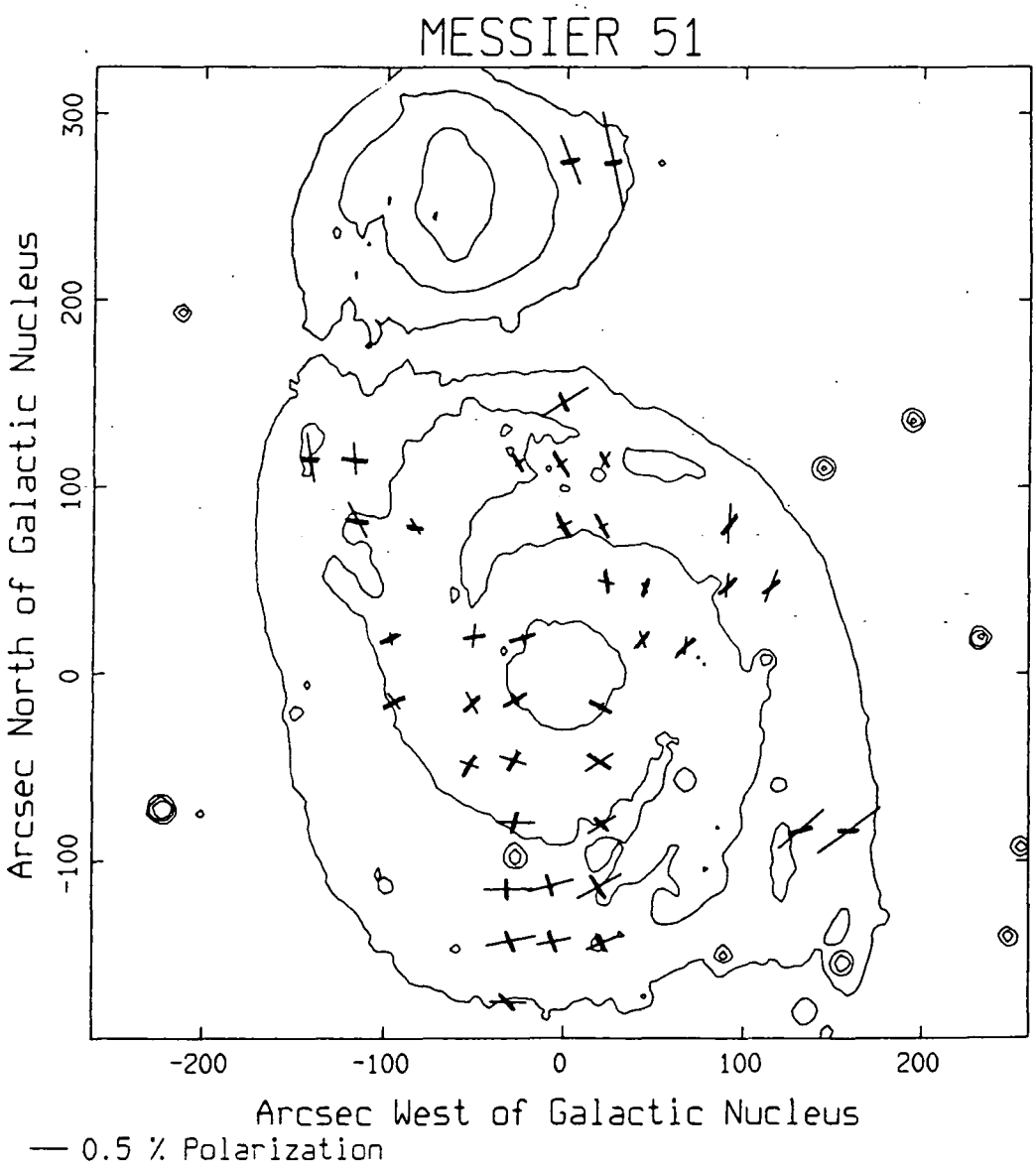

Figure 3.4: Comparison of the optical polarisation (light vectors) with the 6cm radio polarisation measurements (dark vectors) of Segalowitz et al. (see text)

within 30*degrees*. The exceptions all lying in a region centred around 100arcsec west of the nucleus.

The polarisations in Fig 3.4 can-not be explained in terms of simple scattering considerations, so a different mechanism must be invoked to explain the results. As described in the previous chapter, perpendicularity is expected between radio and optical polarisation measurements when both are caused by the same magnetic field. Synchrotron radiation gives a polarisation perpendicular to the magnetic field, while preferential absorption by magnetically aligned grains produces a polarisation parallel to the field. Also note that the levels of polarisation observed in both radio and optical polarisations are consistent with this model.

Thus there is a spiral magnetic field in M51, as was deduced by Segalowitz et al. (1976), and the optical polarisation observed is due to preferential absorption by dust grains aligned in this magnetic field. Returning to Fig 3.3 it can be seen, furthermore, that the spiral field extends to within 10arcsec of the galactic nucleus.

Recently Beck et al. (1987) produced radio polarisation maps of M51 at 6*cm* and 21*cm*. They corrected for Faraday rotation and then plotted the orientation of the **B**-field as a series of vectors at each position where they had made a measurement. Of all their measurements it was only possible to make an optical polarisation measurement in the same place for 28 positions. The resulting map is shown in Fig 3.5, superposed on the same intensity map as Fig 3.2. The dark vectors are the radio polarisations rotated through 90*degrees* to give the orientation of the field, the light vectors are the optical polarisations. The scale in the diagram is for the optical polarisation

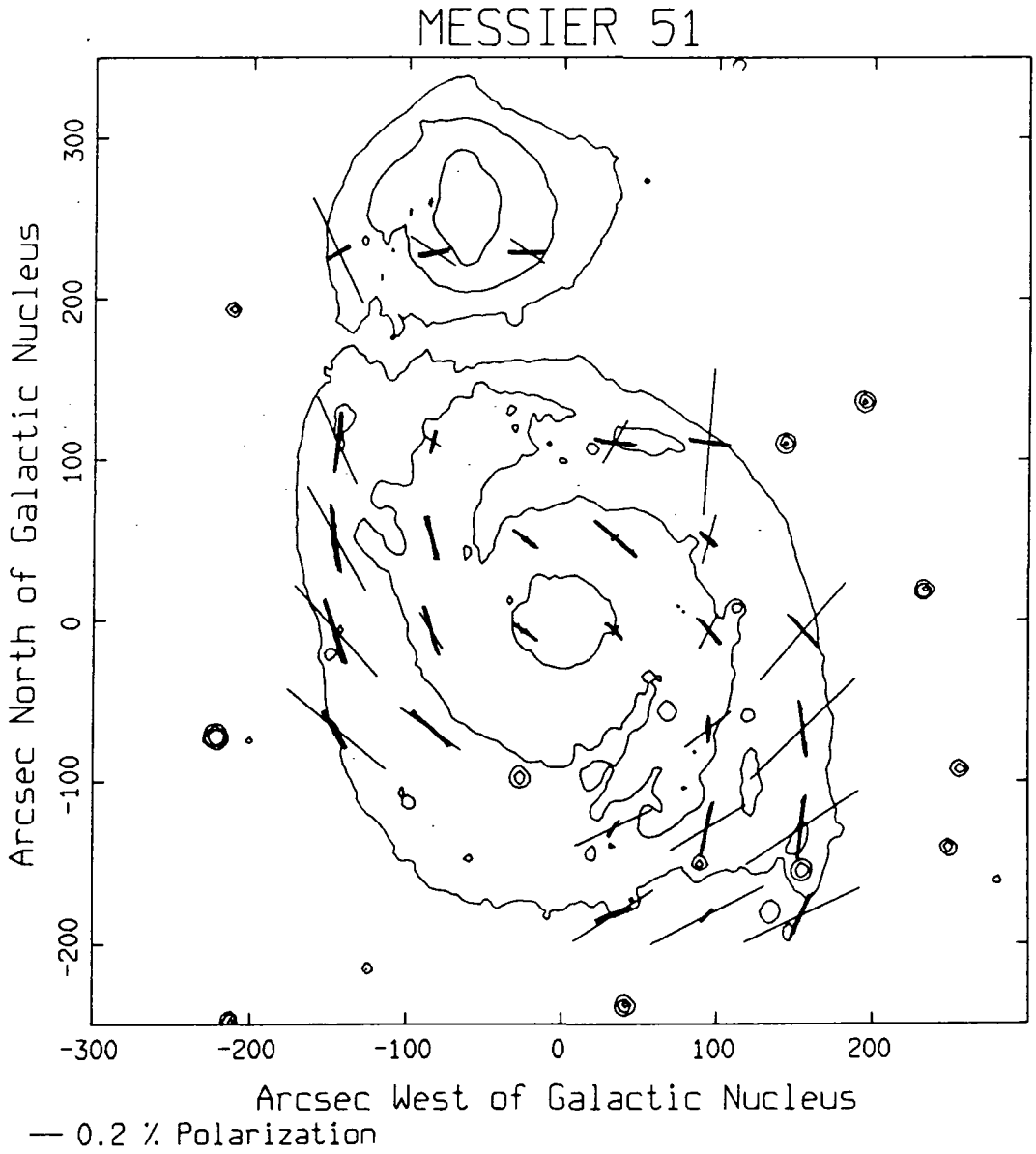

Figure 3.5: Comparison of the optical polarisation (light vectors) with the B-field orientation (dark vectors) measured by Beck et al. (see text)

vectors. The same length of vector corresponds to 20% radio polarisation.

Of the 28 coincident measurements, 4 optical measurements did not record any polarisation, 12 measurements agreed to within 30 degrees and 12 did not. The 4 null results occurred because of their proximity to the galactic nucleus, and of the large diameter of the measurement aperture (over $2arcmin$). That is to say that the optical polarisations cancelled out over such a large area. The majority of the disagreement occurred once more to the west of the nucleus of M51. It is possible that some systematic error may have occurred in the optical data in this region.

There is some disagreement over the distance to M51. Burb idge and Burb idge (1964) quote a distance of $4 \pm 0.5 Mpc$, and various authors since then have quoted approximately the same distance. Sandage and Tammann (1974) used a method of measuring the magnitude and apparent size of HII regions in M51 and arrived at a figure for the distance of $9.7 \pm 0.1 Mpc$. All authors since these have merely quoted one or another.

For the purposes of this thesis a value of $9.7 Mpc$ will be adopted, as being the more recent, and possibly more reliable, estimate. This makes the radius of the visible disk of M51 to be some $12 kpc$. This would then make it roughly the same size as our own Galaxy, and other galaxies. (Note that this does not change qualitatively any of the arguments in this chapter).

Hence $1 arcsec$ on the sky corresponds to $47 pc$. Thus the spiral magnetic field can be seen in Fig 3.3 to extend to within $470 pc$ of the nucleus. To illustrate this more clearly the data were binned once more and the resultant polarisation map is

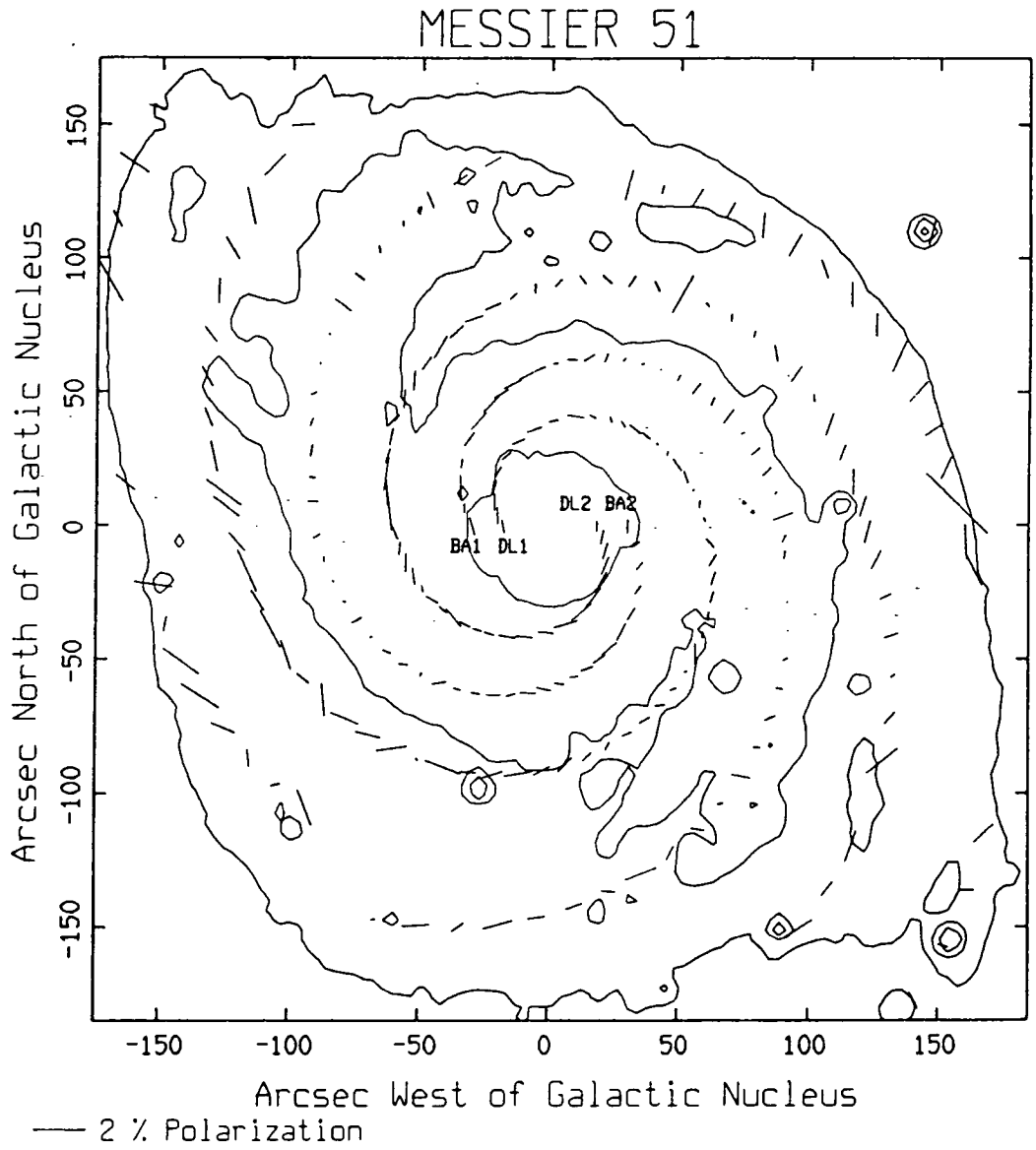

Figure 3.6: A series of aperture polarisation measurements tracing the spiral arms and dark lanes of M51 (see text)

illustrated in Fig 3.6. This time circular apertures were used, of diameter 6*arcsec*, which were placed so as to coincide with the two bright spiral arms (BA1 and BA2) and with the dark interarm lanes (DL1 and DL2). This was superposed on an isophotal contour map with logarithmic contour spacing at intervals of 1.1*magnitudes*.

It can be seen clearly from this that a spiral pattern exists in both bright arms and dark lanes out to a radius of 70*arcsec*. Beyond this radius the dark lane polarisation remains spiral, while the bright arm polarisation turns through 90^o to run perpendicular to the spiral pattern. At large radii both appear random.

This reinforces what was mentioned earlier: The polarisation in the inner 70*arcsec* is spiral regardless of whether it is a bright arm or a dark lane which is under consideration. Here preferential absorption by magnetically aligned grains is the dominant polarising mechanism. Beyond this radius Kunkel's scattering regime dominates—alternately parallel and perpendicular to the spiral arms. In the outer regions the individual scattering geometries contain a random element, and hence the polarisation pattern becomes random. Furthermore the signal to noise ratio decreases in the outer galaxy, and the error on each measurement consequently increases.

To test exactly how close to the nucleus the field remains spiral, a polarisation map was made of just the nuclear region of M51. This is shown in Fig 3.7. Here the data are binned in 6*arcsec* square integration bins, spaced at 3.6*arcsec* intervals. The contour map has logarithmically spaced contours at intervals of 0.75*magnitudes*. Note the very small vector scale of this map. Within a radius of 5*arcsec* of the nucleus itself (ie:

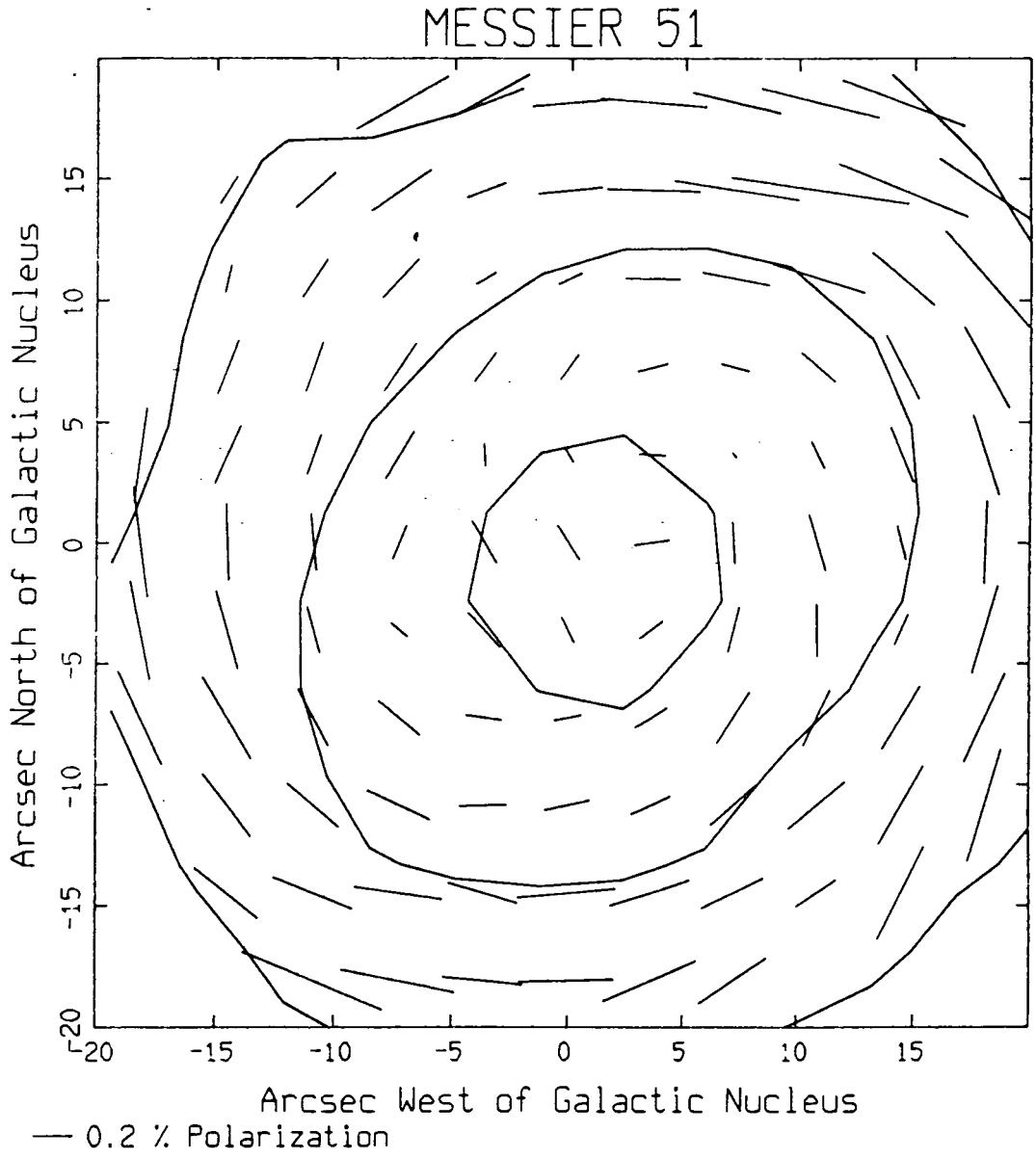

Figure 3.7: Polarisation map of nuclear region of M51 (see text)

within the innermost contour) the errors on the measurements are so large that no measurement has been made. However, outside of this radius a spiral pattern is seen.

Thus from these observations it can be seen that the magnetic field of M51 continues to be spiral right into the centre of the galaxy. The limiting factor is the resolution of the observations. The minimum radius at which the observations can prove that the field is spiral is $5arcsec$, or $235pc$, but the spiral field configuration may in reality continue even closer to the nucleus.

The results seen in all five polarisation diagrams can be explained as follows: There are two independent polarising mechanisms at work in the light from M51. These are preferential absorption by magnetically aligned dust grains, and scattering from dust grains. Polarisation by scattering is heavily dependent upon the scattering geometry. In an aperture which lies solely in a bright arm, or entirely in a dark lane, the scattering polarisation mechanism is dominant. This occurs at radii greater than $1.5kpc$, and can be seen in Fig 3.2 and Fig 3.6. In an aperture which crosses bright arm and dark lane magnetic alignment dominates, as seen in parts of all five polarisation maps.

In the inner $1.5kpc$ preferential absorption is the dominant polarising mechanism—see Fig 3.3, Fig 3.6 and Fig 3.7. Furthermore it has already been shown that the magnetic field of M51 extends over the larger part of the visible disk (Segalowitz et al. 1976). Fig 3.4 confirms this.

So it has been shown that there is a well ordered, large scale magnetic field throughout the major part of M51. This field is spiral in nature, as has been suggested by previous authors.

However what has been shown in this chapter, which was not known previously, is that the field extends to within $235pc$ of the galactic centre.

3.4 NGC 5195

Turning now to the companion galaxy of M51—NGC 5195: Examination of Fig 3.2 shows some interesting features. The galaxy is irregular, and has a nucleus which is elongated in the north-south direction. The polarisation of the nucleus is around $0.6 \pm 0.3\%$, with position angle $70 \pm 15 degrees$.

Comparison of Fig 3.2 with the results of Elvius and Hall (1964) shows agreement on the nuclear polarisation. The results also agree for the areas to the east and south of the nucleus. However disagreement between the two sets of results is observed to the west of the nucleus. Fig 3.2 also shows that there is a region some $30 arcsec$ southwest of the nucleus where no polarisation has been measured.

If the polarisation of NGC 5195 was due only to scattering of starlight, emanating from the nucleus, by interstellar dust grains, then the expected pattern would be the following: The major illuminating source is extended in a north-south direction, thus creating an elliptical polarisation pattern, also extended in the north-south direction. The polarisation would also be expected to be near zero on the brightest part of the nucleus.

As this is not observed, it is suggested that what in fact is happening is that there are two competing polarisation mechanisms at work. One is scattering, as just outlined, and the other is preferential absorption by magnetically aligned dust

grains between NGC 5195 and the observer.

Elvius and Hall (1964) stated that the nuclear polarisation may be due to absorption in a dark band crossing over the nucleus in an east-west direction. Examination of the image in the Hubble Atlas (Sandage 1961), shows that one of the spiral arms of M51 appears to extend as far as NGC 5195. Furthermore, Toomre and Toomre (1972) and Tully (1974) state that this arm continues across the face of NGC 5195 and lies well in front of it.

It is here suggested that this spiral arm of M51 does in fact cross in front of NGC 5195, and further, that there is a magnetic field lying parallel to this arm. Then the polarisation of NGC 5195 can be explained in terms of two competing polarising mechanisms: scattering of light from the nucleus by dust throughout the galaxy, and preferential absorption by foreground magnetically aligned grains within a spiral arm of M51. It is the vector addition of an elliptical pattern and a linear pattern which creates the complex pattern observed.

One result of this argument is that it is then seen that the spiral magnetic field of M51 extends from within $235pc$ of the nucleus, right out to the aparent position of NGC 5195, at a radius of some $14kpc$, and possibly beyond. It is not possible to tell if the field is open to intergalactic space.

3.5 Discussion

A pattern of polarisation has been seen across the visible disk of M51. Kunkel (1977) explained the optical polarisation of M51 in terms of scattering. It has been shown in this chapter that, although scattering can account for some of the results,

where the combination of illuminator, scatterer and observer's aperture size is favourable, Kunkel's model does not explain all of the data, and there is also another polarisation mechanism responsible for the observations.

A spiral magnetic field has been shown to exist throughout the spiral galaxy M51. This field is strong enough to align interstellar dust grains, thus showing it to be comparable in strength to that of our own Galaxy. (Note that this is merely the large scale field, small scale structure being beyond the resolution of these observations).

The field is most clearly seen in the central regions of M51, and in the dark lanes on the inside edges of the spiral arms. It was outlined in Chapter 1 that these dark lanes correspond in some theories to the compression regions of a spiral density wave pattern. Furthermore, Segalowitz (1976) showed that there was a concentration of nonthermal radio emission coincident with the dark lanes, which suggests an increase in magnetic field strength in these compression regions.

The magnetic field of M51 has been shown to be spiral to less than $300pc$ from the galactic nucleus. The radius of the inner Lindblad resonance of M51 is not known. However a typical value for this for a spiral galaxy is $1.5kpc$ (Teuben et al. 1986). If the field continues to be spiral within the inner Lindblad resonance of M51, then this goes beyond what is predicted by spiral density wave theories. Furthermore, theories which only create spirality in the outer regions, such as tidal influence by a neighbouring galaxy (Vallee 1984), clearly need to be modified, or discarded altogether.

Just what is happening to the kinematics of the matter in the central region of M51 is quite difficult to tell. For instance

CO emission as mapped by Lo et al. (1985) shows no measurements in the innermost $400pc$. However, many authors have written about an energetic outflow from the M51 nucleus—see, for example: Rose and Searle (1982), Rose and Cecil (1983), Cecil and Rose (1984), Goad and Gallagher (1985) and Ford et al. (1985). It is merely noted here that this outflow does not appear to disturb the polarisation pattern. This is discussed again in Chapter 6.

One facet of the field which is a possible alternative explanation to that already put forward, is that the observation of perpendicularity within a bright spiral arm could be due to the field direction there, and not as indicated previously to scattering. That is to say that the field could be compressed in the interarm lanes, and drawn out perpendicular to the spiral arms in the arms themselves. This is, however, purely speculative.

Note finally that, even if the distance estimate used were changed, the qualitative results are not affected. For instance, if the estimate of $4.6Mpc$ preferred by some authors is correct, then this means that the magnetic field of M51 is ordered in a spiral manner from within about $100pc$ of the nucleus, out to a radius of $7kpc$.

3.6 Conclusions

It has been seen that there is a large scale magnetic field throughout the spiral galaxy M51. This field is spiral in nature. It persists from within $235pc$ of the nucleus to the outer regions of the visible disk of the galaxy at a radius of $14kpc$, and possibly beyond. The repercussions of this discovery on theories of magnetic fields in galaxies are pursued in Chapter 6.

Chapter 4

NGC1068 (M77)

4.1 Introduction

In this chapter the results are presented of an optical polarimetric survey of the galaxy NGC 1068 carried out between August 1984 and December 1986 by the Durham University Polarimetry Group. These results are then compared with the polarisation measurements of previous researchers, and some conclusions are drawn. Note that some of the data presented in this chapter (specifically: Fig 4.3) have already been briefly summarised by Scarrott et al. (1987b).

NGC 1068 (M77) is a spiral galaxy of type Sb, seen at an angle of $32 degrees$ from directly face-on (de Vaucouleurs 1958). It exhibits a spiral structure in an optical image, although the spiral arms are less clearly defined than those seen in M51 in the previous chapter, and it lies at a distance of 18.1Mpc (Sandage and Tammann 1974). It was classified as a Seyfert galaxy of Type II, although this is debated later.

The first Seyfert galaxy was discovered by Carl Seyfert in 1943, and the distinguishing features of Seyfert galaxies are as

follows: They have very dense active nuclei which have substantial non-thermal emission. Their nuclei are highly luminous in the X-ray, ultraviolet, optical and infrared wave bands. Their nuclei are also variable on very short timescales, of order months, indicating a very compact region responsible for the emission, only a few light-months in diameter. Seyferts are believed to be less energetic examples of quasars.

Seyfert nuclei are surrounded by a region of hot gas, at a typical temperature of around $2 \times 10^5 K$, which is accelerated outwards by the central energy source. Seyferts are divided into Type I and Type II by the following means:

Type I Seyferts have spectra closely resembling those of quasars. The hydrogen lines are broader than the metal lines, indicating very high velocity outflows of gas, in excess of $10^4 km/s$.

Type II Seyferts have spectra in which the line widths are more nearly equal, indicating gas outflows of less than $10^3 km/s$. The further from the nucleus these outflows are seen, the less energetic they are observed to be. It is further believed that all spiral galaxies go through a transitory Seyfert period, lasting for around 10% of their lifespan.

4.2 Previous observations of NGC 1068

The nucleus of NGC 1068 has been studied by several authors. Condon et al. (1982) discovered an elongated region of radio emission extending from the nucleus in a direction roughly north-northeast. This was deduced to be a jet-like outflow from the galactic nucleus. The counter-jet in the opposite direction is also visible in their data, but at a lower intensity, as

if obscured. The significance of this is discussed in Section 4.5.

Wilson and Ulvestad (1982 and 1983) also observed the nucleus of NGC 1068. They used VLA observations at $4.9GHz$ and $15GHz$, with a resolution of just over $1arcsec$. Their maps are very similar to that of Condon et al. (1982), in that they show an apparently bipolar feature centred on the nucleus, whose northern half is of higher intensity than the southern half.

Van der Hulst et al. (1982) presented a $2cm$ map of the nucleus of NGC 1068. This was similar to those just discussed, except that the northern half of the outflow was seen to be misaligned with the southern half by about $20degrees$. They argued that this indicated that what was being observed was not a bipolar outflow at all. They claimed that this was merely a supermassive burst of stellar activity. However they require a very high supernova rate to explain the radio luminosity. So even they are forced to admit that a more exotic explanation may be necessary.

Pedlar et al. (1983) presented MERLIN observations of NGC 1068 at $18cm$ and $73cm$. This showed the same elongated feature, which in this case was not misaligned. Note that none of these authors mentioned here succeeded in resolving this linear feature in the direction perpendicular to its longer axis. However Pedlar et al. did resolve the jet into knots along its length.

Most recently, Tresch-Fienberg et al. (1987) mapped the nucleus of NGC 1068 at $10microns$. They discovered an elongated source, coincident with the north-eastern radio jet. Furthermore, one bright spot in their map was associated with a knot observed in the radio jet. They claimed that these results

considerably strengthen the case for jet-induced star formation in NGC 1068.

So it appears that the observational evidence is in favour of a bipolar outflow, emanating from the nucleus of NGC 1068. A similar feature is seen in another Seyfert galaxy: NGC4151—see Harrison et al. (1986) and references therein.

In the near infrared Telesco et al. (1984) observed a disk-like structure of about $3kpc$ in diameter. They claimed that this represents a disk of young stars, such as has been seen in galaxies which show no Seyfert activity. However this disk must be very heavily obscured by interstellar dust in order to account for its relative luminosity in the infrared compared to the optical waveband.

Wynn-Williams et al. (1985) also detected this disk in the radio. They found a very strong radio emission region of radius about $2kpc$, which they accounted for in terms of a burst of recent star formation which occurred around 10^7 years ago. Schild et al. (1985) detected a young star-forming region within a radius of $900pc$ of the nucleus, using CCD photometry. However, note that this star-forming region is not necessarily linked with the Seyfert activity of the galaxy.

Work of other authors on polarisation measurements of NGC 1068 is discussed in Section 4.4, but first the results of the current survey are presented.

4.3 Polarimetry of NGC 1068

The data available for this galaxy are summarised in Table 3.1. The observation and reduction notes are as for M51, and are outlined in Section 3.2, with the following exception: The reso-

lution of the results derived from observations on the $1-metre$ telescope of the Wise Observatory is $3.1arcsec$ for the unfiltered data, $2.6arcsec$ in the V-band and $2.8arcsec$ in the R-band, while that for the Isaac Newton Telescope is $1.5arcsec$ in the R-band. This was measured from the FWHM of the optical intensity of stars in the field of view. It arises from atmospheric seeing conditions when the observations were made, as well as the effect of combining many images.

Grey-scale intensity images of NGC 1068 are presented in Fig 4.1. North is at the top, east is at the left, and each image is $2arcmin$ square. Three images at different density levels are shown in order to illustrate both the bright nucleus and the fainter body of the galaxy. Note how the bright Seyfert nucleus dominates the intensity image of the galaxy. Also note that the spiral arms are less clearly defined than in M51, although still visible.

The polarimetric results for the whole galaxy are illustrated in Fig 4.2. This map represents the total unfiltered CCD data available for the galaxy—12 short exposures of the galactic nucleus, and 20 longer exposures for the remainder of the galaxy, all taken on the $1-metre$ telescope of the Wise Observatory. The integration bin size of each measurement is $6 \times 6arcsec$, with each bin stepped $3.6 \times 3.6arcsec$ relative to its neighbours. The map is superposed on an isophotal contour map, whose logarithmically spaced contours are placed at $0.5magnitude$ intervals. North is at the top, east is at the left.

Examination of Fig 4.2 shows several interesting features: The whole galaxy shows an overall pattern of polarisation, which shows a tendency to parallel the contours of the intensity image. However, close inspection shows that the pattern

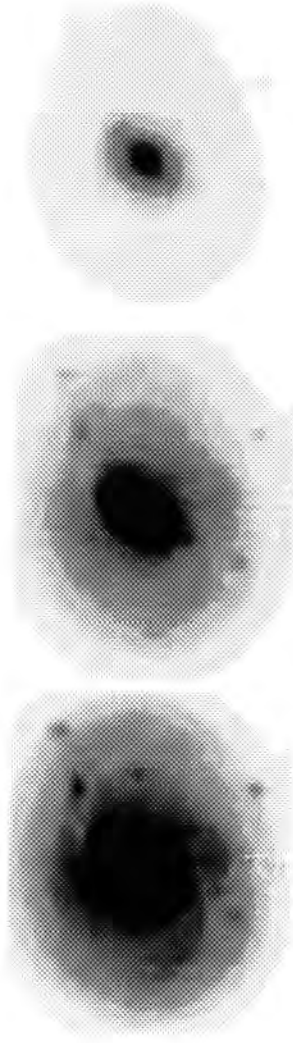

Figure 4.1: Intensity images of NGC 1068 (see text)

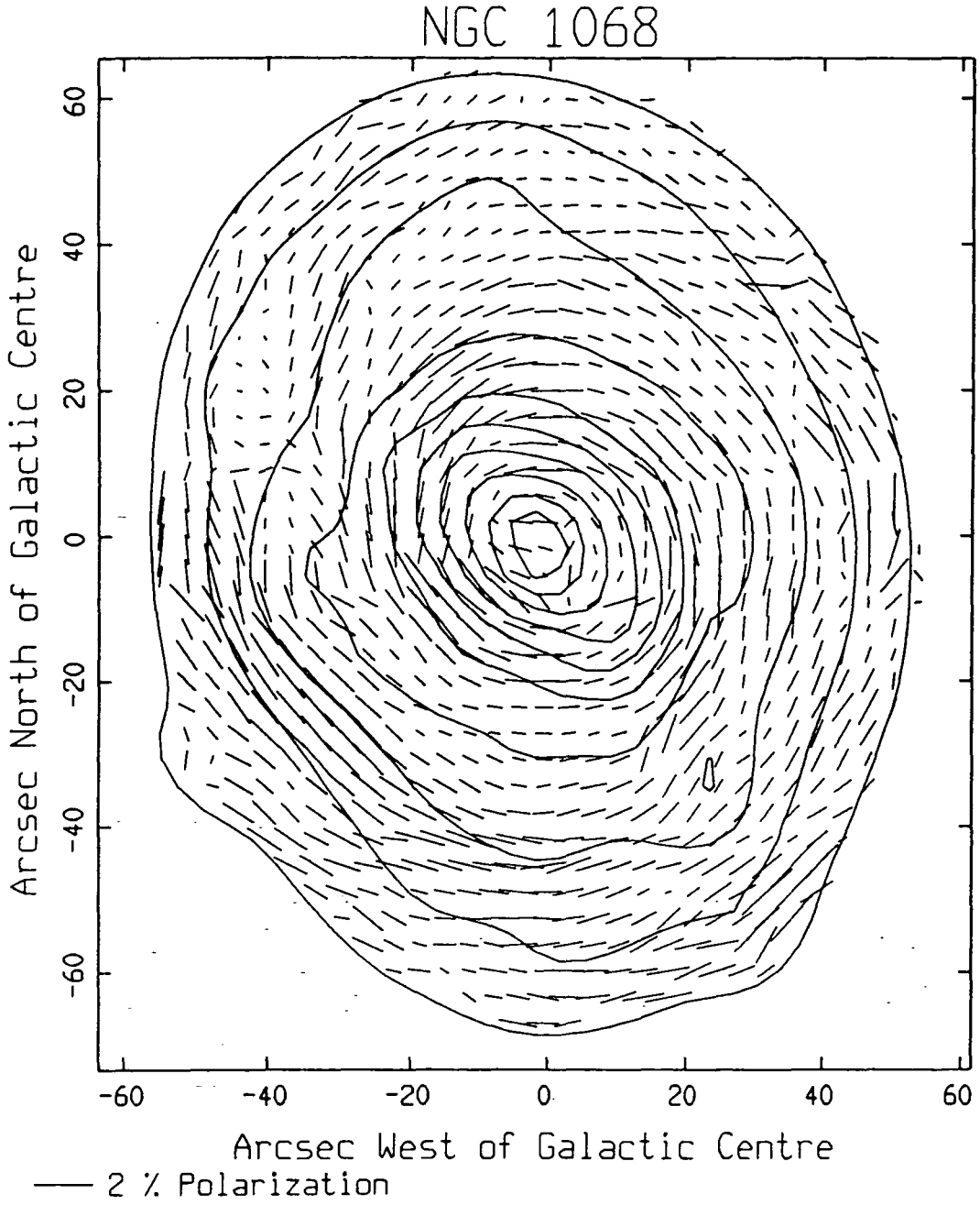

Figure 4.2: Unfiltered polarisation map of NGC 1068 (see text)

is more spiral than elliptical. Typical levels of polarisation are $0.8 \pm 0.3\%$ with angle errors $\pm 10 degrees$, although various regions display higher levels of polarisation. For example, the area around $40 arcsec$ southeast of the nucleus exhibits polarisation at $1.5 \pm 0.3\%$, with angle errors $\pm 5 degrees$.

It could be argued that the polarisation vectors merely parallel the vaguely elliptical contours of the intensity image, and for large parts of the map this is true. However there are specific areas where the polarisation vectors lie at up to 45 degrees to the intensity contours, while all angle errors lie between 10 and 15 degrees. These regions are centred on: $40 arcsec$ due north of the nucleus; $15 arcsec$ northeast of the nucleus; $20 arcsec$ due south; and $50 arcsec$ south-southeast of the nucleus. This all tends to indicate that the pattern is spiral rather than elliptical.

The spiral pattern just mentioned appears less marked than the equivalent pattern observed for M51 in Fig 3.2. In an endeavour to test whether the spiral pattern was real, a similar technique to that used in Chapter 3 was employed. That is to measure the polarisation in a series of apertures on the galaxy, which are coincident with the spiral arms, as was done for M51 in Fig 3.6.

This map is seen in Fig 4.3, where a series of circular apertures of $10.8 arcsec$ diameter have been placed in an array on the galaxy, using the same data as were used for Fig 4.2. One of the spirals in the array lies on the bright arms (BA1 and BA2), and the other on the dark lanes (DL1 and DL2) of the galaxy. The resulting polarisation map is superposed on the same isophotal contour map as Fig 4.2.

Inspection of this map shows that a series of linear polar-

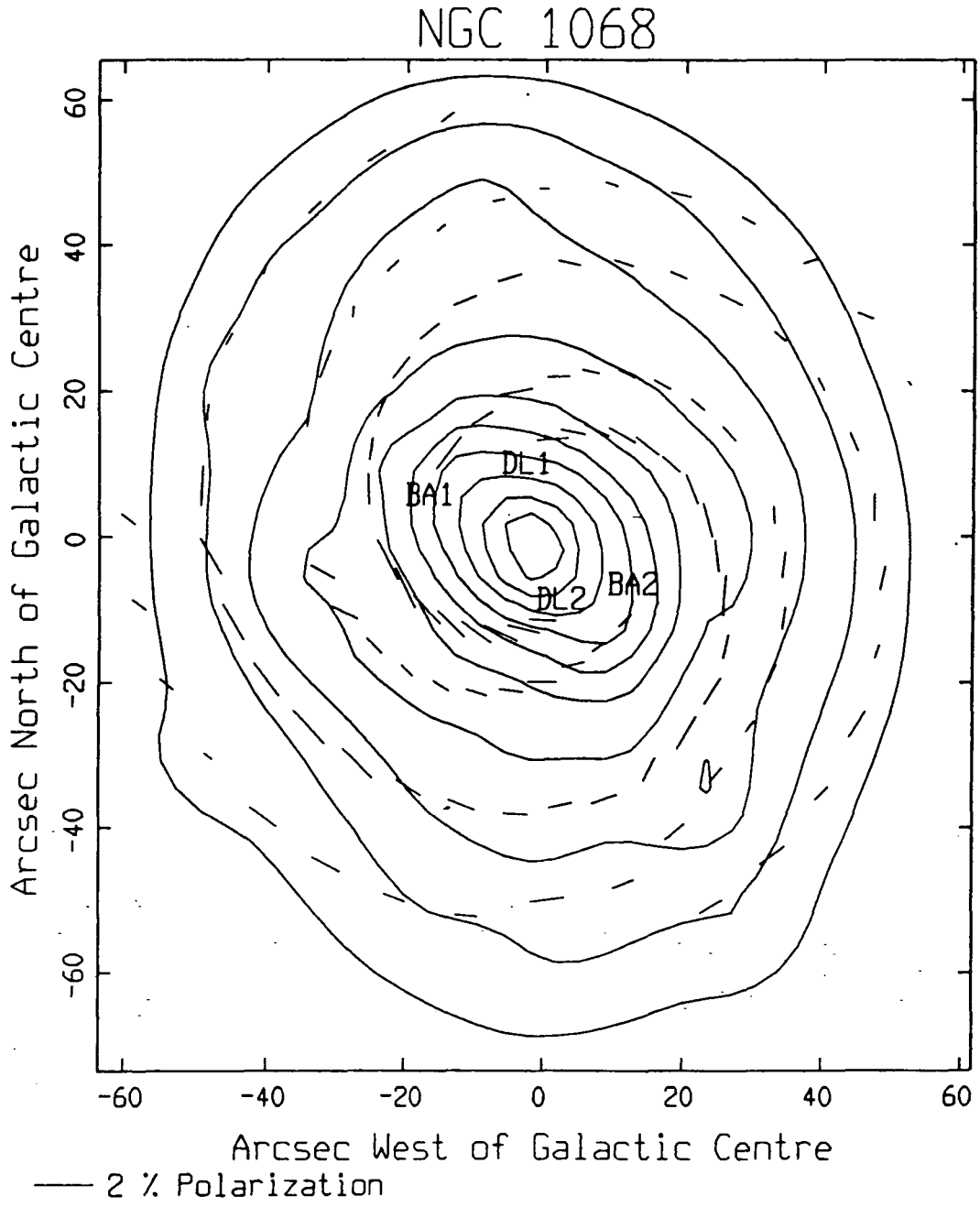

Figure 4.3: A series of unfiltered aperture polarisation measurements tracing the spiral arms and dark lanes of NGC 1068 (see text)

isations are seen across the whole visible disk of NGC 1068, from a radius of $10 arcsec$ to a radius of about $1 arcmin$, which form a spiral pattern at typical levels of $0.8 \pm 0.3\%$, with typical angle errors of $\pm 10 degrees$. At a distance of $18.1 Mpc$ this can be seen to be from a radius of about $900 pc$, to a radius of around $6 kpc$. This then confirms what was suggested earlier.

Returning to Fig 4.2 it can be seen that there is a departure from a purely spiral pattern on the nucleus itself. In order to see this more clearly a polarisation map of just the nucleus is presented in Fig 4.4. These are the same unfiltered data as were presented in Fig 4.2. Here again the polarisation bin size is $6 \times 6 arcsec$, with each bin stepped $3.6 \times 3.6 arcsec$ relative to its neighbours. The superposed isophotal contour map has logarithmically spaced contours at $0.75 magnitude$ intervals.

Examination of Fig 4.4 shows that the spiral pattern continues to within about $5 arcsec$ of the galactic nucleus, or about $450 pc$, at typical levels of $0.9 \pm 0.3\%$ with angle errors of $\pm 10^o$. Within this radius a region of polarisations, with parallel orientations, is seen. The polarisation of the nucleus is equal to $1 \pm 0.2\%$ at position angle $88 \pm 6 degrees$. Note that this is measured in a $6 arcsec$ square integration bin, and, as the polarisation bins all overlap their neighbours in this map, it is not possible to exactly ascertain the true extent of the linear pattern.

This nuclear polarisation could possibly be due to some foreground effect, such as interstellar polarisation in our own Galaxy. NGC 1068 is at right ascension $2^h 40.1^m$ and declination -00.14^o. In galactic coordinates this is at latitude $-55 degrees$ and longitude $170 degrees$. Axon and Ellis (1976) record no measurable interstellar polarisation in this direction,

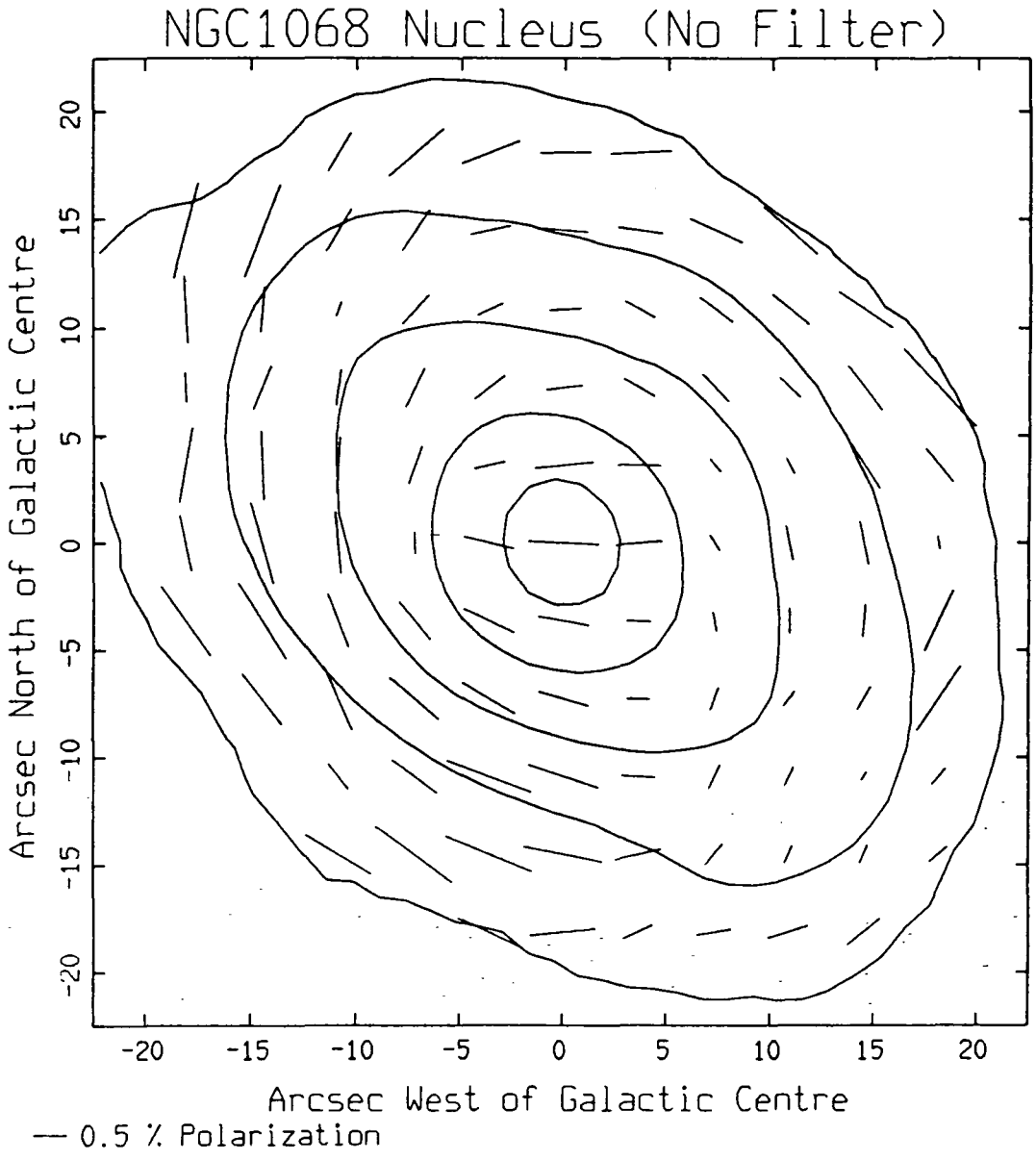

Figure 4.4: Unfiltered polarisation map of NGC 1068 nucleus (see text)

so the observed nuclear polarisation must be associated with NGC 1068 itself. This point is discussed later in the chapter, but first the remainder of the data are presented.

It can be seen from Table 3.1 that some broadband multicolour polarimetry is also available for NGC 1068, although it is only the nucleus which is available in each case. The reason for this is that the integration time required for reliable results on a faint object increases dramatically when a filter is inserted in front of the CCD (see Draper 1987), hence much more telescope time is required to make filtered polarisation maps of fainter objects. The multicolour data are now presented:

Fig 4.5 shows a V-band ($480-660nm$, peak response $550nm$) polarisation map of the nucleus of NGC 1068 taken on the $1-metre$ telescope of the Wise Observatory. The polarisation bin size is $6arcsec$ square, with the bins placed on a square grid at $3.6arcsec$ spacing. The superposed V-band isophotal contour map has logarithmically spaced contours at $1magnitude$ intervals.

A similar pattern to that seen in Fig 4.4 is observed. However there are slight differences also. The nucleus is polarised at $1.3\pm0.2\%$ at position angle $87\pm4degrees$ in a $6arcsec$ square integration bin. A pattern of roughly parallel polarisations is seen extending to a radius of about $6arcsec$ ($550pc$) from the nucleus. The polarisation outside of this region tends to follow the intensity contours as in Fig 4.4.

The areas in Fig 4.5 centred on a radius of about $15-20arcsec$ northwest and $10-15arcsec$ southeast of the nucleus show levels of polarisation around $2\pm0.6\%$, with angle erors of $\pm10degrees$, whereas $10arcsec$ northeast and $15arcsec$ southwest of the nucleus the levels of polarisation are only around

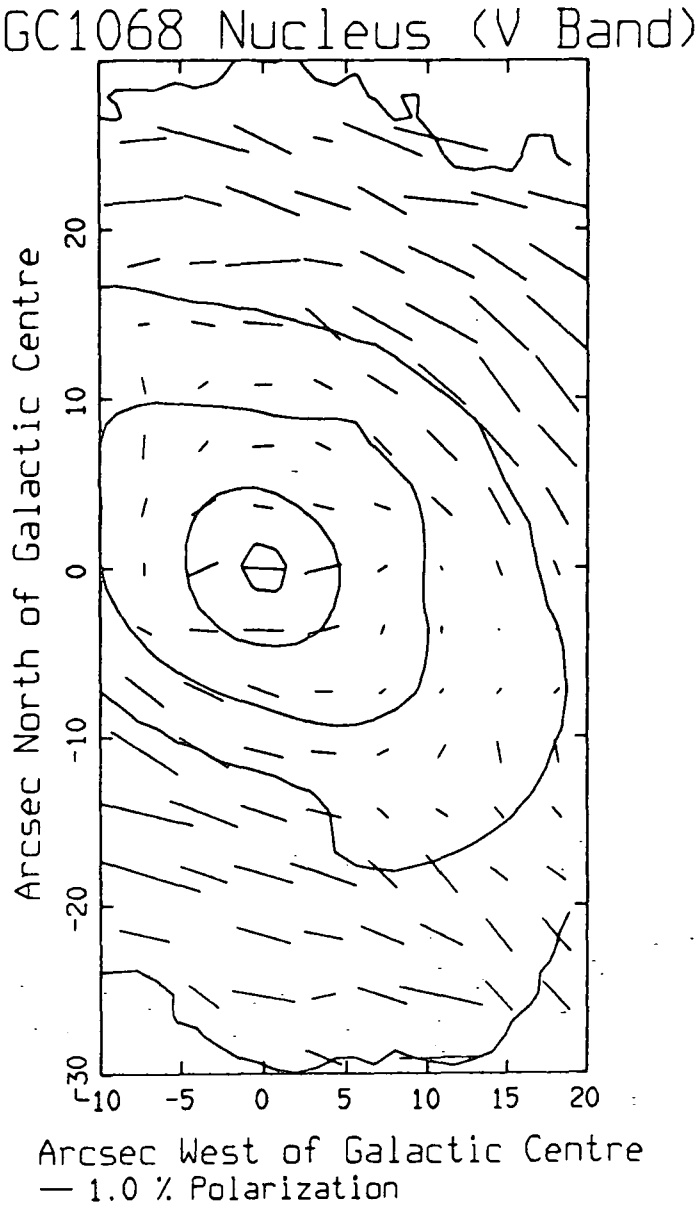

Figure 4.5: V-band polarisation map of NGC 1068 nucleus (see text)

$0.5 \pm 0.3\%$ with angle errors $\pm 20 degrees$. This was not observed in the unfiltered data. Note also that departure from a spiral pattern is observed in the southwest corner of the map. However the errors in this region are large, presumably due to the lower signal-to-noise ratio inherent in each filtered exposure, and also to the smaller number of exposures available in this waveband, so no polarisation has been measured here.

Fig 4.6 shows a polarisation map of the R-band ($560 - 890nm$, peak response $650nm$) data taken with the $1 - metre$ telescope of the Wise Observatory. The measurements are taken in $6arcsec$ square integration bins spaced at $3.6arcsec$ square intervals. The logarithmic spacing of the superposed R-band isophotal contours is $0.75 magnitudes$.

A similar pattern is seen to that in Fig 4.4 and Fig 4.5, but again with slight differences. The majority of the map shows polarisations which form a roughly spiral pattern at typical levels of $1.3 \pm 0.4\%$, with angle errors typically $\pm 10 degrees$. The region within a radius of around $5arcsec$ ($450pc$) of the nucleus shows a linear pattern, with the polarisation of the nucleus in a $6arcsec$ square integration bin being $1 \pm 0.2\%$, at position angle $86 \pm 6 degrees$.

Fig 4.7 shows a polarisation map of the nuclear region of NGC 1068 taken in the R-band ($560 - 890nm$, peak response $650nm$) with the $2.5 metre$ Isaac Newton Telescope. Here the integration bins for each measurement are $2.5arcsec$ square, spaced at $1.5arcsec$ square intervals. The logarithmic spacing of the isophotes is $1 magnitude$.

Similarities are seen between Fig 4.6 and Fig 4.7, although, as was mentioned earlier, the seeing is considerably better in Fig 4.7. It can now be seen that the linear pattern on the

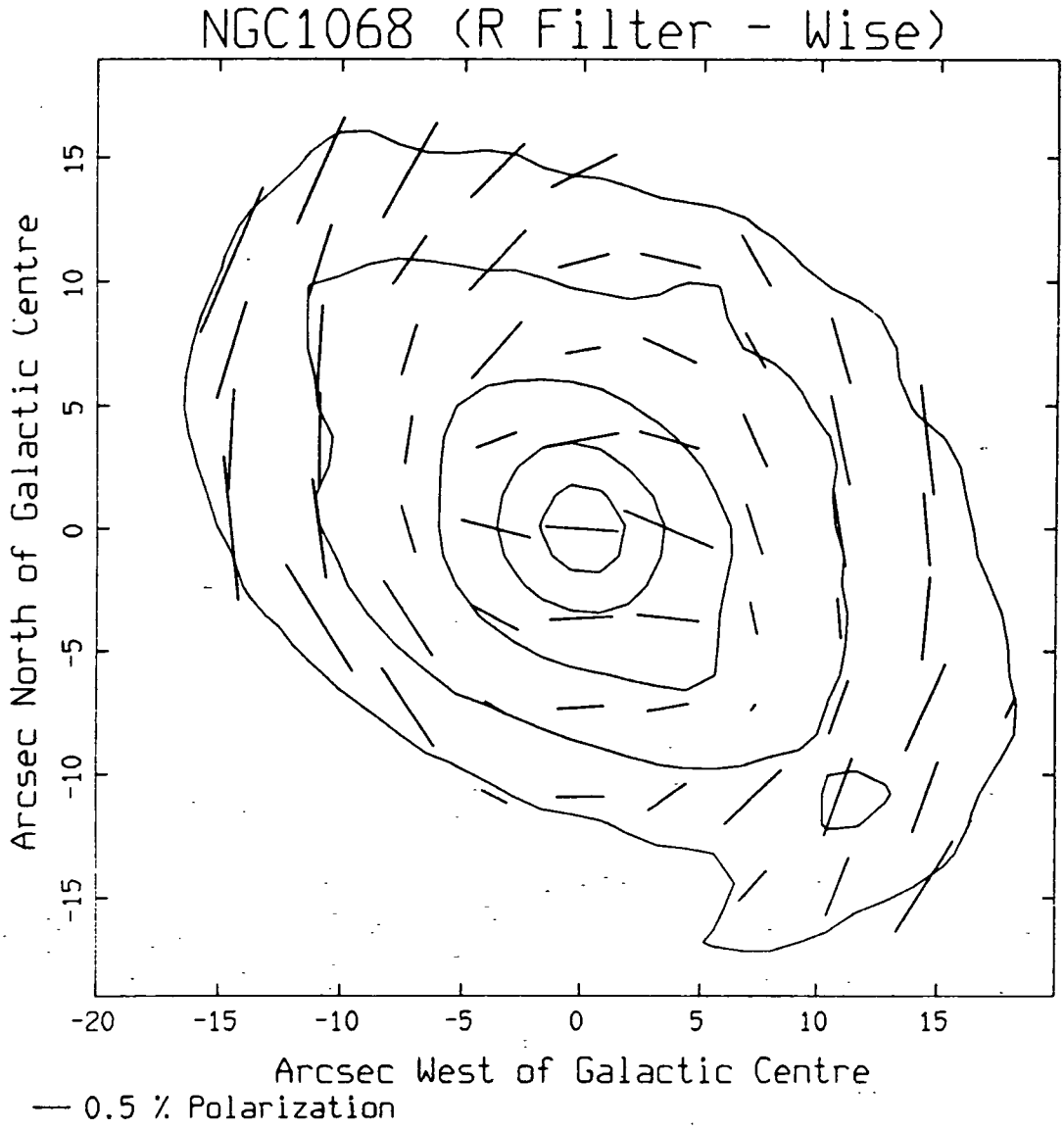

Figure 4.6: R-band polarisation map of NGC 1068 nucleus taken at the Wise Observatory (see text)

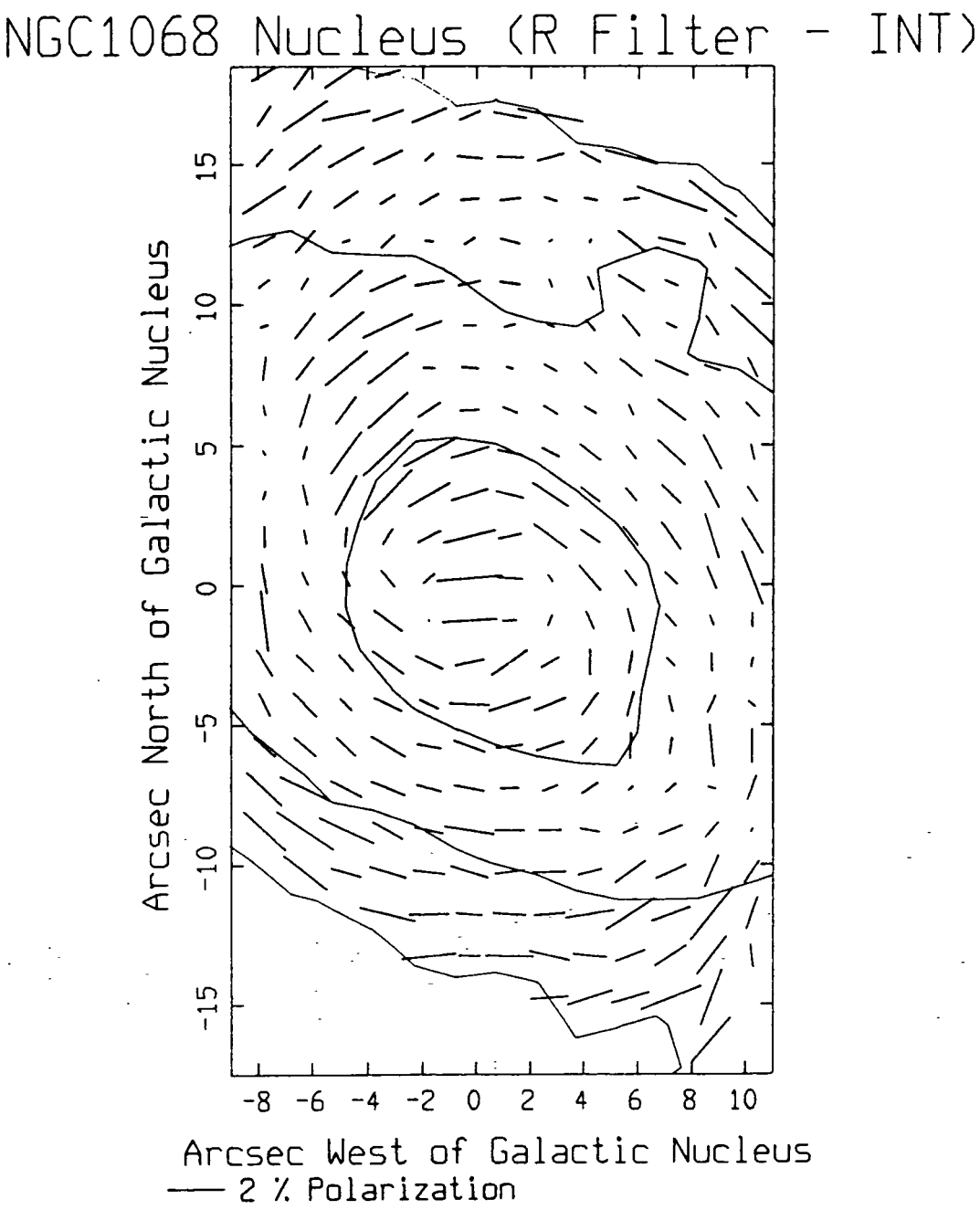

Figure 4.7: R-band polarisation map of NGC 1068 nucleus taken with the INT (see text)

nucleus only actually covers a region comparable in size to the resolution of the data (about $2arcsec$) and must be confined to less than $180pc$ of the nucleus itself. The level of polarisation in a $2.5arcsec$ square integration bin on the nucleus is $1.5 \pm 0.2\%$ at position angle $94 \pm 4degrees$. Outside of this radius the polarisation again appears spiral at polarisation levels of around $1.2 \pm 0.7\%$ with typical angle errors $\pm 15degrees$.

Discussion and interpretation of all of the features observed in the data is pursued in Section 4.5, but first a comparison is made of these data with previous researchers' work.

4.4 Comparison with other authors

Several authors have made polarisation measurements of NGC 1068. These include Angel et al. (1976), Elvius (1978 a & b), Mclean et al. (1983) and Antonucci and Miller (1985). Some of their chief results for the nucleus of NGC 1068 are summarised in Table 4.1.

Authors	A		M		A and M		E	
Aperture	2.8c		2c		2.2x1.7		5x20	
λ	%	PA	%	PA	%	PA	%	PA
370	7.0	100	-	-	8.0	95	-	-
420	4.2	100	6.6	100	5.2	95	-	-
550	1.4	100	1.8	100	2.3	95	-	-
650	0.5	96	1.6	100	1.9	95	-	-
NF	-	-	-	-	-	-	4.25	97

Table 4.1: Previous polarisation results of NGC 1068 nucleus (See text)

In this Table, **A** represents Angel et al; **M** stands for McLean et al; **A and M** is Antonucci and Miller; and **E** stands for Elvius. The aperture size used is annotated by giving its dimensions if rectangular, or its diameter followed by the letter **c** if circular. A percentage polarisation and position angle is given for each measurement. No errors are recorded as none were quoted except by Antonucci and Miller, who claim $\pm 5 degrees$ in position angle.

The first column details the peak wavelength of the observations in question. Note that Elvius uses no filter, but from the details which are given it can be surmised that the peak response of her results occurs at a shorter wavelength than that of the Durham CCD.

All of the position angles appear consistent at $95 - 100^{o}$, and all agree that the percentage polarisation decreases with increasing wavelength. However, comparison of the actual data values show that errors of $\pm 1\%$ appear likely throughout all of the measurements quoted. Although note that disagreements could occur because of the slightly different aperture sizes used.

Table 4.2 lists the results of this current survey for the nucleus of NGC 1068. Note that only the peak wavelength is recorded for each filter. The telescope on which the observations were made is also noted. Again a general decrease with increasing wavelength is observed. The different polarisation position angles measured on the two telescopes in the R-band can be accounted for by the different resolution of the data sets. The INT results agree most closely with previous authors.

The unfiltered measurement cannot be compared with that of Elvius, as the mean wavelength of that author's results is much shorter than that of the Durham CCD. Elvius (1978a)

Waveband	Polarisation	Angle	Telescope
530	2.7% (0.3)	110 (3)	Wise
650	1.4% (0.2)	113 (4)	Wise
650	1.5% (0.2)	95 (4)	INT
NF	1.3% (0.2)	92 (5)	Wise

Table 4.2: Polarisation results of this survey for NGC1068 nucleus in a 2.4 arcsec diameter circular aperture. Errors in brackets (See text)

further records a polarisation measurement for a point $10 arcsec$ northeast of the nucleus of 4% at position angle $135 degrees$, again in unfiltered data. The unfiltered data available in this survey give a result of $0.6 \pm 0.25\%$ at position angle $137 \pm 10 degrees$.

Antonucci and Miller used their data to derive several conclusions. The difference in polarisation states of the continuum and broad line emission of the galaxy, and of the narrow line emission, lead these authors to an interesting conclusion: They hypothesised that the highly polarised continuum and broad line emission is light from the nucleus of NGC 1068 which has been scattered from free electrons in the ISM of the galaxy, and that the less polarised narrow line emission is light seen directly from the main part of the galaxy. They went on to conclude that the nucleus of NGC 1068 is actually a Type I Seyfert which is heavily obscured.

The consistency of the position angle of their results and previous workers lead them to deduce that an optically thick torus of dust surrounds the nucleus of NGC 1068. They stated that the plane of this torus, in the plane of the sky, lies at

position angle $95 degrees$. This is roughly perpendicular to the direction of the collimated radio outflows from the nucleus of NGC 1068 (see Section 4.2), and the spatial extent of the torus is less than the resolution of the observations.

Thus light, emanating from the nucleus along the axis of the torus, is scattered towards the observer, causing the observed nuclear polarisation parallel to the torus. Furthermore, the torus is responsible for collimating the radio outflows from the nucleus, which occur out of the plane of the galaxy, and the southern outflow is obscured by the main body of the galaxy. The results presented in this chapter are consistent with all of these conclusions.

McLean et al. (1983) stated that the polarisation of the continuum spectrum is wavelength independent. They then said that this is indicative of scattering from free electrons. However, interstellar dust grains with a power law grain size distribution also give rise to polarisation which is wavelength independent. This can be shown by study of the Mie scattering functions, where, on choosing the power-law grain size distribution, the wavelength dependence of percentage polarisation disappears (Warren-Smith 1979). So dust grains, as well as free electrons, could be responsible for the scattering which causes the observed nuclear polarisation.

So it has been seen that, where comparisons can be made with other authors, the data provided by the Durham Polarimeter are at least of a comparable standard for single polarisation measurements. Where these new data are superior is in providing a map of the spatial variation of polarisation across an extended object such as NGC 1068. There now follows a discussion and interpretation of the polarisation patterns ob-

served in the previous section.

4.5 Discussion and conclusions

Data have been presented of the variation of optical linear polarisation across the visible disk of NGC 1068 at a number of broad wavebands. An overall spiral pattern of polarisation has been shown to exist throughout NGC 1068 from a radius of $180pc$ from the nucleus, to a radius of $6kpc$, at polarisation levels typically of order 1%.

It is now suggested that there is a large-scale magnetic field throughout NGC 1068 which is spiral in nature. This field aligns non-spherical dust grains in the interstellar medium by means of the Davis-Greenstein mechanism (see Chapter 2). The aligned grains cause the observed polarisations by preferential absorption. The main body of the field appears to lie parallel to the spiral arms of the galaxy, as was seen in M51 in Chapter 3. It is therefore suggested that the magnetic fields in these two galaxies are similar.

The main difference between M51 and NGC 1068, as seen from their respective polarisation maps, is that in the former galaxy the field is observed to continue to be spiral in nature right into the centre of the galaxy, whereas in the latter it is not.

The centre of NGC 1068 is polarised and it was noted in Section 4.2 that there is a bipolar radio outflow from the nucleus, whose nearer half is seen to be directed towards position angle roughly $11degrees$. This is very nearly perpendicular to the nuclear polarisation. Antonucci and Miller (1985) noted this and claimed that there is a dust torus which is responsible

for obscuring the nucleus and collimating the radio outflows. This is supported by the current data.

Note that the outflows do not appear to affect the polarisation map, and, by inference, the magnetic field in the plane of the galaxy, hence the outflows probably occur out of the galactic plane, as was surmised earlier. Exactly how a torus is formed around a Seyfert nucleus is not clear. Antonucci and Miller (1985) discussed an embedded black hole in the centre of the galaxy, and accretion onto a disk around this, which may be the case.

In Chapter 6 the conclusions of this chapter are compared with those of other chapters. The repercussions of the findings are then explored with regard to the origins of galactic magnetic fields in general.

Chapter 5

NGC4594 (M104) and NGC4565

5.1 Introduction

In this chapter data are presented for two spiral galaxies, which are seen nearly edge-on. The two galaxies in question are NGC 4594 (M104) and NGC 4565.

The optical images of the two galaxies show similarities. Both galaxies have a very obvious dark lane foreground to the galactic nucleus. These are believed to be dust lanes in the plane of each galaxy. Both galaxies have a nuclear bulge which can be seen to either side of the dark lane. NGC 4594 has a much larger nuclear bulge than NGC 4565, thus the former is denoted type Sab and the latter is type Sb (The Hubble Atlas, Sandage 1961).

The data are presented for each galaxy in turn, and a discussion and interpretation of the data given. Section 5.2 deals with NGC 4594, and Section 5.3 details NGC 4565. Then in Sections 5.4 and 5.5 a comparison is made of the two galaxies, and conclusions are drawn.

5.2 NGC 4594 (M104)

NGC 4594, or M104, has been called the Sombrero Galaxy, because of its appearance in an optical image—namely the prominent dust lane and the nuclear bulge mentioned above. It is inclined to such an extent that the angle between the plane of the galaxy and the line of sight to the observer is only $6 degrees$ (de Vaucouleurs 1958), and the estimated distance to M104 is $18.2 Mpc$ (Schweizer 1978).

Scarrott et al. (1977) observed M104 with the Durham Polarimeter, using an electronographic camera detector system. They found a polarisation pattern in the dust lane lying parallel to the lane at levels around $2 - 4\%$. This current survey, using a CCD detector system, should be more sensitive, and the improved data reduction software ensures that this survey is more accurate.

5.2.1 The data

The observational details of the data presented here are described in Chapter 3 and outlined in Table 3.1, except where stated otherwise. Typical seeing of the unfiltered data is $3.6 arcsec$, and that of the colour data is $3.1 arcsec$ in the V waveband, $4.1 arcsec$ in the R waveband and $3.7 arcsec$ in the I waveband.

Fig 5.1 shows a grey-scale intensity image of M104. North is at the left, east is at the bottom, and the east-west diameter of the visible part of the disk is $5 arcmin$. Note the large nuclear bulge, and the foreground dust lane, which give this galaxy its name of the sombrero.

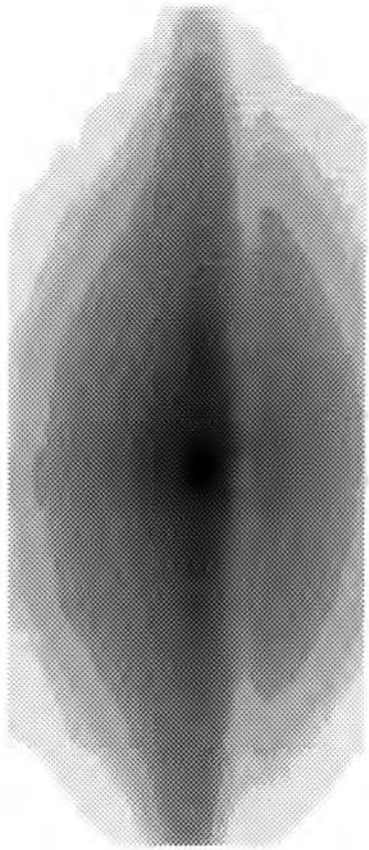

Figure 5.1: Intensity image of M104 (see text)

Fig 5.2 is a linear polarisation map of M104. This map has been formed from a combination of all of the unfiltered data available for this galaxy. The integration bin size of each measurement is 15.6*arcsec* square, and the measurements are placed at 9.6*arcsec* square intervals. The offsets are measured from the brightest part of the visible nucleus. Several interesting features of this map can be seen:

Firstly, the polarisation of the brightest part of the visible nucleus is not zero. Secondly, a pattern of linear polarisation is observed to lie approximately parallel to the dust lane, throughout the major part of its length. Finally, it can be seen that the polarisation at each end of the dust lane turns through roughly 90*degrees* to lie at position angle approximately north-south.

Taking each of these points in turn: The nuclear polarisation was measured to be $0.5 \pm 0.1\%$ at position angle $52 \pm 5 degrees$. The coordinates of M104 are $R.A = 12^h37.3^m$ and $Dec = -11°21'$. In galactic coordinates this is latitude $+51.2°$ and longitude $298.4°$. Axon and Ellis (1976) catalogued an interstellar polarisation, which was measured by Mathewson and Ford (1970), local to our neighbourhood of the Galaxy (within 400*pc*), within a few degrees of M104, of 0.3% polarisation at position angle 56*degrees*.

Thus this recorded nuclear polarisation of M104 is clearly a foreground interstellar polarisation, arising from preferential extinction by aligned dust grains in the magnetic field of our own Galaxy in the solar neighbourhood. As linear polarisation obeys the laws of vector addition it is possible to subtract a foreground polarisation from an entire map. Therefore Fig 5.3 illustrates the same map as Fig 5.2 with 0.5% at position angle

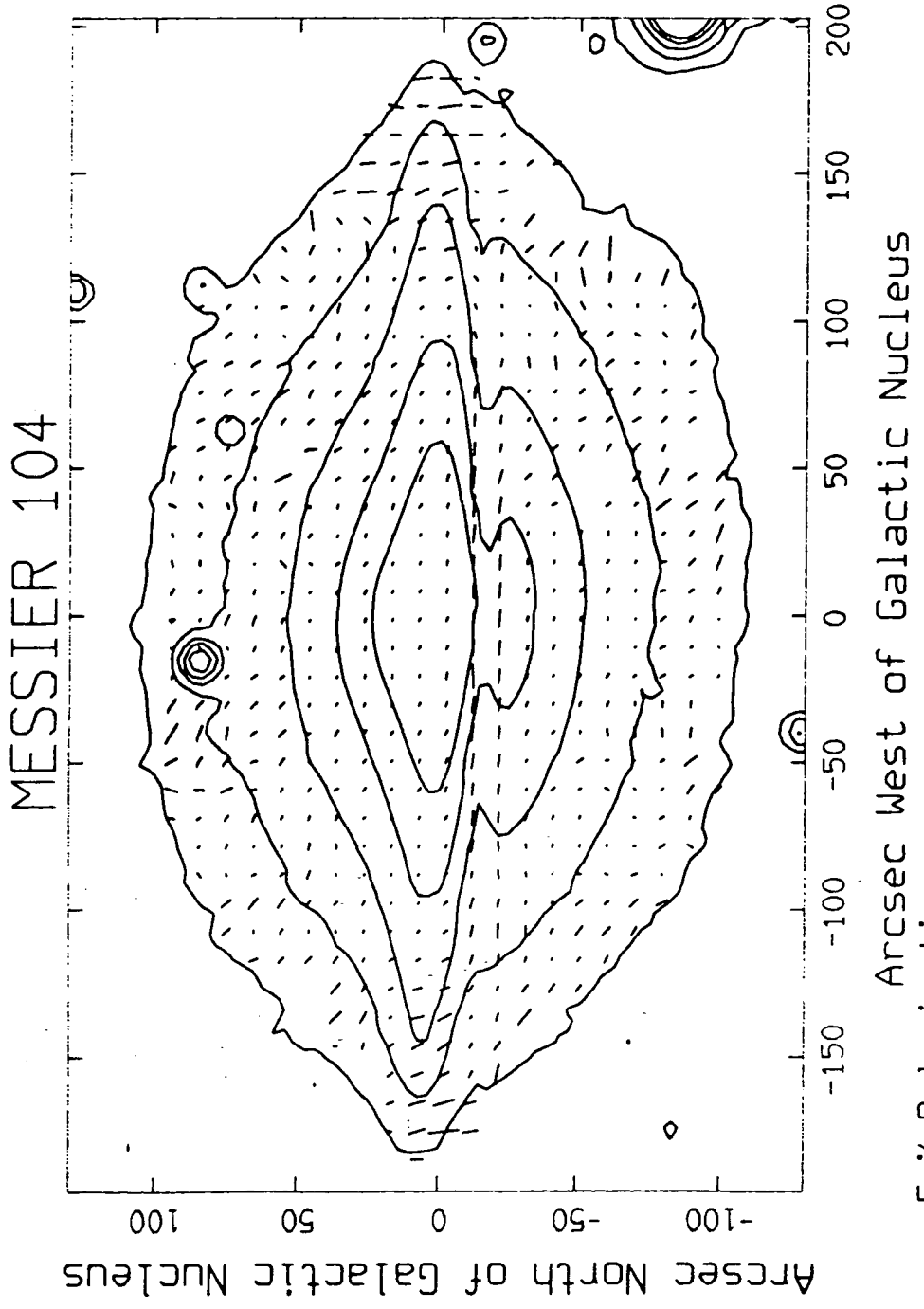

Figure 5.2: Unfiltered polarisation map of M104 (see text)

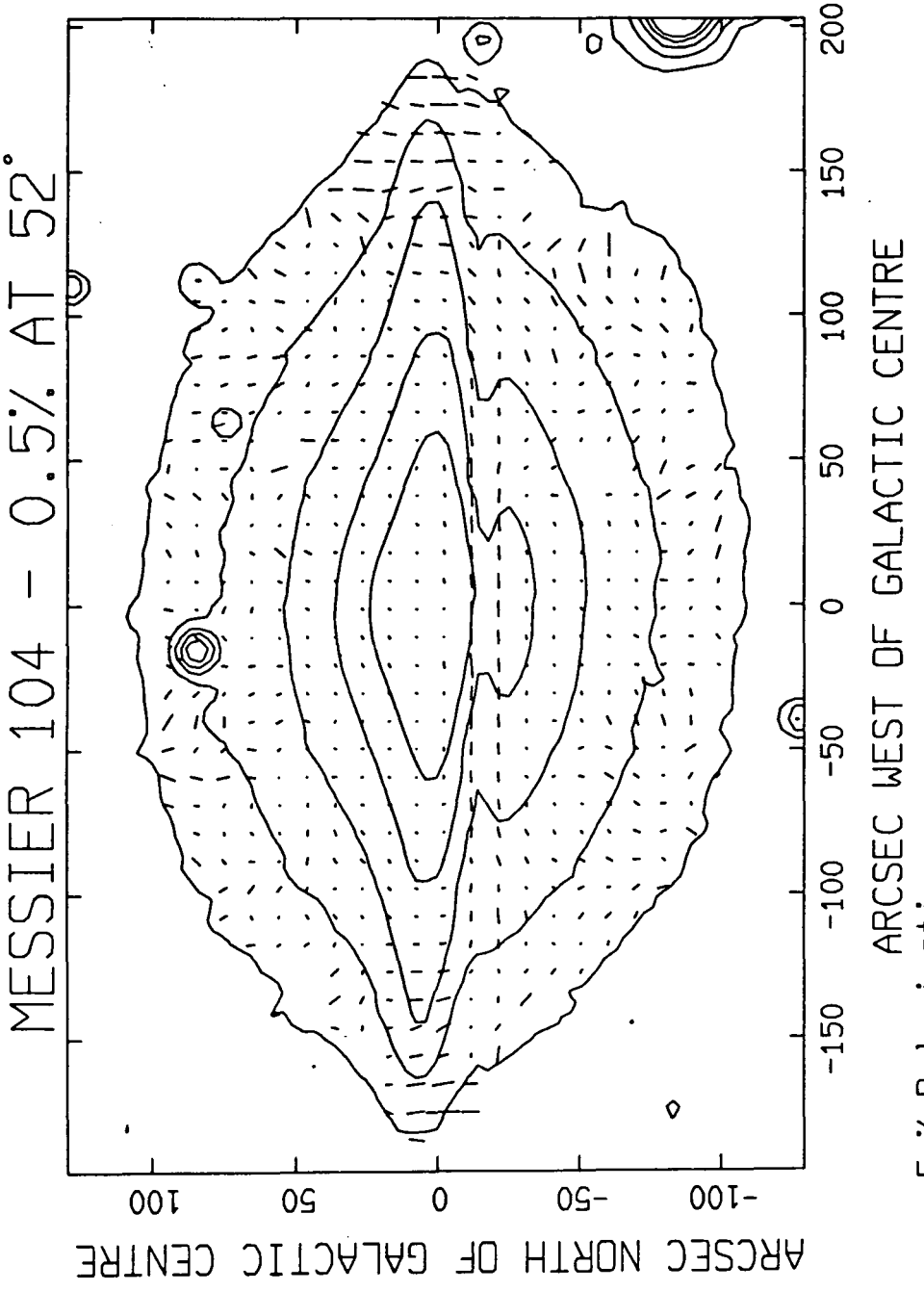

Figure 5.3: Unfiltered polarisation map of M104, with foreground polarisation (ISP) removed (see text)

$52 degrees$ subtracted from the whole map.

Examination of Fig 5.3 reveals several points of interest. The majority of M104 has very low levels of polarisation ($\leq$ 0.1%), indicating that no polarisation has been measured. The exception to this is the dust lane mentioned earlier. The polarisation of this lane is at levels around $2\% \pm 0.4\%$, as measured in a $15.6 arcsec$ square integration bin, at position angle parallel to the lane itself, $\pm 5 degrees$. At each end of the dust lane there is a region of polarisation which is at position angle roughly north-south, and at levels of polarisation up to $3\% \pm 0.5\%$, with angle errors $\pm 5 degrees$.

Fig 5.4 shows a linear polarisation map of just the dust lane of M104. The integration bin size of each measurement is $8.4 arcsec$ square, and the measurements are spaced at $6 arcsec$ square intervals. The logarithmic spacing of the superposed isophotes is $0.75 magnitudes$. Again the foreground interstellar polarisation has beeen subtracted from the map.

It can be seen again in this polarisation map that the polarisation of the dust lane lies parallel to the lane itself (within $\pm 5 degrees$) at levels around $3.5\% \pm 0.5\%$, with angle errors $\pm 4 degrees$, as measured in an $8.4 arcsec$ square integration bin. Note the contrast in levels of polarisation between the dust lane and the remainder of the galaxy.

Fig 5.4 also illustrates the two regions at either end of the dust lane very clearly. It can be seen that the change of polarisation position angle occurs in a very small area. The polarisation changes from lying east-west to north-south within about $20 arcsec$ in each case. The significance of this abrupt change will be discussed later.

Reference to Table 3.1 shows that multicolour data are avail-

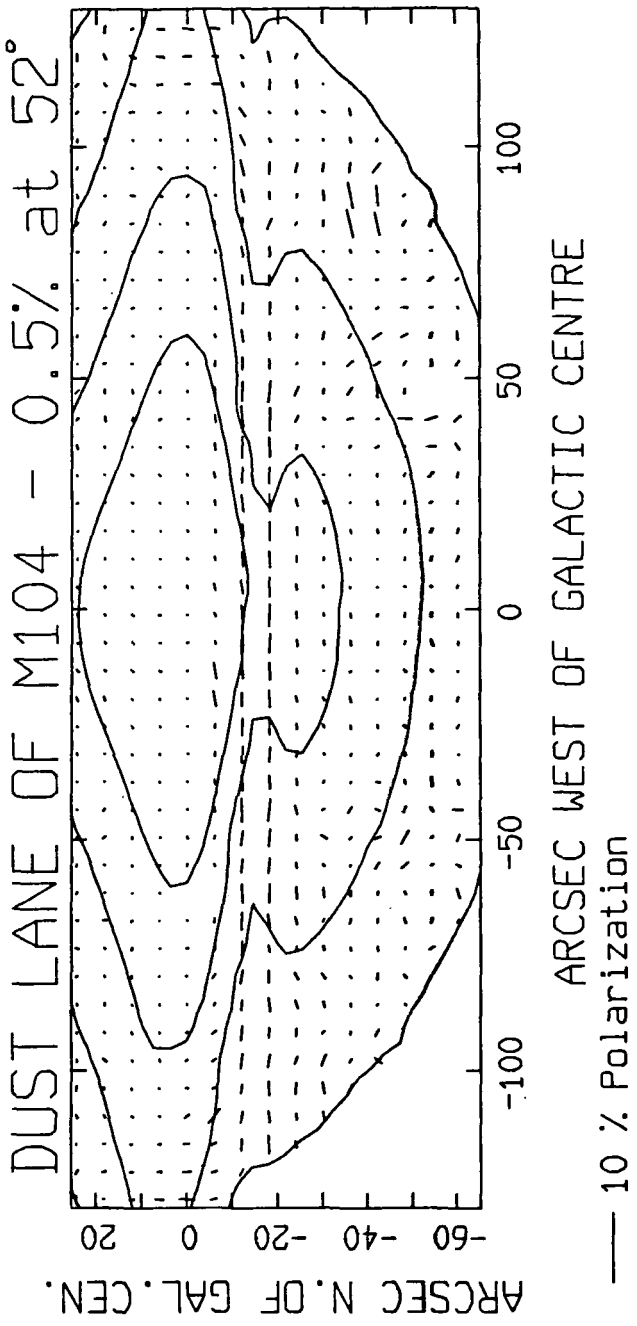

Figure 5.4: Unfiltered polarisation map of M104 dust lane with ISP removed (see text)

able for M104. Due to the greater amount of telescope time required to make a colour polarisation map than an unfiltered one, only part of the galaxy was observed at each waveband. This part includes the galactic nucleus, but not all of the galactic dust lane. The three wavebands used were V, R and I, covering $480-660nm$, $560-890nm$ and $680-1000nm$ respectively. The peak wavelengths of these bands are $550nm$, $650nm$ and $745nm$ respectively.

The nuclear polarisation was measured in each waveband and found to be $0.4\pm0.1\%$ in V, $0.5\pm0.3\%$ in R and $0.7\pm0.4\%$ in I. The position angles were 63 ± 7, 41 ± 7 and 39 ± 6 degrees respectively. These are all similar to the previously measured interstellar polarisation for the unfiltered data. Hence they are believed also to be foreground polarisations. These values were subtracted from each set of data before plotting the polarisation maps.

Figs 5.5, 5.6 and 5.7 show linear polarisation maps of M104 in the V, R and I wavebands respectively, where the integration bin size of the measurements in each map is $8.4arcsec$ square, spaced at $6arcsec$ square intervals. Each is superposed on an isophotal contour map in the same waveband, where the logarithmic spacing of the isophotes is $0.5magnitudes$ in each case.

It appears from these maps that the only regions for which significant results have been measured are the central part of the dust lane, which is seen to be polarised parallel to its length. The value of this polarisation in an $8.4arcsec$ square integration bin is around $3-5\%$ in V, $3-4\%$ in R and $2-3\%$ in I. For comparison the value of the dust lane polarisation in the unfiltered data was seen to be around $3-4\%$. The errors

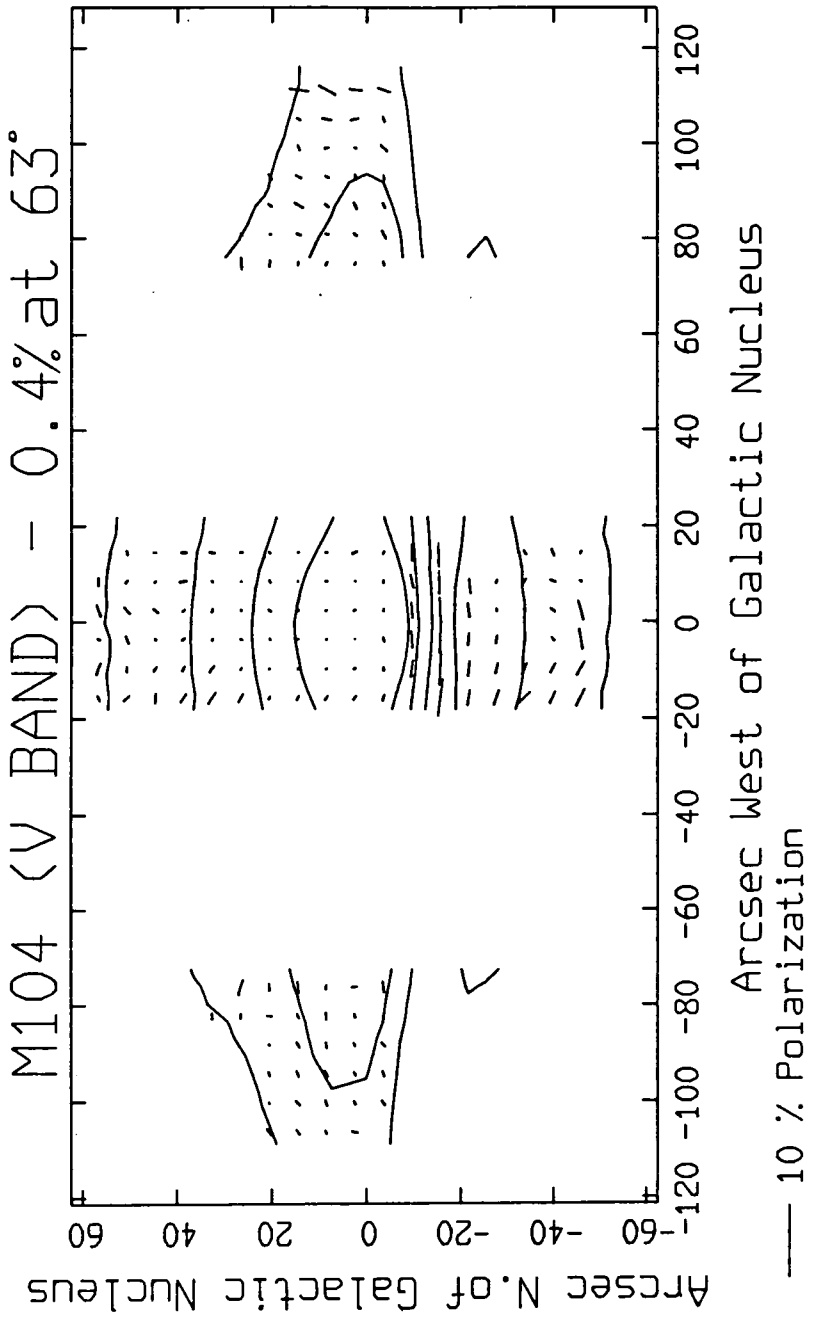

Figure 5.5: V-band polarisation map of M104 with ISP removed (see text)

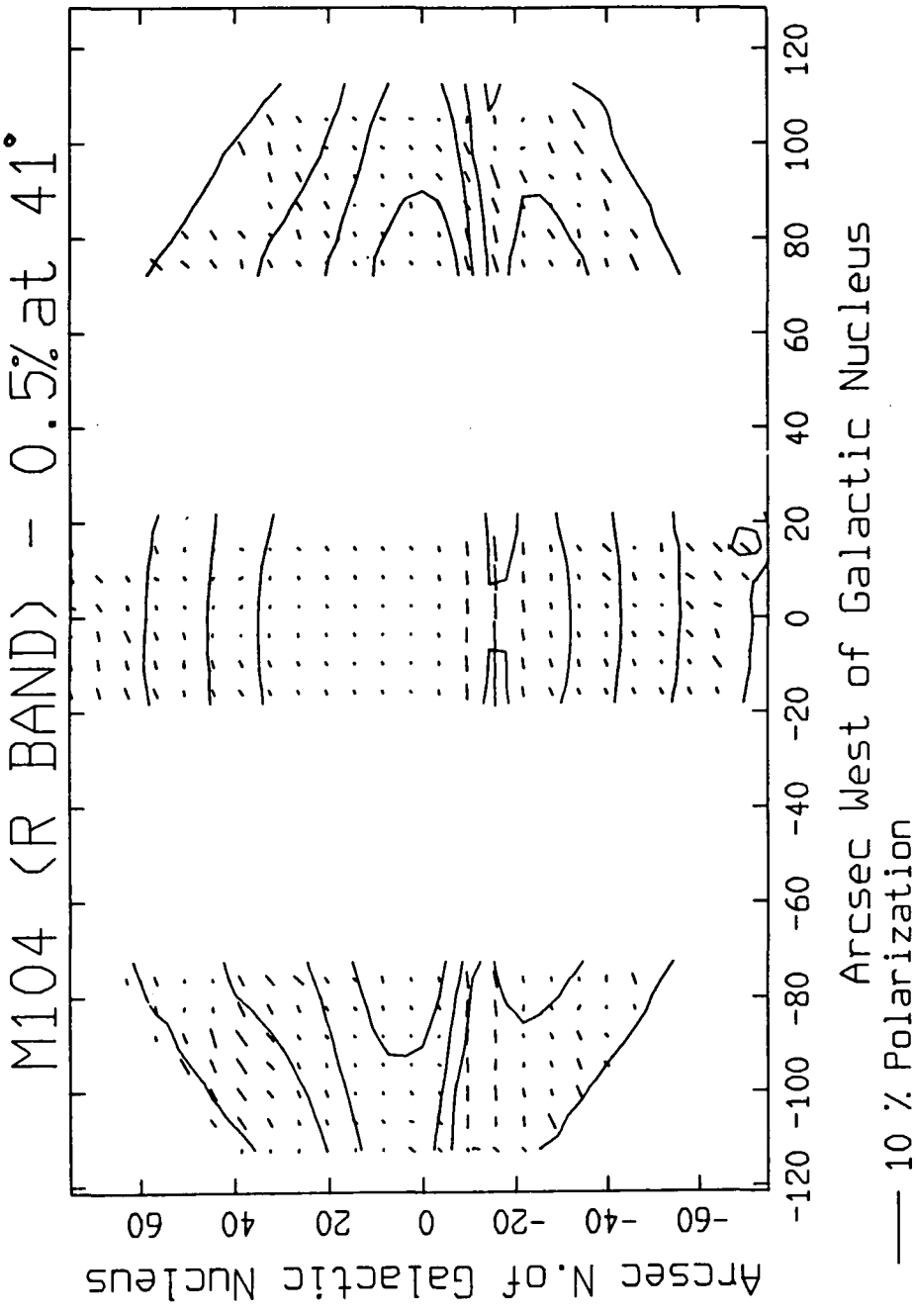

Figure 5.6: R-band polarisation map of M104 with ISP removed (see text)

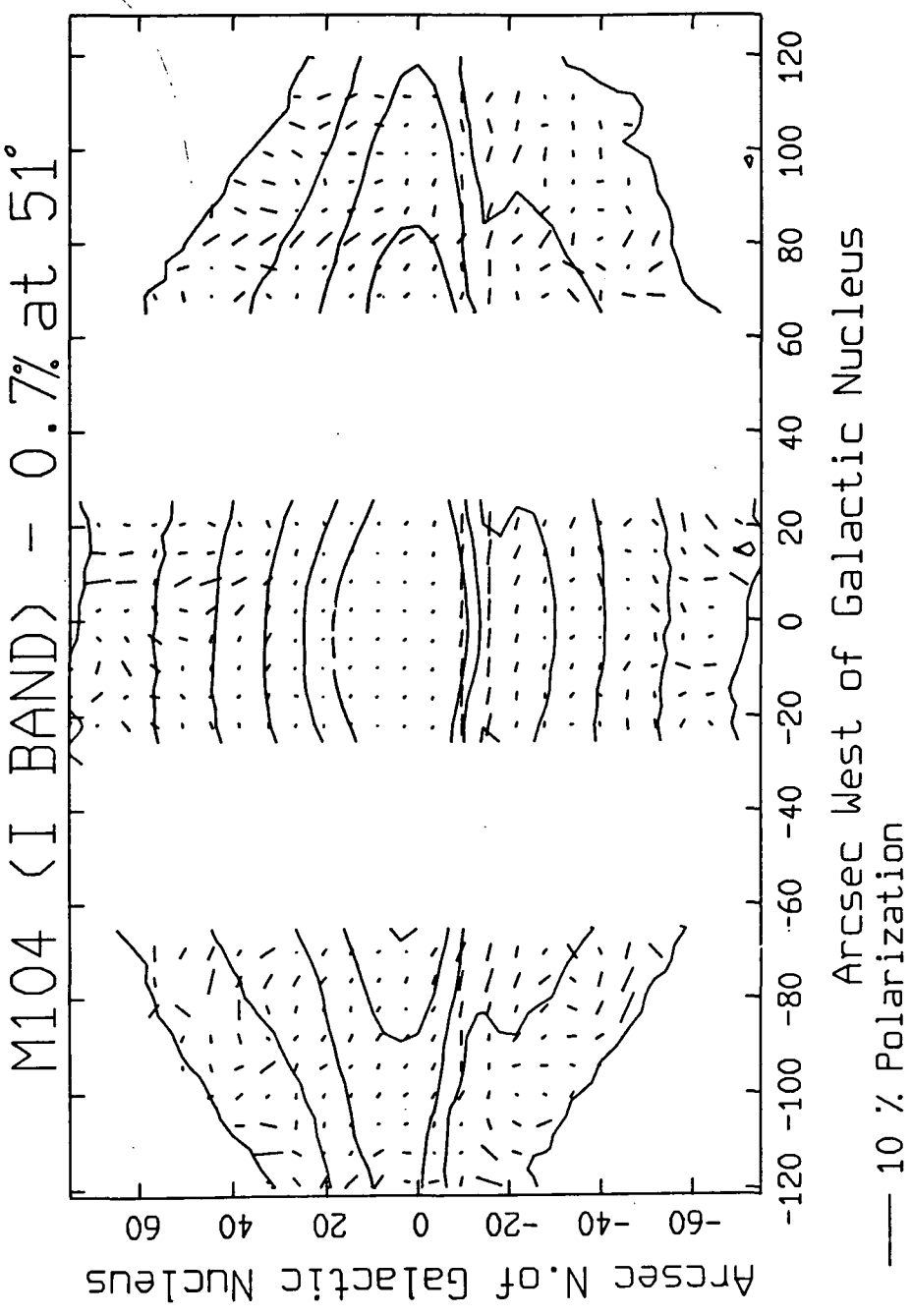

Figure 5.7: I-band polarisation map of M104 with ISP removed (see text)

in the dust lane measurements are typically ±0.5% in polarisation and ±5*degrees* in position angle, while those on the data covering the remainder of the galaxy are so large as to make multicolour analysis of the data apart from the dust lane impossible.

In order to ascertain the extinction in the dust lane, intensity profiles were made through the nucleus of M104, perpendicular to the dust lane, in each waveband. It was assumed that the intensity of the underlying nucleus is symmetrical about a line parallel to the dust lane. This assumption was then used to reflect the unaffected profile so that it overlies the profile which is affected by the dust lane. Note that this is similar to the technique of Burkhead (1986) of assuming the galaxy to be composed of the sum of a symmetrical nuclear bulge and a foreground disk component containing dust.

Fig 5.8 shows these intensity profiles in the V, R, I and unfiltered bands respectively (the latter is merely included for comparison). The upper curve in each case is that part of the profile unaffected by the dust lane, the lower curve is the profile through the centre of the dust lane. The ordinate scale of each graph is measured in magnitudes, although the zero-point of each scale is arbitrary, and the width of the profile is 6*arcsec*.

The extinction caused by the dust lane in each waveband is obtained by subtracting the lower curve from the upper. The close match of each pair of curves away from the region of the dust lane appears to validate the assumption of symmetry. The profiles were used to measure the maximum extinction in the dust lane in each waveband, that point where the difference between the two curves is greatest.

The values of maximum extinction are recorded in Table 5.1

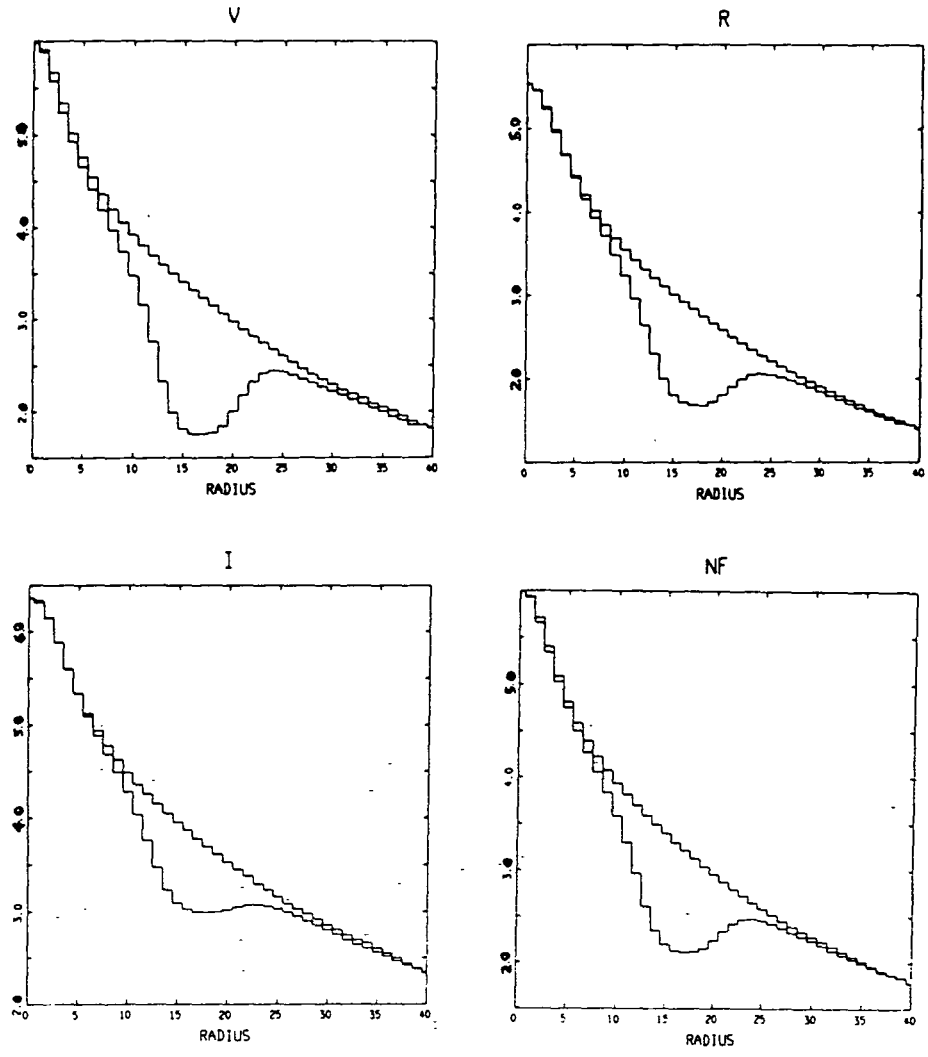

Figure 5.8: Intensity profiles to show the dust lane extinction in M104 at each waveband (see text)

together with the foreground interstellar polarisation (ISP) in each waveband, and a measure of the dust lane polarisation. This was taken in an integration aperture measuring 6*arcsec* east-west by 2.4*arcsec* north-south, thus enclosing that part of the dust lane which was included in the profile and only that. Once again the unfiltered results are included for comparison.

Wave band	Interstellar Polarisation				Dust lane					
					Extinction		Polarisation			
(nm)	%		Angle		DWT	B	%		Angle	
V(550)	0.4	(0.1)	63	(7)	1.5	1.6	4.4	(1.1)	82	(6)
R(650)	0.5	(0.3)	41	(7)	1.2	1.5	3.1	(0.5)	93	(5)
I(745)	0.7	(0.4)	51	(6)	0.8	1.4	2.4	(0.6)	108	(5)
NF	0.5	(0.1)	52	(5)	1.1	-	3.5	(0.7)	92	(5)

Table 5.1: Multicolour polarimetry of M104. Errors in brackets. Errors in extinction are 0.01mag. DWT refers to this survey, B to Burkhead (1986) (see text)

Examination of the data in Table 5.1 shows that the foreground interstellar polarisation in this direction is varying to an extent less than that which is measurable, whilst the dust lane polarisation decreases with increasing wavelength.

The extinction measured by Burkhead (1986) at each wavelength is included in Table 5.1 for comparison. It can be seen that a lesser extinction has been measured in this survey than in that of Burkhead, although both agree that the extinction decreases with increasing wavelength, and note that the figures quoted for Burkhead were measured from a graph, so errors

could arise from this source. All results of M104 are discussed in the next subsection.

5.2.2 Discussion

A similar picture has been observed in all wavebands of M104 and a foreground interstellar polarisation has been subtracted from each. A map has then been seen of an unpolarised nucleus, and a polarised dust lane, where the absolute value of this polarisation decreases with increasing wavelength.

As was discussed in Chapter 2, Serkowski et al. (1975) derived a wavelength dependence of polarisation caused by aligned grains in our Galaxy from observations of the polarisation of stars. This gives the polarisation P at wavelength λ to be:

$$P(\lambda) = P_{max} e^{-1.15 ln^2(\lambda_{max}/\lambda)} \tag{5.1}$$

where the wavelength λ_{max}, at which maximum polarisation P_{max} occurs, lies between 450 and $800nm$. However Wilking et al. (1980) modified this relation, in view of more observations, chiefly at infra-red wavelengths, to be:

$$P(\lambda) = P_{max} e^{-1.7\lambda_{max} ln^2(\lambda_{max}/\lambda)} \tag{5.2}$$

This new relation does not significantly affect the results obtained at optical wavelengths, although it does become significant in the infra-red.

It can be seen from Table 5.1 that λ_{max} occurs somewhere around the range of observations described in this chapter. So an endeavour was made to see if these current results were consistent with the theory of Serkowski et al.

Serkowski et al. (1975) plotted P/P_{max} against λ_{max}/λ for their data. This curve was used to see if the data in this chapter

would fit the same relation as their data. It was found that values for $\lambda_{max} = 0.4\mu m$, and $P_{max} = 4.85\%$ were required for a fit. The data are tabulated in Table 5.2.

$\lambda/\mu m$	λ_{max}/λ	$P_{observed}/\%$	$P_{calculated}/\%$
0.400	1.00	- --	4.85
0.550	0.72	4.4 (1.1)	4.37
0.650	0.60	3.1 (0.5)	3.40
0.745	0.53	2.4 (0.6)	2.60

Table 5.2: Comparison of observations with theory. Errors in $P_{observed}$ in brackets. $P_{calculated}$ is from the relation of Serkowski et al. (1975) (see text)

The first column gives the peak wavelength of each observation in *microns*, the second column divides the wavelength at which P_{max} occurs by the wavelength of the observations and the third column lists the measured dust lane polarisation of M104 at each wavelength. The fourth column gives the polarisation calculated from the relation of Serkowski et al. from their observations of our own Galaxy.

It can be seen from Table 5.2 that this author's results for M104 are consistent with the theoretical predictions of Serkowski et al. for polarisation caused by extinction by magnetically aligned dust grains in our Galaxy, although the errors are large. However, note that the wavelength λ_{max} required to fit the M104 data is shorter than that required by Serkowski et al. for our own Galaxy. Using Equn 2.4, this gives a value of the ratio of total to selective extinction in M104 to be: $R = 2.2$, compared to $R = 3.1$ for our Galaxy (Savage and Mathis 1979).

Compare this with the value of $R = 1.9$ found for IC4320 by

Warren-Smith and Berry (1983). IC4320 is an elliptical galaxy with a dust lane, and so it would not be expected to show similarities to M104. However these latter authors explained their low value of R as being caused by a deficiency, relative to our Galaxy, of large dust grains, and hence a smaller mean particle size. It is here hypothesised that this may also be true for M104.

The relation between polarisation and extinction caused by aligned interstellar dust grains in our own Galaxy has been studied by many workers. Greenberg (1978) studied the ratio of polarisation (P) to extinction (A), with inverse wavelength (λ^{-1}). He used the polarisation expressed in terms of a magnitude difference in intensity between the orthogonal states parallel (I_{max}) and perpendicular (I_{min}) to the direction of polarisation. This polarisation is denoted Δm_p, where:

$$\Delta m_p = 2.5 log(I_{max}/I_{min}) \tag{5.3}$$

This can be expanded as a polynomial in P, which simplifies, for $P << 100\%$, to:

$$\Delta m_p \times 100\% = 2.172P \tag{5.4}$$

Greenberg (1978) used the results gathered from various sources and catalogued by Aanestadt and Purcell (1973), and normalised at inverse wavelength $\lambda^{-1} = 1.93 \mu m^{-1}$.

Their results have been normalised by this author to the results of this survey at inverse wavelength $\lambda^{-1} = 1.54 \mu m^{-1}$, where both Greenberg (1978) and this author have a data point. Interpolation was then used to calculate what they would derive for the values of the ratio for interstellar grains in our own Galaxy at the wavelengths used in this chapter to

study M104, assuming a linear relation. All of these data are tabulated in Table 5.3.

λ^{-1}	Δm_p	A	$R = \Delta m_p / A$	G'berg
1.34	0.052 (0.013)	0.8 (0.01)	0.065 (0.017)	0.071
1.54	0.067 (0.011)	1.2 (0.01)	0.056 (0.010)	0.056
1.82	0.096 (0.025)	1.5 (0.01)	0.064 (0.016)	0.046

Table 5.3: Polarisation vs. extinction in M104 dust lane. Errors in brackets. G'berg refers to Greenberg (1978) (see text)

The first column lists the inverse wavelength in μm^{-1}, the second column gives the value of Δm_p calculated from P in Table 5.1, the third column is the dust lane extinction in magnitudes, and the fourth column is the ratio of these latter two. The last column gives the values for this ratio which would be expected at these wavelengths in our own Galaxy under the relation discussed by Greenberg (1978).

The agreement is fair when it is considered that Greenberg's study is of interstellar dust grains in our own Galaxy, and this survey is of M104. Thus it is here suggested that this is further confirmation of the magnetic alignment diagnosis of the polarisation observed in M104. It is also suggested that this is evidence that the interstellar dust grains of M104 may be of similar composition to those of our Galaxy.

So it is here hypothesised that there is a magnetic field parallel to the plane of M104 which causes grain alignment within the dust lane. This alignment then produces the observed polarisation, and extinction, which are of the correct order of

magnitude, and are consistent with the relation between these parameters, for this polarising mechanism (see Chapter 2 for an explanation of the Davis-Greenstein grain alignment).

However the regions of the galaxy which display polarisations perpendicular to the plane of the disk are believed to be caused by scattering of nuclear light from the dust grains of the interstellar medium. The main argument in favour of this hypothesis, as opposed to the belief that all the observed polarisation arises from preferential absorption, comes from the areas where the two patterns meet. At each end of the dust lane there is a very sharp transition from polarisations parallel to the galactic plane to perpendicular polarisations.

Furthermore, there is a region where the two polarisation patterns appear to be competing, and cancelling one another out: At a point $100 arcsec$ to either side of the galactic nucleus in the dust lane the polarisation is seen in Fig 5.3 and Fig 5.4 to vanish to zero, indicating competing polarisation mechanisms. This appears to corroborate the above diagnosis. Further discussion of this galaxy is pursued in Section 5.4, where a comparison is made with NGC 4565.

5.3 NGC 4565

NGC 4565 is similar in appearance to M104, and has a prominent dark lane foreground to the luminous part of the galaxy. This is believed to be a dust lane, as was seen in M104. The angle between the plane of the galactic disk and the line of sight to the observer is $4 degrees$ (de Vaucouleurs 1958). The galaxy is classified as type Sb, and lies at a distance of approximately $10 Mpc$ (Richmond and Knapp 1986).

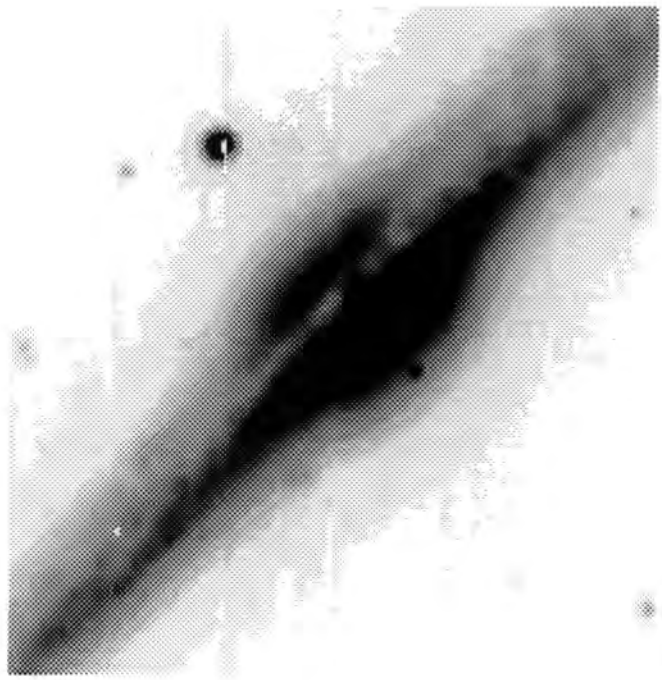

Figure 5.9: Intensity image of NGC 4565 (see text)

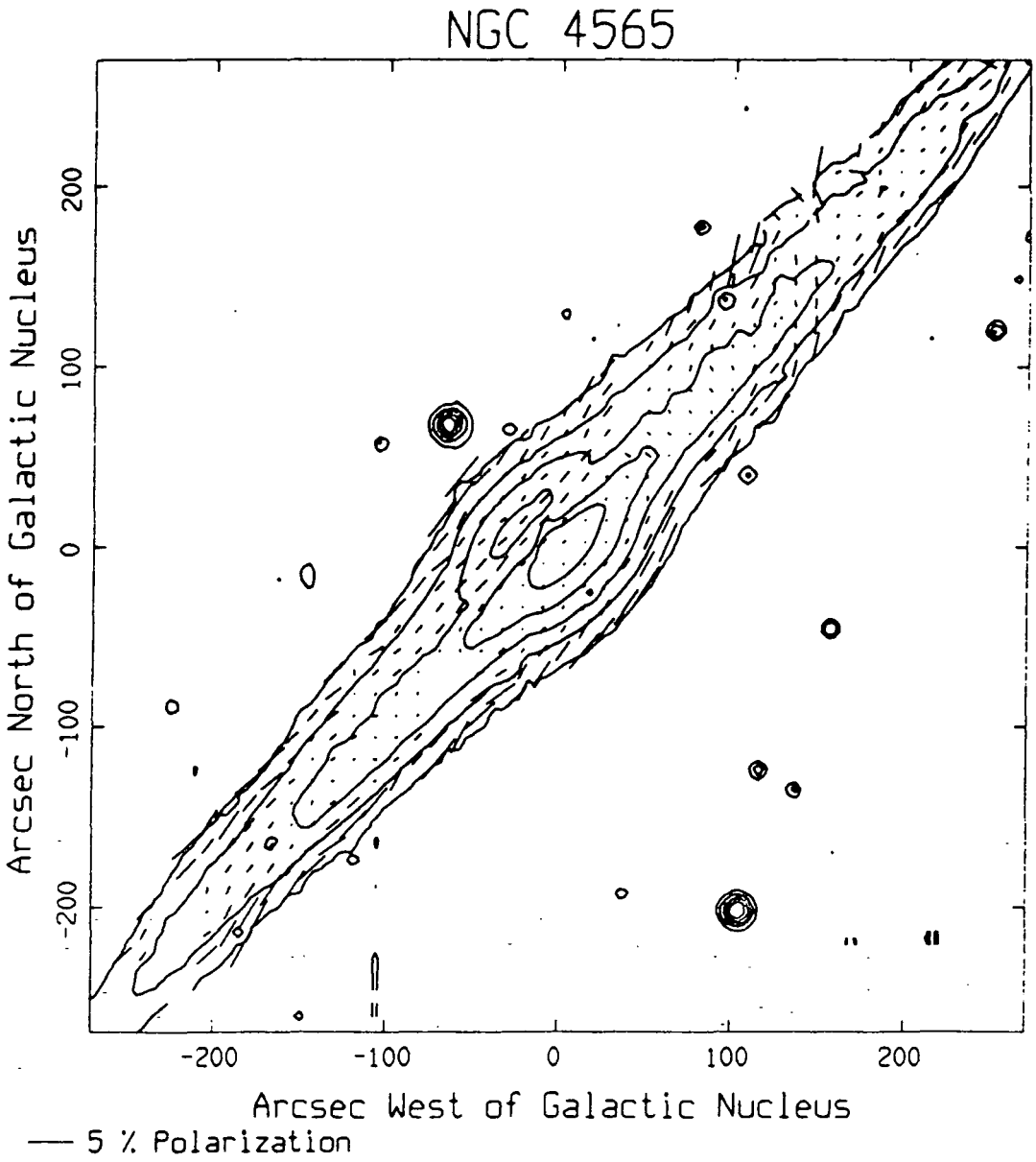

Figure 5.10: Polarisation map of NGC 4565 (see text)

Elvius and Hall (1964) attempted to measure polarisation in NGC 4565, but without success. However, Elvius (1973) did succeed in measuring the polarisation of this object, and found polarisation parallel to the dust lane at levels of $1 - 3\%$.

5.3.1 The data

Chapter 3 lists the observational details, and Table 3.1 the data available, for this object in the current survey. The mean seeing of the data is $3.8 arcsec$. Fig 5.9 shows a grey-scale intensity image of NGC 4565. North is at the top, east is at the left, and the diameter of the visible part of the galactic disk from southeast to northwest is $5 arcmin$. Note the foreground dust lane, and the smaller nuclear bulge than is seen in M104.

Fig 5.10 shows an optical linear polarisation map made from a combination of all of the observations made of NGC 4565, north is at the top, east at the left. No filter was used in this case. The integration bin size of each polarisation measurement is $18 arcsec$ square, and the measurements are spaced at $12 arcsec$ square intervals. The logarithmic spacing of the superposed isophotes is $1 magnitude$.

Examination of Fig 5.10 shows that the polarisation of NGC 4565 shows some similarities to M104. The dust lane shows a linear band of polarisation, just as in M104. This linear pattern extends to the extreme edges of the visible disk. Typical levels of polarisation in the dust lane are $1.5\% \pm 0.5\%$, parallel to the dust lane, with angle errors $\pm 10 degrees$.

However, unlike M104, the polarisation of the nucleus of NGC 4565 is so small as not to have been measured ($\leq 0.1\%$). The coordinates of NGC 4565 are: $R.A. = 12^h35^m$, $Dec. =$

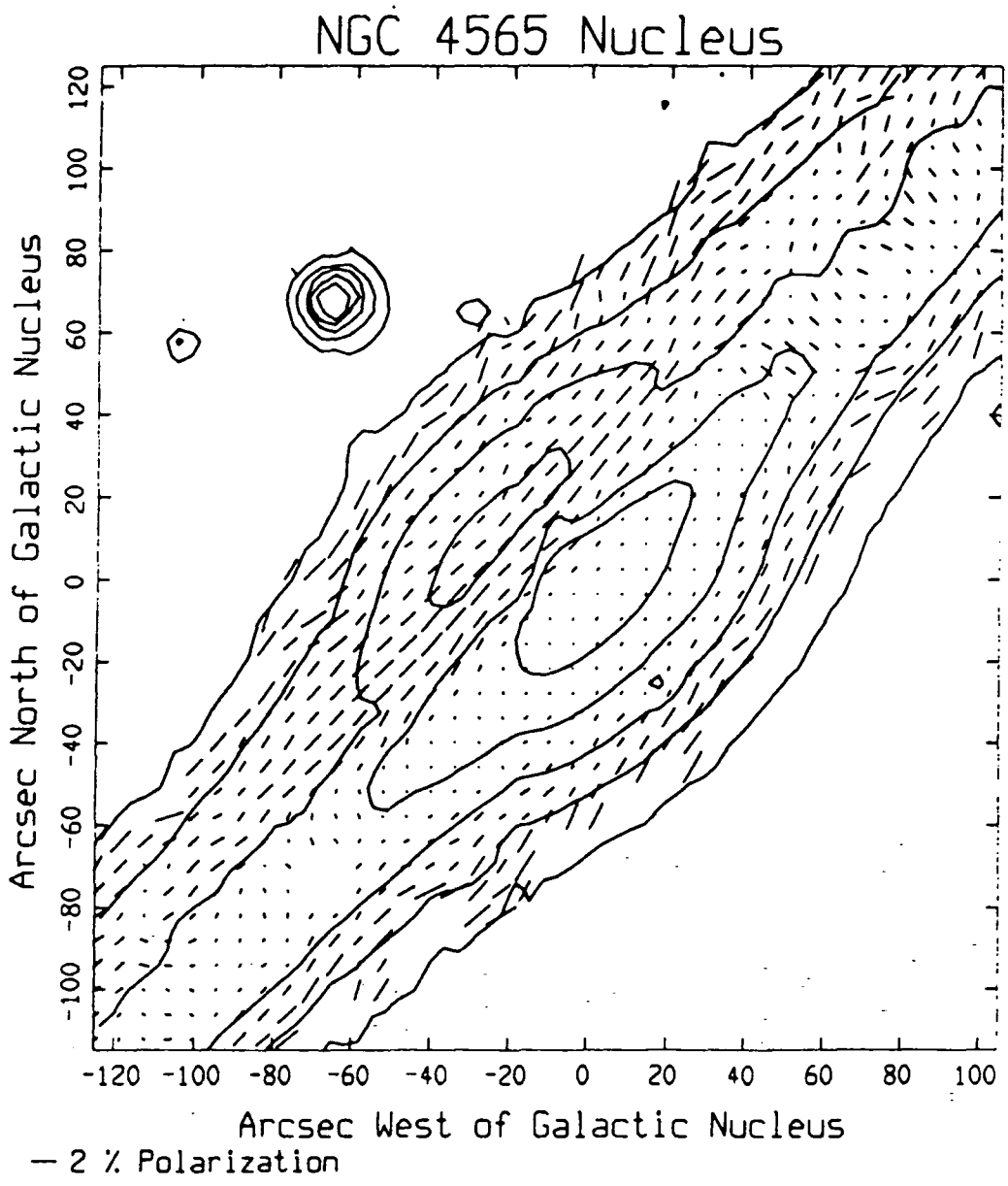

Figure 5.11: Polarisation map of central region of NGC 4565 (see text)

$26^o8'$, which, in Galactic coordinates is: longitude 230.7^o, and latitude 86.4^o. Axon and Ellis (1976) record no interstellar polarisation at, or near to, this position, as it is well away from the Galactic Plane.

Further study of Fig 5.10 shows that there is a region around $100 arcsec$ northwest of the nucleus in which a pattern of polarisations perpendicular to the plane of NGC 4565 is seen. Typical levels of polarisation in this region are $0.75\% \pm 0.25\%$, with angle errors $\pm 10 degrees$. A similar feature on the diametrically opposite side of the nucleus cannot be seen in this map.

However it can be seen that the polarisation of the regions above and below the galactic plane is at levels of around $3\% \pm 1\%$, with angle errors $\pm 10 degrees$, in a direction such as to parallel the isophotal intensity contours. Discussion of each of these separate areas of polarisation will be pursued, but first a closer look at the polarisation of the central regions of the galaxy is presented.

Fig 5.11 shows an optical linear polarisation map of the central region of NGC 4565. The integration bin size of each measurement is $10.8 arcsec$ square, and the measurements are spaced at $6 arcsec$ square intervals. The logarithmic spacing of the superposed isophotes is $1 magnitude$.

This map shows that no polarisation has been recorded for the galactic nucleus. Once again the polarisation of the dust lane can be seen to lie parallel to the plane of the disk at levels of around $1.5\% \pm 0.5\%$ with angle errors $\pm 10 degrees$. The region to the north-west of the nucleus can now be clearly seen to contain polarisations which are perpendicular to the plane of the galaxy, at levels of up to $1\% \pm 0.5\%$, with angle

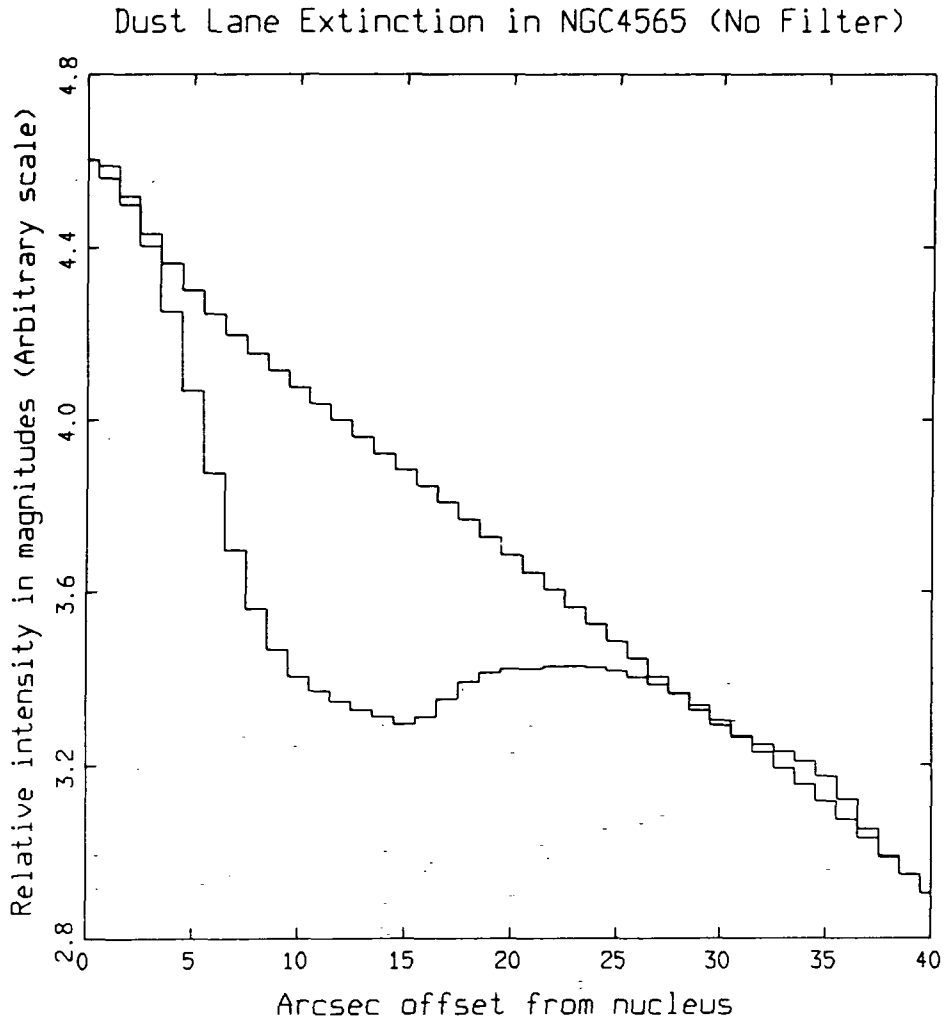

Figure 5.12: Intensity profiles to show dust lane extinction in NGC 4565 (see text)

errors $\pm 15 degrees$. A trace of a similar pattern can be seen to the south-east of the nucleus, but only at levels of $0.5\% \pm 0.3\%$ or less, with angle errors $\pm 15 degrees$. Note also that the polarisation of the areas above and below the plane appears to parallel the contours.

5.3.2 Discussion

The explanation of the observed results for NGC 4565 is believed to be the following: The levels of polarisation, and the position angles, in the linear pattern along the dust lane, indicate that there is a magnetic field parallel to the galactic plane of that galaxy. This field aligns non-spherical dust grains within the dust lane, which in turn create the observed polarisation by preferential absorption after the manner of the Davis-Greenstein effect (see Chapter 2). Thus NGC 4565 is similar both to our own Galaxy and to M104, in that it contains a magnetic field parallel to the galactic plane.

The dust lane extinction of NGC 4565 was measured in the same way as was done for M104. The profiles are shown in Fig 5.12. Again the scale is in magnitudes, but the zero point is arbitrary. The upper curve is an intensity profile through the half of the galaxy unaffected by the dust lane, the lower curve is an intensity profile through the dust lane. The width of the profiles is $6 arcsec$.

The maximum measured extinction in the dust lane is $0.6 \pm 0.05 magnitudes$, while the polarisation measured in the dust lane is $1.5 \pm 0.5\%$. This extinction is slightly lower than the unfiltered measurement of M104, although the ratio of polarisation to extinction ($= 2.5\%/mag$) is correct for the polarising

mechanism hypothesised. As no multicolour data is available for this galaxy, it is not possible to make any more detailed analysis than to state that this is consistent with the magnetic grain alignment mechanism for the production of the observed polarisation.

It is also hypothesised that the small regions of low polarisation (of order 1%) centred on 1*arcmin* to the northwest and southeast of the galactic nucleus, where the polarisation is roughly perpendicular to the galactic plane, are caused by scattering of nuclear light by interstellar dust grains. Further justification of the scenario here outlined is given in the next section. A comparison of this galaxy with NGC 4594 is also presented. A discussion of magnetic fields in galaxies is pursued in Chapter 6.

5.4 Magnetic alignment vs scattering

In this chapter data have been presented of two spiral galaxies. The observed polarisations have been interpreted in terms of preferential absorption of light by a magnetic field, which aligns non-spherical grains in a galactic dust lane. This interpretation is after the manner of previous workers who have discovered similar phenomena (eg: Scarrott et al. 1977, Berry 1985).

However, a serious objection to this type of interpretation has been raised by Jura (1982). He claimed that polarisations of this nature can be explained simply in terms of scattering of nuclear light from non-aligned grains in the dust lane, without any recourse to a magnetic field whatsoever. In this section an attempt is made to show that this explanation is inadequate for the two galaxies discussed in this chapter.

Note that two galaxies, which have a similar optical appearance, have been found to have very similar polarisation results. Therefore it is logical to assume that the same polarising mechanism is responsible for both sets of data, and that the same physical explanation holds true for both galaxies. Hence any argument must explain all of the features of all the polarisation maps in this chapter.

Firstly, it may be noted that the polarisation versus extinction relations at three wavebands for M104 are consistent with the magnetic alignment hypothesis. It is also noted that the ratio of polarisation to extinction in NGC 4565 is consistent with the mechanism of preferential absorption by aligned dust grains. However, none of these relations can rule out scattering as the polarising mechanism, due to experimental errors.

However Hough et al. (1987) made measurements of the polarisation of a supernova, which was seen through the dust lane of NGC 5128. They carried out these measurements over a wide range of wavelengths, covering the optical and infra-red. Their measurements were fitted by a Serkowski-type relation for preferential extinction by magnetically aligned dust grains. Furthermore, their results were inconsistent with a model for polarisation caused by scattering, and could not be explained without recourse to aligned grains.

For the data in this chapter: Fig 5.3 clearly shows evidence of two polarising mechanisms being present: There are vectors around $140 arcsec$ east of the nucleus, and around $2 arcmin$ west, which appear to indicate that two perpendicular polarisations are in competition in these regions. Likewise the fact that the polarisation pattern turns through $90 degrees$ so sharply, rather than in a smooth curve, after the manner of a

centrosymmetric pattern, also indicates that scattering is not the only mechanism present.

Jura (1982) claims that a galaxy of type Sa should show a polarisation pattern parallel to the plane of the galaxy. The polarisation of a galaxy of type Sb should be more nearly perpendicular to the galactic plane, while a galaxy of type Sc should have polarisations which are all perpendicular to the plane of the galaxy. This is because later type galaxies have a smaller nuclear bulge and a galaxy with only a very small nuclear bulge should exhibit polarisation perpendicular to the plane of the disk, at a point far from the nucleus, if scattering is the mechanism responsible for the polarisation. This arises from simple scattering geometry considerations.

M104 is of type Sab and so should be polarised parallel to its plane, however NGC 4565 is of type Sb and so should be polarised perpendicular to the plane of the galaxy. However, examination of Fig 5.10 shows that, all the way from that part of the dust lane which is nearest to the galactic nucleus out to some 280*arcsec* northwest and southeast of the nuclear bulge respectively, the polarisation observed is parallel to the plane of the disk. This can not be explained by scattering, so Jura's hypothesis is not valid for these data, as Hough et al. (1987) deduced in the case of NGC 5128.

5.5 Conclusions

The two galaxies studied in this chapter exhibit similar polarisation maps. It has been deduced from these polarimetric results that both M104 and NGC 4565 contain a magnetic field which is parallel to the plane of the galaxy. In this respect both

are similar to our own Galaxy. The alternative interpretation of results of this nature, as proposed by Jura (1982), has been discounted, on the grounds that it does not explain all of the features of the data presented.

Muticolour polarimetry of M104 has been used to demonstrate a consistency with the magnetic alignment interpretation. Furthermore, the similarity between these data and those discussed by Greenberg (1978) has lead to the hypothesis that the interstellar dust grains of M104 are similar to those of our Galaxy. A more detailed discussion of magnetic fields in galaxies is pursued in the next chapter.

Chapter 6

Discussion

6.1 Introduction

A review was presented in Chapters 1 and 2 of spiral structure in galaxies and of existing theories of magnetic fields in galaxies. The ensuing chapters then presented new data of magnetic fields in spiral galaxies. This chapter now considers how these new results affect the theories.

Firstly the individual conclusions for each galaxy are described, and then more general conclusions are drawn. The three-dimensional shape of galactic magnetic fields is discussed. The relationship is also discussed between the magnetic field and each of: matter, spiral density waves and spiral shocks. The ways in which they interact are then explored. Finally the arguments for and against a primordial origin of galactic magnetic fields are summarised as they are affected by the new observations.

6.2 The results of this survey

Polarisation maps were presented, in Chapter 3, of M51. From these it was concluded that there is a spiral magnetic field in M51, which persists from within $300pc$ of the galactic centre, to a radius of $14kpc$. This large-scale spiral field is well ordered, and of sufficient intensity to align non-spherical interstellar dust grains. It is suspected that this field continues to be spiral within the ILR of M51.

In Chapter 4 polarisation maps were presented of NGC 1068, and it was surmised from these that this galaxy also contains a spiral field, of a similar nature to that of M51. In this case the field was seen to be spiral from within $400pc$ of the galactic centre, to a radius of $6kpc$. However, also observed was a dust torus surrounding, and obscuring, the Seyfert nucleus of NGC 1068.

Polarisation maps of NGC 4565 were presented in Chapter 5. From these, the presence of a galactic magnetic field aligning interstellar dust grains was inferred. Study of both the magnitude of extinction and percentage polarisation in the dust lane of that galaxy further indicated a magnetic field parallel to the galactic plane.

Results of a multicolour polarimetric survey of M104 were also presented in Chapter 5. A magnetic field parallel to the galactic plane was inferred from the overall polarisation maps of that galaxy. Closer inspection of the multicolour data tended to confirm this interpretation and lead to the hypothesis that interstellar dust grains in M104 may be smaller than those in our own Galaxy.

6.3 Magnetic fields in three-dimensions

The disadvantage of optical polarimetry over other methods, in the study of magnetic fields, is that it only determines the direction of a magnetic field and not its sense. However several galaxies have been studied in this work, at different angles of inclination to the observer, and an attempt is here made to discuss what may be discerned of the overall three-dimensional structure of the large-scale magnetic fields of these galaxies.

The studied galaxies are two which are seen at inclination close to face-on and two which are seen close to edge-on. The two edge-on galaxies, NGC 4565 and M104, both have magnetic fields which are parallel to the planes of those galaxies. Similarly our own Galaxy has a magnetic field which is parallel to the Galactic Plane (Mathewson and Ford 1970). It therefore seems reasonable to assume that the fields which have been observed in M51 and NGC 1068 are also parallel to their respective galactic planes, there being no evidence to the contrary.

The specific example of M51 is taken first and the structure of its magnetic field is conjectured. (The reason for choosing M51 first is that not only are very clear optical linear polarisation measurements available, but also radio linear polarisations and radio rotation measurements). Indications from data presented in this thesis lead to several possible alternatives for the three-dimensional shape of the magnetic field of M51:

(1) Bisymmetric open spiral (BSS)—in which the field is open to intergalactic space, and may link with the fields of other galaxies.

(2) Closed spiral—the direction of the field reverses from

arm to inter-arm and thus is a closed system.

(3) Spiral in the plane, but closed via a poloidal component—the field relinks from the outer edges of the disk to the galactic centre by means of a poloidal component not unlike that of the earth or the sun.

Optical polarimetry alone can not distinguish between these three, however radio rotation measures (RM) help clarify the situation. Sofue et al. (1986) gave details of RM analysis of M51, and found it to be best fitted by a bisymmetric open spiral structure. Thus option (1) above appears to be the option closest to the observational evidence.

However, note that (3) is not ruled out by the available observations. Our own Galaxy has been observed to have a poloidal field component (Seiradakis et al. 1985, Uchida et al. 1985), so it is possible that M51 may also have such a field component.

The next example to consider is NGC 1068: The optical polarisation maps presented of this galaxy show many similarities to those of M51. However in this case it is not possible to state what is the configuration of the magnetic field near to the galactic centre. As no equivalent RM analysis has been made of this galaxy, it is also not possible to distinguish between options (1), (2) and (3) above, but merely to note that one of these is the magnetic field configuration of NGC 1068.

In the case of both M104 and NGC 4565 the configuration of the field in the galactic plane remains a matter for conjecture, and may be different for each. In each case either options (1) or (2) above may be the true configuration, and option (3) cannot be ruled out as no measurements were made far from the plane of either galaxy. Furthermore, the fields of these galaxies could

be circular within their galactic planes, and hence closed, or some more complex configuration not yet mentioned.

The relevance of whether a galactic magnetic field is open to intergalactic space or closed has a bearing on the origin of the seed field. An open field seems to favour a primordial model, whereas a closed field appears to favour a later origin. However this is an over-simplification for the following reasons: An intergalactic seed field can become wrapped up in a galaxy and relink to form a closed system. Likewise a field which was created by dynamo action within a galaxy can leak out to seed intergalactic space.

Thus other arguments must be employed to determine whether or not the observed magnetic fields are primordial in origin. These arguments are discussed in Section 6.7, but first a discussion is presented of why the observed magnetic fields show any spiral structure at all.

6.4 Magnetic fields and matter

It has been shown in this thesis that two spiral galaxies have spiral magnetic fields - namely M51 and NGC 1068. Other authors have also found evidence for spiral magnetic fields in these and other spiral galaxies. For instance spiral fields have already been reported in M51 (Segalowitz et al. 1976), M33 (Beck 1982) and M81 (Sofue et al. 1980, Krause et al. 1987a). However, to the author's knowledge, these data represent the first detailing of a spiral magnetic field in NGC 1068.

There are several constituents of the material of a galaxy - these include stars, dust, neutral gas and ionised gas. All of these components are orbiting at velocities dependent on

radius from the galactic centre. Thus any element of spiral structure, which is linked solely to the matter in a galaxy, would be expected to be destroyed by differential rotation in a small percentage of the galaxy's lifetime. Hence, for a spiral magnetic field to exist for a substantial part of the lifetime of a galaxy the field lines can not be coupled to the matter.

However the magnetic field is only expected to be coupled to the ionised gas, and not to the neutral gas and dust. The ionised gas is coupled weakly to the neutral gas in a way which is dependent upon the product of the two gas densities and the scattering cross-sections. Thus the field may be only weakly coupled to the galactic matter.

Sofue et al. (1980) stated that the problem of differential rotation may be overcome if a spiral galaxy has a massive halo containing diffuse gas and a magnetic field. Turbulent diffusion and the mixing of the disk and halo fields were then invoked by these authors to maintain the open spiral nature of the disk field. Other solutions to the same problem are presented later in this chapter.

It was mentioned in Chapters 3 and 4 that ionised outflows, which have been observed from the nuclei of M51 and NGC 1068, do not affect the observed magnetic field orientation. However, it has just been suggested that the field would be expected to be coupled to any ionised gas flow. One possible explanation for this is that the outflows may occur out of the plane of the disk, where the field has not been measured (see previous section).

Ruzmaikin (1987) calculated that the motions of charged particles in the interstellar medium can sustain the magnetic field of our own Galaxy, provided that the efficiency of this

process is around 10%. Thereafter the back emf. of the motions stabilises the field. Thus the behaviour of the magnetic field in a galaxy is governed by the velocity field of the charged particles, and also by the characteristics of the spiral density waves within that galaxy (Klein et al. 1983). This is pursued in the next section.

6.5 Magnetic fields and spiral density waves

Spiral density wave theory was discussed in Chapter 1. Here the relation between this theory and observations of magnetic fields in spiral galaxies is discussed.

Mathewson et al. (1972) and Segalowitz (1976) reported a concentration of non-thermal radio emission along the dark lane regions on the inner edges of the spiral arms of M51. This is believed to be because the magnetic field is enhanced in the compression regions associated with such lanes in spiral density wave theories (Roberts 1974). Thus it is here hypothesised that the magnetic field of M51 is coupled to the spiral density waves of that galaxy.

However one of the interesting features of the theory of spiral density waves is that there are two resonant orbits—the inner and outer Lindblad resonances, ILR and OLR—which form the boundaries of the spiral structure. That is to say that spiral density waves do not exist within the ILR or beyond the OLR.

In Chapter 3 the data presented of M51 appear to indicate that the magnetic field continues to be spiral within this radius, and in fact right into the galactic centre. If this is the case then the field cannot be coupled to spiral density waves throughout

its entire length.

6.6 Magnetic fields and spiral shocks

Spiral shocks are found in association with spiral density waves (Roberts 1974), and have been studied in detail on a small scale (Draine et al. 1983). It is here hypothesised that it is possible that galactic magnetic fields may be coupled to galactic shock waves. This theory was propounded by Roberts and Yuan (1970), who performed mathematical derivations for large-scale spiral hydromagnetic shocks within our Galaxy, and showed that a two-armed spiral structure could be the result.

This means that, where a shock front exists in the interstellar medium, there is an increase in the local magnetic field strength. Furthermore, if the local field was initially not parallel to the shock front, then it would soon be forced to be more nearly parallel by its interactions with the matter which was being shocked.

In order to explain, consider a region of the interstellar medium within a spiral galaxy, away from corotation, in which there exists part of a spiral shock front. The neutral matter of the interstellar medium flows through the shock, and experiences various shock-induced phenomena such as star formation (Elmegreen 1985).

The ionised component of the matter, coupled to the magnetic field, also flows through the shock front, and also experiences shock-related phenomena. Some of this ionised matter accretes onto other matter and takes part in the star-forming processes of the region. Similarly, some neutral matter is ionised by shock excitation. The net result of this is that, when viewed on a large scale, the magnetic field lines tend to

align with, and be compressed together by, the shock front, as was observed in M51 by Mathewson et al. (1972).

Giant HII regions, which contain large volumes of ionised gas, might be expected to disrupt the overall spiral design of galactic magnetic fields which have been here postulated. Such regions would be strongly coupled to the local magnetic field. However, one way in which this disruption may be avoided is the following:

When a giant HII region passes through a galactic arm, with its associated shock wave and more intense magnetic field, it would carry with it that part of the field through which it passes. This would create a magnetic bubble which, through local field annihilation, relinks behind the cloud. Such a bubble has been shown (Parker 1979) to annihilate itself on a timescale which is short relative to the orbiting travel time between spiral arms, with a consequent heating of the ISM. In this way, the spiral nature of the field is maintained, and the problems of differential rotation are overcome.

This hypothesis could be tested by the study of a spiral galaxy for which greater angular resolution of the spiral arms is possible. For instance M31 could be studied in this way. Optical linear polarisation measurements of the giant HII regions could then ascertain whether they had disrupted a purely spiral magnetic field pattern.

6.7 The origin of galactic magnetic fields

A review was presented in Chapter 2 of various theories concerning the origin of magnetic fields in galaxies and the different theories were discussed. The model of a primordial field

being wrapped up into a spiral pattern (Piddington 1964) was outlined. The galactic dynamo theory (Parker 1979) was also detailed. These theories may now be assessed in view of the data presented in this thesis.

It has already been pointed out in this chapter that the magnetic field of M51 has a BSS structure. This could not be created by the dynamo as it was described by Parker (1979), as this latter creates a circumferential field in a spiral galaxy. Thus the primordial field model of Piddington (1964) may appear to be favoured. However Scarrott et al. (1987a) concluded that it may be possible to revise the dynamo model to account for the observations. This has since been undertaken and is now discussed.

Fujimoto (1987) found BSS solutions of the dynamo equations, and showed that, for a substantial range of galactic radii, a spiral field configuration can be sustained. However, he did not find solutions which sustained a BSS field for all galactic radii.

Ruzmaikin (1987), expanding on the work of Ruzmaikin et al. (1985), considered a galactic magnetic field with a component in the plane of the disk. He invoked differential rotation in the galactic plane to twist this field into some form of spiral. He then considered different modes (m) of excitation of the field, where $m = 0$ is a circular field, $m = 1$ corresponds to a BSS configuration etc. He studied a local rate of exponential growth of the mean magnetic field at some point in the galactic disk.

He deduced that the mode $m = 0$ is the preferred mode for galactic magnetic fields, but that the mode $m = 1$ has a significant probability of occurring, while all higher modes

decay exponentially. However, he was also forced to admit the need for a seed field. He dismissed any cosmological origin of such a seed as being too weak, and concluded that the most likely origin is in fields ejected from supernovae or leakage of stellar fields. Furthermore he put an estimate on the probable magnitude of a seed field as $10^{-3} microgauss$.

Finally, he admitted that galactic magnetic field theories still have some way to go to explain all aspects of the observations. However, his work has shown that galactic dynamo theories can probably explain all of the observations which have been made of galactic magnetic fields. Furthermore, he has removed the necessity to resort to a primordial magnetic field.

6.8 Conclusions

Data have been presented of magnetic fields in spiral galaxies and a suggestion has been made that galactic magnetic fields may be linked to galactic shock waves. The observations have been used to test current theories of the origin of galactic magnetic fields. The dynamo theory of Parker (1979) proved unable to explain the results, but the refinements of Ruzmaikin (1987) have shown that interstellar magnetic fields can be explained by galactic dynamo action without recourse to a primordial magnetic field. However there is much scope for further theoretical and observational studies.

Acknowledgements

The author would like to thank Dr. S.M.Scarrott for supervising, overseeing and leading astray this student during times observational, theoretical, reductional and aquatic.

Collingwood College are very gratefully acknowledged for the Collingwood Scholarship which made this thesis possible.

Rodney Warren-Smith, Peter Draper and Tim Gledhill are thanked for their assistance, friendship and home-brews.

Thanks also go to Alan Lotts for keeping the Durham node of STARLINK operational despite my efforts. SERC is acknowledged for funding polarimetry in Durham.

The author would also like to thank the following for their help in many ways: David Berry, Janice Shirt, David Mannion, Nick Eaton, Mike Lee, Cathy Swift, Dr. Tuck, Eric Halliday, Gerald Blake and Durham University Boat Club.

References

Aanestadt P A & Purcell E M (1973) Ann Rev A & Ap **11**, 309.

Allen R J, Baldwin J E & Sancisi R (1978) A & Ap **62**, 397

Ambastha A & Varma R K (1983) Ap J **264**, 413

Angel J R P, Stockman H S, Woolf N J, Beaver E A & Martin P G (1976) Ap J Lett **206**, L5

Antonucci R R J & Miller J S (1985) Ap J **297**, 621

Axon D J & Ellis R S (1976) MNRAS **177**, 499

Beck R (1982) A & Ap **106**, 121

Beck R, Klein U & Wielebinski R (1987) A & Ap (in press)

Berkhiujsen E M, Beck R & Grave R (1987) in Interstellar Magnetic Fields, ed: R Beck & R Grave (Springer-Verlag), Heidelberg

Berry D S (1985) PhD Thesis, Univ of Durham

Bingham R G, MacMullan D, Pallister W S, White C, Axon D J & Scarrott S M (1976) Nature **259**, 463

Buczilowski U R (1987) in Interstellar Magnetic Fields, ed: R Beck & R Grave (Springer-Verlag), Heidelberg

Burb idge E M & Burb idge R G (1964) Ap J **140**, 1445

Burkhead M S (1986) A J **91**, 777

Burn B J (1966) MNRAS **133**, 67

Byrd GG (1983) Ap J **264**, 464

Cecil G & Rose J A (1984) Ap J **287**, 131

Chesterman J F & Pallister W S (1980) MNRAS **191**, 349

Condon J J, Condon M A, Gisler G & Puschell J J (1982) Ap J **252**, 102

Cugnon P (1985) A & Ap **152**, 1

Davis L Jnr & Greenstein J L (1951) Ap J **114**, 206

De Vaucouleurs G (1958) Ap J **127**, 487
Draine B T, Roberge W G & Dalgarno A (1983) Ap J **264**, 485
Draper P W (1987) PhD Thesis, Univ of Durham (in preparation)
Elmegreen B G (1985) IAU Symp **115**, 457
Elvius A (1951) Stockholms Obs Ann **17**, no.4
Elvius A (1956) Stockholms Obs Ann **19** no.1
Elvius A (1973) IAU Symp **52**, 209
Elvius A (1978a) IAU Symp **77**, 65
Elvius A (1978b) A & Ap **65**, 233
Elvius A (1978c) A & Space Science **55**, 49
Elvius A & Hall J S (1964) Lowell Obs Bull **No.123**, vol.VI, no.4
Ford H C, Crane P C, Jacoby G H, Lawrie D G & van der Hulst J M (1985) Ap J **293**, 132
Fujimoto M (1987) in Interstellar Magnetic Fields, ed: R Beck & R Grave (Springer-Verlag), Heidelberg
Goad J W & Gallagher J S (1985) Ap J **297**, 98
Gott J R III (1977) Ann Rev A & Ap **15**, 235
Grave R & Beck R (1987) in Interstellar Magnetic Fields, ed: R Beck & R Grave (Springer-Verlag), Heidelberg
Greenberg J M (1978) in Cosmic Dust, ed: J A McDonnell (Wiley)
Hall J S (1949) Science **109**, 166
Harrison B, Pedlar A, Unger S W, Burgess P, Graham D A & Preuss E (1986) MNRAS **218**, 775
Harrison E R (1970) MNRAS **147**, 279
Hausmann M A & Roberts W W Jnr (1984) Ap J **282**, 106
Hegyi D J & Gerber G L (1977) Ap J Lett **218**, L7
Hiltner W A (1949) Science **109**, 471
Hohl F (1971) Ap J **168**, 343

Hohl F (1974) in La Dynamique des Galaxies Spirales, Coll Int du Cen Nat de Recherche Scientifique, ed: L Weliachew (CNRS), Paris
Hough J H & Bailey J A (1987) MNRAS **227**, 1P
Illingworth G (1981) in The Structure and Evolution of Normal Galaxies, NATO Adv Study Inst, ed: S M Fall & D Lynden-Bell (Cambridge)
Jones B J T & Gonzalez E M (1984) in Lectures at Univ of Menendez Pelayo, Nordisk Inst fur Teoretisk Atomfysik
Jones R V & Spitzer L (1967) Ap J **147**, 943
Jura M (1982) Ap J **258**, 59
Kalnajs A J (1973) Proc Ast Soc Aust **2**, 174
Kalnajs A J (1976a) Ap J **205**, 745
Kalnajs A J (1976b) Ap J **205**, 751
Kalnajs A J & Athanassoula-Georgala E (1974) MNRAS **168**, 287
Klein U, Beck R, Buczilowski U R & Wielebinski R (1982) A & Ap **108**, 176
Klein U, Urbanik M, Beck R & Wielebinski R (1983) A & Ap **127**, 177
Krause M, Beck R & Hummel E (1987a) in Interstellar Magnetic Fields, ed: R Beck & R Grave (Springer-Verlag), Heidelberg
Krause M, Hummel E & Beck R (1987b) in Interstellar Magnetic Fields, ed: R Beck & R Grave (Springer-Verlag), Heidelberg
Kunkel T D (1977) PhD Thesis, Univ of Hawaii
Lin C C & Shu F H (1964) Ap J **140**, 646
Lindblad B (1964) Astrophys Norv **9**, 103
Lindblad P O (1974) IAU Symp **58**, 399
Lo K Y, Berge G, Claussen M, Heiligman G, Keene J, Masson C, Phillips T, Sargent A, Scoville N, Scott S, Watson D & Woody

D (1984) Proc of URSI Symp, Spain
Loiseau N, Hummel E, Beck R & Wielebinski R (1987) in Interstellar Magnetic Fields, ed: R Beck & R Grave (Springer-Verlag), Heidelberg
Lynden-Bell D (1974) in La Dynamique des Galaxies Spirales, Coll Int du Cen Nat de Recherche Scientifique, ed: L Weliachew (CNRS), Paris
Mathewson D S & Ford V L (1970) Mem RAS **74**, 139
Mathewson D S, van der Kruit P C & Brouw W N (1972) A & Ap **17**, 468
McLean I S, Aspin C, Heathcote S R & McCaughrean M J (1983) Nature **304**, 609
Ondrechen M P (1985) A J **90**, 1474
Ostriker J P & Peebles P J E (1973) Ap J **186**, 467
Pallister W S (1976) PhD Thesis, Univ of Durham
Parker E N (1971) Ap J **168**, 239
Parker E N (1975) Ap J **202**, 523
Parker E N (1979) Cosmical Magnetic Fields (Clarendon), Oxford
Pedlar A, Booler R V, Spencer R E & Stewart O J (1983) MNRAS **202**, 647
Perkins H G (1978) PhD Thesis, Univ of Durham
Piddington J H (1964) MNRAS **128**, 345
Purcell E M (1973) in The Dusty Universe, ed: G B Field & A G W Cameron (Neale Watson)
Rees M J (1986) in Ginsberg Zeitschrift, (Springer-Verlag), Heidelberg
Richmond M W & Knapp G R (1986) A J **91**, 517
Roberts W W Jnr (1974) in La Dynamique des Galaxies Spirales, Coll Int du Cen Nat de Recherche Scientifique,

ed: L Weliachew (CNRS), Paris
Roberts W W Jnr, Roberts M S & Shu F H (1974) IAU Symp **58**, 439
Roberts W W Jnr & Hausmann M A (1984) Ap J **277**, 744
Roberts W W Jnr & Yuan C (1970) Ap J **161**, 887
Rose J A & Cecil G (1983) Ap J **266**, 531
Rose J A & Searle L (1982) Ap J **253**, 556
Ruzmaikin A A (1987) in Interstellar Magnetic Fields, ed: R Beck & R Grave (Springer-Verlag), Heidelberg
Ruzmaikin A A, Sokoloff D D & Shukurov A M (1985) A & Ap **148**, 335
Sandage A (1961) The Hubble Atlas of Galaxies, (Carnegie Inst), Washington
Sandage A & Tammann G A (1974) Ap J **194**, 559
Sanders R H & Bania T M (1976) Ap J **204**, 341
Sanders R H & Huntley J M (1976) Ap J **209**, 53
Savage B D & Mathis J S (1979) Ann Rev A & Ap **17**, 73
Scarrott S M, Ward-Thompson D & Warren-Smith R F (1987a) MNRAS **224**, 299
Scarrott S M, Ward-Thompson D & Warren-Smith R F (1987b) in Interstellar Magnetic Fields, ed: R Beck & R Grave (Springer-Verlag), Heidelberg
Scarrott S M, Warren-Smith R F, Pallister W S, Axon D J & Bingham R G (1983) MNRAS **204**, 1163
Scarrott S M, White C, Pallister W S & Solinger A B (1977) Nature **265**, 32
Schild R, Tresch-Fienberg R & Huchra J (1985) A J **90**, 441
Schweizer F (1978) Ap J **220**, 98
Segalowitz A (1976) PhD Thesis, Univ of Leiden

Segalowitz A, Shane W W & de Bruyn A G (1976) Nature **264**, 222
Seiradakis J H, Lasenby A N, Yusef-Zaheh F, Wielebinski R & Klein U (1985) Nature **317**, 697
Sellwood J A & Carlberg R G (1984) Ap J **282**, 61
Serkowski K, Mathewson D S & Ford V L (1975) Ap J **196**, 261
Shanks T (1985) Vistas in Astronomy **28**, 595
Shu F H (1973) Lecture at Adv Study Inst on ISM, Germany
Shu F H (1974) in La Dynamique des Galaxies Spirales, Coll Int du Cen Nat de Recherche Scientifique, ed: L Weliachew (CNRS), Paris
Shu F H, Dones L, Lissauer J J, Yuan C & Cuzzi J N (1985) Ap J **299**, 542
Sofue Y (1987) in Interstellar Magnetic Fields, ed: R Beck & R Grave (Springer-Verlag), Heidelberg
Sofue Y & Fujimoto M (1983) Ap J **265**,722
Sofue Y, Fujimoto M & Kawabata K (1979) Pub Ast Soc of Japan **31**, 125
Sofue Y, Fujimoto M & Wielebinski R (1986) Ann Rev A & Ap **24**, 459
Sofue Y, Takano T & Fujimoto M (1980) A & Ap **91**, 335
Telesco C M, Becklin E E, Wynn-Williams C G & Harper D A (1984) Ap J **282**, 427
Teuben P J, Sanders R H, Atherton P D & van Albada G D (1986) MNRAS **221**, 1
Toomre A (1977) Ann Rev A & Ap **15**, 437
Toomre A (1981) in The Structure and Evolution of Normal Galaxies, NATO Adv Study Inst, ed: S M Fall & D Lynden-Bell (Cambridge)
Toomre A (1982) Ap J **259**, 535

Toomre A & Toomre J (1972) Ap J **178**, 623
Tosa M & Fujimoto M (1978) Pub Ast Soc of Japan **30**, 315
Tresch-Fienberg R, Fazio G G, Gezari D Y, Hoffmann W F, Lamb G M, Shu P K & McCreight C R (1987) Ap J **312**, 542
Tully R B (1974) in La Dynamique des Galaxies Spirales, Coll Int du Cen Nat de Recherche Scientifique, ed: L Weliachew (CNRS), Paris
Turner L (1986) Ap J **305**, 668
Uchida Y, Shibata K & Sofue Y (1985) Nature **317**, 699
Vallee J P (1984) A & Ap **136**, 373
Van Albada G D & Roberts W W Jnr (1981) Ap J **246**, 740
Van den Bergh S (1960a) Ap J **131**, 215
Van den Bergh S (1960b) Ap J **131**, 558
Van der Hulst J M, Hummel E & Dickey J M (1982) Ap J Lett **261**, L59
Ward-Thompson D (1984) MSc Thesis, Univ of Durham
Ward-Thompson D, Warren-Smith R F, Scarrott S M & Wolstencroft R D (1985) MNRAS **215**, 537
Warren-Smith R F (1979) PhD Thesis, Univ of Durham
Warren-Smith R F & Berry D S (1983) MNRAS **205**, 889
Welter G L, Perry J J & Kronberg P P (1984) Ap J **279**, 19
Wielen R (1974) in La Dynamique des Galaxies Spirales, Coll Int du Cen Nat de Recherche Scientifique, ed: L Weliachew (CNRS), Paris
Wilking B A, Lebofsky M J, Martin P G, Rieke G H & Kemp J C (1980) Ap J **235**, 905
Wilson A S & Ulvestad J S (1982) Ap J **263**, 576
Wilson A S & Ulvestad J S (1983) Ap J **275**, 8
Wright J S & Mackay C D (1981) Proc Soc Phot Inst Eng **290**, 160
Wynn-Williams C G, Becklin E E & Scoville N Z (1985) Ap J **297**, 607